THE UNIVERSITY OF SYDNEY

ANALYSIS OF FLUID STRUCTURE-INTERACTION (FSI) PROBLEMS IN ANSYS

FREDDY SANTIAGO CARO DIAZ

SID 430542013

A thesis submitted in partial fulfillment of
requirements for the degree of
Master of Professional Engineering (Aerospace)

School of Aerospace, Mechanical & Mechatronic Engineering
Faculty of Engineering and Information Technologies
University of Sydney
2015

Declaration

I certify that the work in this Capstone Project does not incorporate, without acknowledgement, any material previously submitted for a degree or diploma in any university. It does not contain any material previously published or written by another person except where due reference is made in the text.

Signature of Student:

Freddy Santiago Caro Diaz
10/10/2015

Declaration

This thesis was completed between February and October of 2015 under the supervision of Dr. Gareth Arthur Vio from the School of Aerospace, Mechanical and Mechatronic Engineering, University of Sydney.

The following areas of original work were carried out for this thesis:

- Background investigation and literature review of Fluid-Structure Interaction (FSI)simulations using commercial programs and programming codes, as well as the main applications of FSI and the problems that usually arise in this type of simulation.

- FSI simulations of two aeroelastic cases using Ansys. The aeroelastic cases are called Delta Wing and Onera M6 wing. The study includes all the pre-processing, configuration of solvers, execution of simulation, and post-processing.

- Validation of results of the FSI simulations through comparisons against experimental results reported in literature or results from other simulations.

- Computational Fluid Dynamics (CFD) simulation in Ansys-Fluent of the Onera M6 wing in steady state and validation of results through comparison against experiments reported in literature.

- Pre-Processing and Post-processing of the simulation in Patran-Nastran of the Onera M6 wing.

……..	……..
Freddy Santiago Caro Diaz	Dr. Gareth Arthur Vio

Acknowledgements

Firstly, I would like to thank and acknowledge my supervisor, Dr Gareth A Vio, for his guidance throughout the year. Always happy to answer questions and give great insights into the subject matter. His prompt and concise feedback was highly appreciated at all stages of the project. Gareth was always ready to help at a moment's notice, and being able to simply drop into his office at any time has been incredibly helpful over the past year. His efforts to make available the necessary technical resources is highly appreciated. I also would like to offer thanks to Gareth for the execution of the simulation in Patran-Nastran of the Onera M6 wing.

I would also like to thank to the Phd candidate Nicholas Giannelis for his valuable support to overcome the multiple problems regarding Ansys. His work in the setup of the necessary hardware and software to run the simulations was vital to the completion of this project.

This thesis represents the culmination of the Master Degree in Aerospace Engineering. My academic stay in this Program has been possible thanks to the support of the Australian Department of Education that has awarded me with The Endeavour Postgraduate Scholarship. This scholarship has given me the opportunity to focus entirely on my studies, professional networking and intellectual development. In addition, it has allowed me to further enrich my multicultural experience.

Finally, thanks to all the members of my family, who consistently encouraged me, and who have given me moral support to carry out the adventure that represent study abroad far away from home.

TABLE OF CONTENTS

List of Figures

List of Tables

Nomenclature

C	Structural Damping Matrix
K	Structural stiffness
M	Structural mass Matrix
p	Force Vector
q	Dynamic Pressure
U,V	Velocity of the Air in the free stream
u	Displacement
ω_n	Natural frequency of the mode i
φ_i	Mode Shape Vector of mode i
ρ	Density
μ	Viscosity
w	Surface function

Acronyms

FEM	Finite Element Models
FSI	Fluid-Structure Interaction
LCOs	Limit Cycle Oscillations
DOFs	degrees of freedom
DNS	Direct numerical simulations
LES	Large Eddy Simulation
RANS	Reynolds-Averaged Navier-Stokes
SKE	Standard k-epsilon model
VLM	Vortex Lattice Method
DLM	Doublet-Lattice Method (DLM)
CAD	computer-aided design

Abstract

The Fluid-Structure Interaction problems occur in many natural phenomena and man-made engineering systems, this fact has promoted the research in this area. The research in this field of study is implementing two different methodologies. The first one is the use of commercial programs that have developed FSI capabilities such as Ansys or ADINA. The second methodology is the development of computational codes to solve specific problems of FSI analysis. This Project in particular focuses in the evaluation of Ansys-Fluent to perform FSI simulations.

Two aeroelastic cases were simulated in Ansys, they were: the delta wing, and the Onera M6 wing. The delta wing simulation is subsonic and its structure is a simple flat plate made out of aluminum. The Onera M6 wing simulation is transonic and its structure has multiple components that are made out of an orthotropic material.

The FSI simulations of the delta wing were validated through comparison with experimental data reported in literature. A turbulence analysis and a mesh independence analysis were carried out as well. The validation showed a limited capability to replicate the results that were obtained in the experiment.

The FSI simulations of the Onera M6 wing were validated through comparison with a simulation that was carried out in Patran-Nastran. In addition, a computational fluid dynamics (CFD) simulation in steady state was performed in Ansys in order to establish the bases of the configuration that was implemented in the FSI simulations in Ansys. The validation showed that Ansys-Fluent is able to reproduce the results obtained in Patran-Nastran.

Chapter 1

Introduction

This chapter presents a literature review of the current state of the research of Fluid Structure Interaction problems using commercial Finite Element Software. It also presents the description of the problem that is studied in this thesis and the methodology that was followed during the project.

1.1 Literature Review

Fluid-Structure Interaction (FSI) is a field that studies the interaction between a fluid flow and an elastic structure. In this kind of interaction, a fluid flow may exert a pressure load or thermal load on a structure. In some cases these loads could cause structural deformation enough to change flow itself.

FSI belongs to a bigger field that is known as Coupled Systems. Other examples of Coupled Systems are the thermal stress analysis (Cook 2007) and the soil-fluid interaction (Zienkiewicz and Taylor 2000).

According with Zienkiewicz and Taylor (2000) , Coupled systems are those applicable to multiple domains and dependent variables which usually (but not always) describe different physical phenomena and in which.

a) Neither domain can be solved while separated from the other

b) Neither set of dependent variables can be explicitly eliminated at the differential equation level.

The Fluid-Structure Interaction problems occur in many natural phenomena and man-made engineering systems. In the area of natural phenomena, there is a wide range of FSI problems in biology and bio-medicine such as the study of the fluid structure interaction in the cardiovascular system in the human body (De Hart, Peters et al. 2003), and the FSI simulation of flapping elastic wings in birds and insects (Ruck and Oertel 2010). In the area of engineering, the study of FSI problems is important because it is crucial in the understanding of many engineering problems such as fatigue, material selection, effect on fluid flow and structural parameters. For example, FSI simulations are conducted to avoid flutter on turbo-machines and aircraft, to evaluate the dynamic response and the environmental loads of offshore structures (Raja 2012), and in the design of bio-medical devices.

Fluid Structure interaction is also an area of study in permanent evolution. This means that there are some FSI problems that have successfully been solved, but there are other types of problems that have not been solved, or they have partially been solved. Therefore, the research and engineering communities are implementing two different methodologies. The first one is the use of commercial programs that have developed FSI capabilities such as Ansys, ADINA, COMMSOL and CD-adapco (Raja 2012). The second methodology is the development of computational codes to solve specific problems of FSI analysis or for specific applications, these codes are developed in a wide range of programming languages like Matlab, or in open software platforms like OpenFoam (Ponweiser, Stadelmeyer et al. 2013).

The reason that explain the use of commercial software to solve FSI problems is that the technical progress in the fields of computational fluid dynamics (CFD), computational structure mechanics (CSM), and numerical algorithms have made the numerical FSI analysis more realistic to be performed in the commercial-industrial programs in a reasonable time frame (Sigrist and Garreau 2007). However, for some aspects of the FSI problems, the use of commercial-industrial programs for design purposes is still not possible or very limited. An example of these limitations is the non-linearity found in structural models that is not taken into consideration in numerical analysis carried out in industrial and commercial programs. This limits the possibility of simulating some cases such as extreme airplane

manoeuvres, in which significant deformation of the structures can occur (Roszak, Posadzy et al. 2009), and cases with the non-linearity of constitutive equation. The non-linearity is also of particular importance for biological flows such as the blood flow in the blood vessels (Guru and Chansup 1993).

In the area of aeronautics, the study of non-linearity behaviours like Limit Cycle Oscillations (LCOs), jump resonance, and period doubling, have become relevant because they could appear in aircraft or machines under specific conditions with potential negative results. For example, the presence of LCOs in wings could compromise the structural integrity of an airplane. FSI simulations are an option to study this kind of problems, in particular, industrial-commercial programs with FSI simulation capabilities have been used to analyse the non-linear aeroelastic behaviour obtaining reasonable accurate results despite the limitation that were mentioned before(Szabo and Kristof 2010) (Dowell, Edwards et al. 2003).

The modelling of turbulence in some aeroelastic problems seems to have a major importance. For example, simulations of flutter in wings and turbomachinery components have shown significant differences in the prediction of flutter boundaries that are attributed to the turbulence models used in the simulations (Chen, Wang et al. 2010). In addition, there is an interest on measuring the performance of turbulence models in FSI simulations, especially in the applications with turbulent flow, because these applications have a high relevance in real-world problems (Reimann, Ali et al. 2014).

Ansys 14.5, which is the software that is used in this study, has the capability of perform coupling analysis between different types of solvers. The typical combination of solvers for an FSI simulation in Ansys is the Transient Structural Solver to solve the mechanical stresses, and Fluent to solve the fluid dynamics. Force and mesh displacement are the variables that pass between the solvers. In addition, there are two types of analysis available, they are: one way co-simulation and two way co-simulation (Raja 2012). According with Tooley (2012), one-way co-simulation may pass force data to Ansys Mechanical, but no displacements pass back to Fluent. On the other hand, two-way simulation passes data in both directions.

A permanent task for the researchers is the validation of the programs with FSI capabilities to determine their strengths and limitations. The validation is usually carried out through

the comparison with reference test cases (Sigrist and Garreau 2007) whose solutions are known from experimental results, theoretical solutions or more accurate simulations.

For the two simulations that are proposed in this study there are experimental studies that can be used to validate the simulation results. For the ONERA M6 wing exists a complete experiment carried out by Schmitt and Charpin (1979). In the case of the Delta Wing, Korbahti, Kagambage et al. (2011) have carried out a complete set of experiments to define the dynamic response of a flexible delta wing in a low speed wind tunnel .

In addition to the experimental studies, there are other CFD simulations that match the experimental results and that could be used as reference. For instance, Slater (2008) simulated the ONERA M6 using WIND which is a programming code developed by NASA to perform CFD simulations. Elfeed and Kostic (2014) and Abobaker, Toumi et al. (2014) also have carried out CFD simulations of the ONERA M6 using Ansys

1.2 General Description of the Project

This project consists in perform FSI simulations in the program Ansys which is one of the leaders in FEM analysis. It is used in a wide range of industrial sectors and research areas. The purposes and methodology of this project are explained below.

1.2.1 Problem Statement

Determine the capabilities of the software Ansys-FLUENT to simulate the 2-way coupling between the Structures and the Aerodynamics, and the simulation parameters that produce the more reliable results for this kind of problems.

1.2.2 Methodology

The finite elements simulation is the tool that will be used in the project. Two Aeroelastic cases are analysed. Therefore, the chapters 3 to 7 are grouped in two parts which correspond to each case. The first case is a delta wing in a subsonic flow, the second case is a wing with the external shape of the Onera M6 wing in a transonic flow. In order to validate the

simulations, the results from Ansys are compared against a reference answer which could be experimental data, a theoretical answer or a simulation obtained in NASTRAN.

The process of simulation and validation in Ansys is repeated many times in order to identify the best combinations of simulation parameters and simulation techniques that produce the best results. This iterative process will focus on the changes of the parameters related with the type of coupling algorithm, the turbulence models and the ways to model the structure. These areas of analysis have been selected since previous simulations have shown that they are critical factors that affect the sensitivity of the results.

The package that is used to perform the CFD simulation in Ansys is FLUENT since it is one of the most developed packages to simulate fluids. Furthermore, it has the capability to be integrated in a FSI simulation.

This thesis is organized in 8 chapters. The chapters one and two cover the literature review and the theoretical background. Then, the content is divided in two parts. The first part is about the simulation of the delta wing and it covers the chapters three and four. The second part is about the simulation of the Onera M6 wing and it covers the chapters five, six and seven. Finally, the chapter 8 explains the conclusions and the future work in this topic.

Chapter 2

Theoretical Background

This chapter presents the theoretical frame work that provides the bases for the development of the FSI simulation models in Ansys-Fluent, especially, It presents all the topics that are related directly with the simulation that are presented in this thesis such as Nonlinear Aeroelasticity, basic concepts of Finite Element Models (FEM) and Computational Fluid Dynamics, turbulence models, theoretical approaches in FSI simulations and types of FSI algorithms.

2.1 Aeroelasticity

Aeroelasticity is a traditional aeronautics discipline that studies the interaction between inertial, elastic and aerodynamic forces than can occur when an elastic body is exposed to a fluid flow. Aeroelasticity involves two physical systems that interact with each other, they are: the fluid system, which is studied by the aerodynamics, and the structural system, which studied by the structural dynamics. This field of study is divided in two big branch: Static Aeroelasticity and Dynamic Aeroelasticity.

Static Aeroelasticity deals with static or steady response of an elastic Body to a fluid Flow. It studies problems such as Divergence and Control Reversal.
Dynamic Aeroelasticity deals with elastic structures that presents considerable motion in a fluid flow. Usually, this motion takes the form of vibrations. It studies problems like Flutter, Buffeting, Effects of Gust, and Transonic Aeroelasticity.

2.1.1 Linear Aeroelasticty

Another aspect that must be take into account in the analysis or Aeroelastic problems is the presence of linear and nonlinear effects because it determines the type phenomena that the aeroelasticity model is able to handle. The static and dynamic aeroelastic problems can be either, linear or nonlinear.

Linear Aeroelasticity is based in classical theories that assume linear aerodynamics and linear structural analysis. For instance, in the case of the structural model, the classical theory assumes that the displacement is linearly proportional to the applied forces. In the case of the Aerodynamic model, the classical theory assumes that the lift is linearly proportional to the angle of attack. Authors like Dowell, Edwards et al. (2003) and Castelló, Preidikman et al. (2014) consider that a wholly linear aeroelastic model is composed of wholly linear structural and aerodynamic models.

For many years the traditional approach has been successful in providing approximate calculations of aircraft response to external excitations, gust, and turbulence. The flutter boundaries are usually predicted accurately when compared to wind tunnel experiments or flight test results, but failed when airspeed grows to transonic regime or high supersonic regime because linear Aerodynamics fails to provide accurate results. For instance, it fails in the detection of transonic dips (Lee, Price et al. 1999). Furthermore, flow separation and shock oscillations introduce phenomena that classical aeroelasticity is not able to calculate. For example, Limit Cycle Oscillations (LCOs)

2.1.2 Nonlinear Aeroelasticity

In contrast to linear aeroelasticity, nonlinear aeroelasticity takes into account the nonlinearities in the aerodynamics or structural models and it is able to describe properly a wide range of aeroelastic behaviours such as: Limit Cycle Oscillations (LCOs), harmonic

and subharmonic resonances, jump resonance, beating (due to linear or non-linear coupling), and period doubling(Dowell, Edwards et al. 2003).

There are several sources of non-linearity in either, the Aerodynamic flow or the elastic structure. Some of them are described below (Dowell and Tang 2002).

The physical sources of nonlinearity in elastic structure include:

- The presence of dry friction, or nonlinear damping that comes from structural components in sliding contact.
- geometric nonlinearity or strain displacement, which comprise the nonlinear stiffness that comes from big displacement gradients
- bilinear stiffness , or free play arising from loosely connected structural Components

The physical sources of nonlinearity in aerodynamic flow include

- Flow separation, which is common at high angles of attack and transonic flow (it also could be induced by shock).

- The presence of shock motions in transonic flow, which are especially significant for low, reduced frequencies.

2.1.3 Limit Cycle Oscillations (LCOs)

LCOs is a finite amplitude steady state oscillation. As described before, it is one of the possible response behaviour of nonlinear aeroelasticity. The LCOs have been observed in wind tunnel models and operational Aircraft (Castelló, Preidikman et al. 2014).

There are two possible main consequences of any non-linear effect. One is that the rapidly growing oscillations calculated by lineal models are reduced due to the nonlinear effects, which could result in the occurrence of LCOs. From this point of view, LCOs could be considered as benign effect since it reduces the amplitude of oscillations that otherwise could increase permanently. However, if the amplitudes of the oscillations are too large, the structural integrity may be compromised. The second main consequence could be considered

detrimental since, in this situation, a system that may be stable to a sufficiently small perturbation can become unstable due to a large disturbance (Dowell and Tang 2002).

2.2 Structural Dynamics

The loads acting on a structural can be of two types. The first type is the static load which does not change in time, and the second type is the dynamic load which varies in time. The structural analysis for static loads only takes into account the stiffness of the structural components. In contrast, the dynamic structural analysis must take into account the effects of the mass, the acceleration and damping of the structure, in addition to its stiffness.

The structural dynamic analysis is based on the equation 2.1. In this equation, **M** is the structural mass matrix, **C** is the structural damping matrix, **K** is the structural stiffness matrix, **p** is a force vector that represents the external forces that applied on the structure, and u is a displacement vector, being $\dot{u}$ and $\ddot{u}$ the corresponding velocity and acceleration vectors. Equation 2.1 is a differential equation where p(t) is function of time that is usually known, and u is an unknown function that satisfies the differential equation.

$$M\ddot{u} + C\dot{u} + Ku = p(t) \tag{2.1}$$

In equation 2.1, u is a vector whose size is determined by the number of degrees of freedom (DOFs) of the structure.

2.3 Finite Elements Method

The finite elements method (FEM) is a numerical technique that allows to solve complex physical problems that are modelled by a set of differential equations that are geometrically difficult, or even impossible to solve through analytic methods. The FEM method can find an approximate solution to the differential equation system, the basic principle of this method is to divide the volume of a structure or system in to smaller (finite) elements such that infinite number of DOFs is converted to a finite value.

The finite elements method is currently applied to a wide range of physical systems. The implementation of FEM in a specific physical system depends on the assumptions and the type of problem that is intended to solve. For example, in the case of structural systems,

there are linear and nonlinear problems, as well as different types of solvers such as buckling or static solvers.

In this thesis, The FEM method is applied to structural systems and the fluid systems. In the field of the structural system, the problem of interest is the dynamic response of the structure. To solve equation 2.1, the FEM method applies a sequence of steps that is described as follows (Raja 2012).

- Conversion of a structure into a system of finite elements which are interconnected at the nodes and defining the DOFs at these nodes. The number DOFs for the whole system is defined as the multiplication of the number of nodes by the number of DOFs of each node. For three dimensional systems, the FEA could have millions of elements and nodes. This process of discretization is called meshing.

  During this process, the relations between the local DOFs of each element and the Global DOFs of the global matrices are defined. This process is called connectivity and it allows the construction of the transformation Matrix and the Global Matrices.

- Calculation of element mass matrix, the element stiffness matrix, and the element force vector for each element in a mesh with reference to the DOF for the element. The force –displacement relation and inertia force- acceleration relation for each element can be written as.

$$(f_I) = M_e \ddot{u}_e$$
$$(fs)_e = K_e u_e \qquad (2.2)$$

  Where M_e is the element mass matrix, K_e is the element stiffness matrix, $\ddot{u}_e$ and u_e are the acceleration and the displacement vector for the element, respectively.

- Construction of transformation matrix (Boolean matrix contains zeros and ones) that relates the values of each element into the global finite element assemblage. It just locates the elements of M_e, K_e and u_e at the proper places of the global matrices.
- Calculation of the values of element mass matrix M_e, element stiffness matrix K_e and element force vector $p_e(t)$. They are determined by a function called element shape function or interpolation function. These interpolation functions depend on the type of element that is used to do the meshing.

- Assembly of global element mass matrix, global element stiffness matrix and Global force vector. The formation of these global matrices is based on the matrices of each element, the transformation matrices and the connectivity.
- Imposing boundary and initial conditions that usually correspond to known values of some physical dimension such as displacements or relation between displacements. The mathematical effect of this process is the simplification of the systems of equations through the elimination of variables and equations which in turns allows the solution of the mathematical problem.
- The final equation system of motion with the global matrices is formulated as in the form of basic governing equation. This equation can be solved for using an appropriate iteration schemes which gives the response of the system in terms of u which is the vector of nodal displacement values.

2.4 Modal analysis

When a solid body, such as a metallic structure, is deformed elastically and suddenly released, it has a tendency to vibrate about its equilibrium position. This vibration, that is produced by the restoring strain energy, is called free vibration (Chandrupatla, Belegundu et al. 1997). The motion of vibration is mainly characterized by two physical properties, which are the amplitude and the frequency. The amplitude is displacement from the equilibrium position. The frequency is number of cycles per unit time and it is usually measured in Hertz (Hz).

In the majority of physical environments, the vibrations diminish with time due to damping action. In the simplest vibration model, the damping effects are ignored, which means that the matrix C in the equation 2.1 is equal to zero, thus the term $C\dot{u}$ disappears. The undamped free vibration model of a structure gives important information about its dynamic behaviour such as the natural frequencies, which are necessary to calculate the modes of motion in a modal analysis.

Modal analysis is often used to define the vibrational characteristics of an Engineering structure. The vibrational characteristics such as mode shapes and natural frequencies are essential in the design of a structure that supports dynamic load. It can be considered as a starting point for a transient dynamic analysis. In addition, the response of a structure can be

assessed when these modes are excited (Raja 2012). The fundamental equation used in undamped modal analysis is the classical eigenvalue problem which is described by the equation 2.3.

$$K\varphi_i = \omega_n{}^2 m\varphi_i \qquad (2.3)$$

The term ω_n is the natural frequency of the mode *i* and the term φ_i is a mode shape vector (eigenvector) of the mode *i.*

It is important to note that if the frequency of the dynamic load that is applied to the structure matches some of the values of the natural frequencies, the phenomenon known as resonance can occur, which means that the amplitude of the vibration becomes so large than in can compromise the structural integrity.

2.5 Computational Fluid Dynamics

Computational Fluid Dynamics (CFD) is the field of study that uses algorithms, mechanic of fluids and numerical analysis to solve problems that involves fluid flows. The techniques developed in CFD have been implemented through industrial and commercial programs which allows to solve a wide range of problems. Other form of implementation has been programming codes which often are developed and used by researchers to solve specialized problems.

CFD techniques carry out two important task that are necessary to find a numerical solution of a fluid flow, the first task is the discretization of the governing equations. The second task is the discretization of the volume that is occupied by the flow which is also called geometrical domain or flow domain.

Transport Phenomena and fluid flow are governed by basic conservation principles which are defined by the fluid model. These conservation principles can be described in terms of differential equations that are called governing equations (Raja 2012). The fluid models are defined to describe properly the behaviour of the type of fluid flow that will be analysed. The type of fluid in turns depends of the problem of phenomena. For example, for subsonic flows the fluid model is assumed as incompressible, while for supersonic flows the fluid model is assumed compressible.

The governing equations and the geometrical domain can be discretized, then, different types of algorithms can be applied to find the numerical solution of the fluid flow.

This section explains the basic aspects of the CFD techniques.

2.5.1 Governing Equations.

The governing equations of fluid flow comprises the conservation of mass and momentum.

The conservation of mass is expressed in the continuity equation (conservation of mass) that can be expressed as (Kesti and Olsson 2014)

$$\frac{d\rho}{dt} + \rho \frac{\partial v_i}{\partial x_i} = 0 \tag{2.4}$$

The conservation of momentum can be expressed through the Navier-Stoke equations. In the general case, these equations are a set of partial differential equations with four major characteristics, they are nonlinear, unsteady, and include the effect of the viscosity and the compressibility. The next equation is the expression of the Navier-Stokes equations in tensor notation, which is one of the several ways to express these equations. In this equation μ is viscosity and ρ is density.

$$\rho \frac{Du_i}{Dt} = -\frac{\partial p}{\partial x_i} + \mu \frac{\partial^2 u_i}{\partial x_i^{\,2}} \tag{2.5}$$

It is important to note that the complete Navier-Stokes equations do not have analytical solution. However, each fluid model introduces simplifications that allow the solution of these equations.

It is also important to point out that in some problems, the continuity equation and the Navier-Stokes equations are not enough to describe the behaviour of the fluid flow. In some cases it is necessary the energy balance equation and the equation of state (NASA 2014).

2.5.2 Finite volume method

Commercial CFD programs have implemented multiple discretization techniques to solve the governing equations such as Finite Volume Method, Finite element method, spectral element method, boundary element method, and Finite difference method (Joaquim Peiro). Here, only the Finite Volume method is described because it is the method that has been implemented in Ansys-Fluent.

The basic and foremost step of CFD is dividing the geometric into multiple smaller regions called control volumes or cells, the collection of these cells is called a grid or a mesh. Then, the governing equations are recast in a conservative form, and solved over the mesh. This discretization guarantees the conservation of fluxes through a particular control volume. Ansys-Fluent uses the finite volume technique to convert the general transport equation into a system of algebraic equations and it uses different iterative methods to solve the algebraic equations(Raja 2012).

The steps of the finite volume method are as follows (Raja 2012).

- Partition of geometry into control volumes using a computational mesh.
- Integration of the governing equations of fluid over grid.
- Discretization – transformation of the resulting integral equations in to a system of algebraic equations.
- Calculation of a solution to the system of algebraic equations by an iterative method.

2.5.3 Turbulence

Turbulence or turbulent flow is a flow regime characterized by considerable seemingly random motion which creates chaotic changes in the fluid properties including high momentum convection, low momentum diffusion, and a rapid variation of pressure and flow velocity in time and space. The velocity fluctuation exists both along the main direction of the flow and perpendicular to it. As a consequence of the perpendicular fluctuation, there are appreciable transports of mass between adjacent layers (Houghton, Carpenter et al. 2012).

2.5.3.1 Turbulent Flow Simulation Approaches

There are three basic approaches that can be used to calculate a turbulent flow. These approaches are also used to simulate the turbulence effects. The three methods are explained as follow.

- **Direct numerical simulations (DNS)**

  In this method, the appropriate equations are solved on a computer without making any approximation. This means that DNS solves numerically the full unsteady Navier-Stokes equations, it also resolves the whole spectrum of scales, therefore, no modelling is required. However its main disadvantage is that the computations cost is prohibitive, which make it not practical for industrial applications. In fact, this method is not available in Ansys –Fluent (ANSYS 2010)

- **Large Eddy Simulation (LES)**

  This method solves the spatially averaged Navier-Stokes equations. It directly solves the large scales (large eddies), but scales smaller than the mesh are modelled. Although it is less expensive than DNS, the amount of computational resources is still very large. Therefore, this method is not practical for the majority of industrial applications.

  The main advantage of LES is its potential for improved accuracy when the resolution of the largest eddies is important or when unsteady data is needed.

  Apart from its high computational cost, LES also has other disadvantages such as, the necessity of higher grid resolution, long run times and large volume of data in unsteady simulations due to the small time steps. In addition, it is an inherently unsteady method (Eggenspieler 2012).

- **Reynolds-Averaged Navier-Stokes (RANS) models**

  This method solves the time-averaged Navier-Stokes equations. In contrast with DNS and LES, All turbulent length scales are modelled in RANS. In addition, steady state solutions are possible with this method.

The main advantages of RANS is that, for many applications, steady state solutions are preferable. In addition, for the majority of industrial problems, a good RANS model with a good quality grid will provide all the required accuracy. Another significant advantage is that many different variations of the model are available in this method.

The main disadvantages of RANS is that, in some cases, challenges associated with RANS modelling can limit the level of accuracy that it is possible to attain

All the characteristics of the RANS method have made it one of the most used methods in the industry. It is available in multiple CFD commercial programs including Ansys-Fluent (Eggenspieler 2012).

2.5.3.2 Main RANS Models

As mentioned before, there are multiple models available in the RANS method. However, as it is illustrated in the figure 2.1, around 2/3 of all simulation reported use some variation of 1 or 2 equation model, which mean that they use the k-epsilon family or the k-omega family.

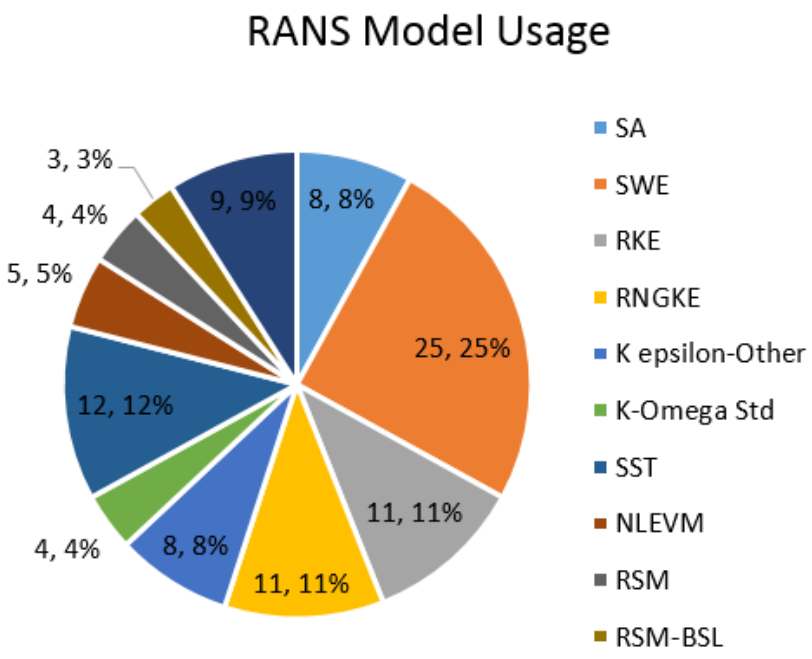

Figure 2. 1: RANS model usage (Eggenspieler 2012)

The relevant RANS models that were used in this thesis are described below.

2.5.3.2.1 k–epsilon Models

The k-epsilon model solves for two variables: epsilon (ε); the rate of dissipation of kinetic energy, and k; the turbulent kinetic energy. Wall functions are used in this model, so the flow in the buffer region is not simulated (Frei 2013).

There are different variation of the k-epsilon model, two of them are mentioned here.

Standard k-Epsilon

The Standard k-epsilon model (SKE) is the most widely-used engineering turbulence model for industrial applications, it contains submodels for compressibility, buoyancy, combustion etc. It also is characterized by its robustness and reasonably accuracy for a wide range of applications (ANSYS 2010). The Model parameters are calibrated by using data from a number of experiments of reference like pipe flow, flat plate etc.

However, this model also has some limitation such as: Inaccurate prediction of the spreading rate of round jets, poor performance in the simulation of flows with strong separation , larger pressure gradient, large streamline curvature, and high swirling component (ANSYS 2006), inaccurate model predictions that can result from excessive production of k in regions with large strain rate (for example, near a stagnation point).

Realizable k-epsilon

This model is often preferred to Standard k-epsilon. Realizable k-epsilon implements changes that allow certain mathematical constraints to be obeyed which eventually increases the performance of this model (ANSYS 2006). Another characteristic is that several realizability conditions are enforced for Reynolds stresses.

The main advantages that this method can offer are the high accuracy in the predictions of the spreading rate of both round and planar jets, and the superior performance in comparison with the k-epsilon model for flows involving boundary layers under strong adverse pressure gradients, recirculation, rotation, and separation (ANSYS 2010).

2.5.3.2.2 k-omega Models

In the k-omega model, the transport equation for the turbulent dissipation rate, ε (epsilon), is replaced with an equation for the specific dissipation rate, ω (omega). However, The turbulent kinetic energy transport equation is still solved (ANSYS 2006) .

Standard k–omega

The Standard k–omega is a two-transport-equation model solving for k and ω. It has options for modelling compressible flows and transitional, free shear.

This model is suitable for complex boundary layer flows under adverse pressure gradient and separation is present (turbomachinery and external aerodynamics) (ANSYS 2010). It also has superior performance for wall-bounded boundary layer, free shear, and low Reynolds number flows. In addition it can be used for transitional flows (although tends to predict early transition). Separation is typically predicted to be excessive and early.

SST k–omega

The SST k–omega model combines the standard k–epsilon model for use away from walls using a blending function, and the original Wilcox model for use close to walls. In addition, it limits turbulent viscosity to guarantee that $\tau_T \sim k$ (ANSYS 2006). The shearing and transition options are taken from standard k–omega. This model does not have options to include compressibility.

This model has comparable benefits as standard k–ω. However, dependency on wall distance makes this less suitable for free shear flows.

2.6 Fluid Structure Interaction

In all applications in FSI exist an interface surface between the fluid and the solid domain. At this interface surface, both the boundary conditions and the governing equations from the Fluid and solid domain have to be satisfied simultaneously. This interface is also useful to Transfer the quantities form one solver to the other.

2.6.1 Types of Approach

The programs with capabilities to solve FSI problems have implemented two different approaches for the numerical discretization, especially at interface surface. These approach are called the monolithic approach and the partitioned approach.

In the monolithic approach, also called fully coupled, the problems in both sub systems (structure and fluid) are formulated as one combined problem (Kesti and Olsson 2014). Therefore, the governing equations of the fluid and structure are solved together. This requires a conformal mesh with matching nodal position between the solid and fluid meshes. This approach is very robust and it offers a better stability of the solution, but it requires a fully integrated solver that is computationally expensive and cannot take advantage of the modularity as the partitioned method does.

In the partitioned approach (also called staggered) the fluid and the structure systems can be solved using separate solvers, in sequential order. This means that the flow does not change while the structural solution is calculated (Raja 2012). The intermediate fluid solution is prescribed as a boundary condition for the structure and vice versa, and the iteration continues until the convergence criterion is satisfied. In addition, the mesh does not need to be conformal, which signifies that nodal positions do not need to be matched. This approach is a very efficient and fast way of solving FSI problems. However, convergence problems are more frequent than for a monolithic approach.

2.6.2 One-way and two-way coupling

In one-way coupling, transfer quantities are sent from one solver to the other, but not in the opposite direction (Kesti and Olsson 2014). This coupling is used when one domain has an important effect in the other domain, but not the opposite. For example, the Fluid flow in a pipeline can affect significantly the stresses in the pipeline but the deformation in the pipeline does not affect significantly the fluid flow. In this case the one-way coupling method is usually a good approximation because there are not large deformations in the pipeline. The figure 2.2 illustrates the Flow chart of the one-way coupling. Initially, the fluid flow calculation is performed until convergence is reached. Next the resulting fluid pressures or forces at the interface from fluid calculation are interpolated to the structural mesh. Then, the structural dynamic calculations are performed until the convergence criterion is met. This is repeated until the end time is reached.

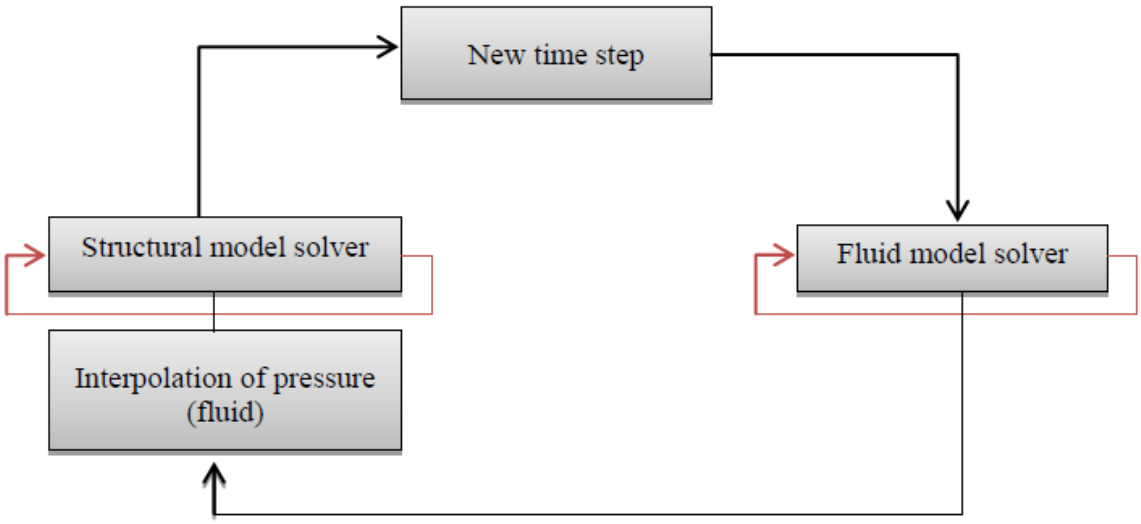

Figure 2. 2 Flow chart of the algorithm for One-way coupling (Raja 2012)

In the two way coupling, the solver data is always transferred both ways between the two systems. This type of coupling is applied to the problem where the motion of a fluid affects significantly a solid structure and at the same time the fluid flow is influenced by the reaction of the solid structure (Raja 2012). For example, fluid pressure is transferred to the solid solver. Then, using the pressure from the fluid as and external load, the resulting displacement of the structure is transferred back to the fluid solver. This process is repeated until both pressure (force) and displacement values are converged below a predetermined limit. The figure 2.3 shows the flow chart of the algorithm for the two-way coupling.

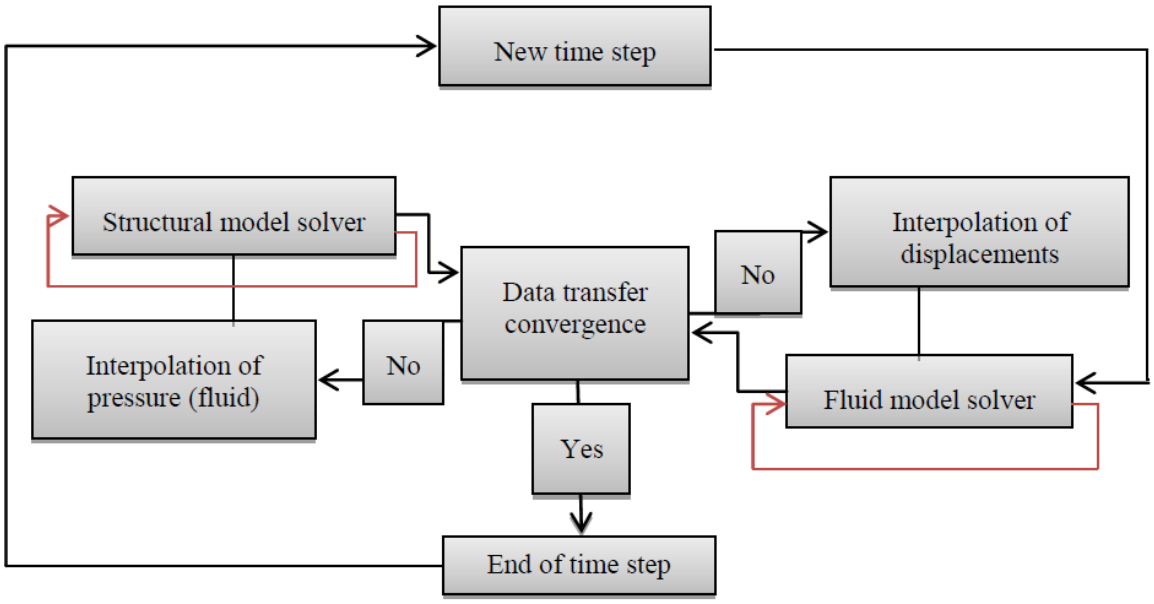

Figure 2. 3: Flow chart of the algorithm for Two-way coupling (Raja 2012)

The figure 2.4 illustrates the relation between the types of approaches and the types of coupling. It can be appreciated that one-way coupling and two-way coupling are methods that only can be applied with the partitioned approach.

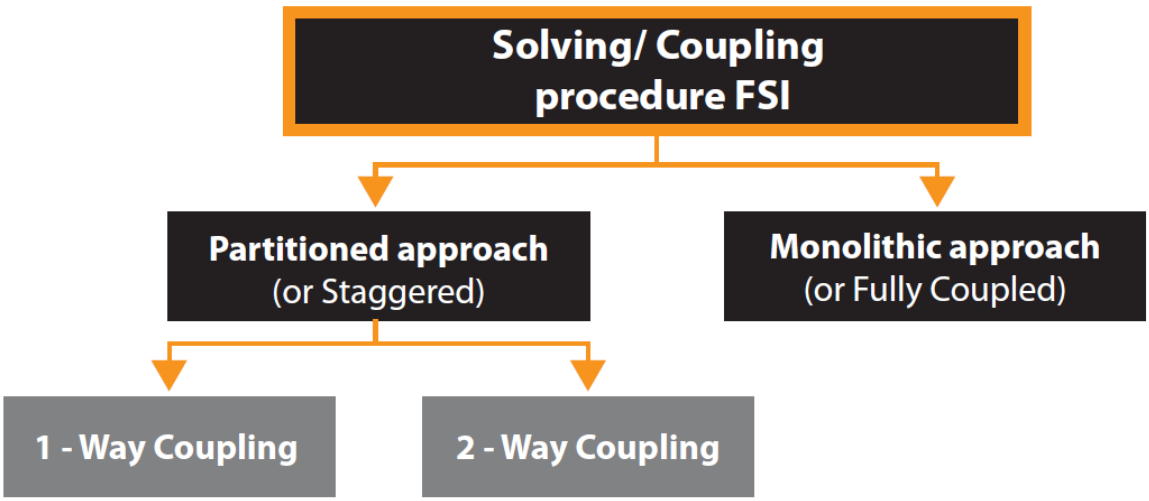

Figure 2. 4: Relation between approaches and coupling methods (Kesti and Olsson 2014)

2.7 Flutter Solution Techniques

There are different methods to solve problems of Aeroelasticity, one of them is the application of FSI methods that were described before. This section present other methods that are widely used to solve Aeroelastic problems, specially, flutter problems. These techniques are relevant in this project because they are the base of the simulation carried out in Patran-Nastran that is presented in the chapter 7.

2.7.1 Vortex Lattice Method (VLM)

The Vortex Lattice Method is widely used in the aerospace industry for aerodynamic estimates in conceptual design and preliminary design predictions. The VLM provides good insight into the aerodynamics of wings. It is based on the theory of Potential flow and its main theoretical assumptions are explained as follows.

- The lifting surfaces are thin. Therefore, the influence of thickness on aerodynamic forces are neglected.

- The flow field is irrotational, inviscid and incompressible. However, small-disturbance can be included in the model

- The angle of sideslip and the angle of attack are both small. Therefore, small angle approximation is used.

The VLM consists in modelling the wing as a set of lifting panels. Each panel will contain a single horse-shoe vortex. A bound vortex is located at the panel 1/4 chord position with two trailing vortex lines shed from each end. Both span-wise and chord-wise variation in lift can be modelled as a set of step changes from one panel to the next (USYD 2015).

The steps to implement of the VLM are described below (Tech 1998). The implementation is shown in the figure 2.5

1. Split the platform up into a lattice of quadrilateral panels, and place a horse-shoe vortex on each panel.

2. Set the bound vortex of the horseshoe vortex on the 1/4 chord element line of each panel.

3. Set the control point on the 3/4 chord point of each panel at the midpoint in the spanwise direction, sometimes the lateral panel centroid location is used.

4. Assume a flat wake.

5. Determine the strengths of each horse-show vortex required to satisfy the boundary conditions by solving a system of linear equations.

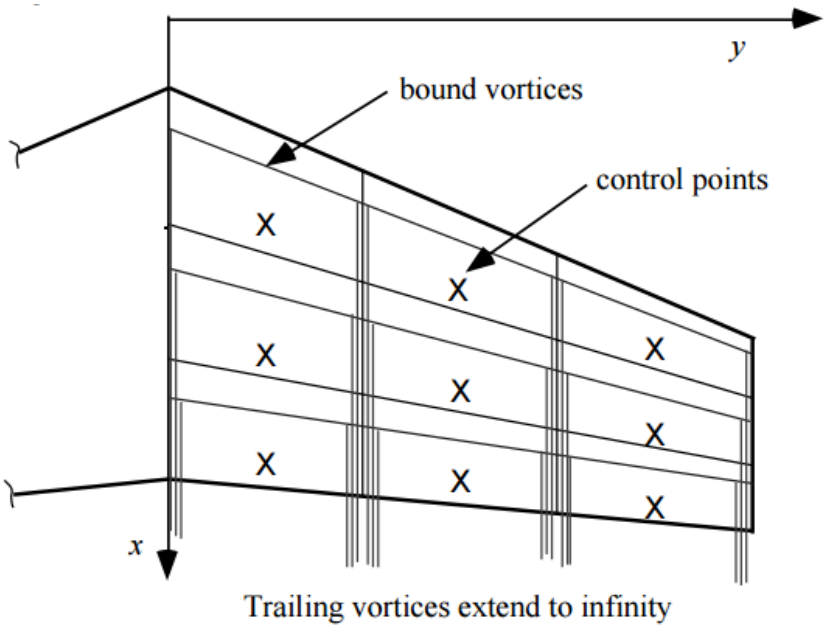

Figure 2. 5 The horseshoe vortex for the Vortice-lattice method (Tech 1998)

The method that is applied in the chapter 7 to calculate the aerodynamics in Nastran is known as Doublet-Lattice Subsonic Lifting Surface Theory (DLM) which is an extension of the steady VLM to unsteady flow. This method is obtained when the vortex is augmented with an oscillating doublet. DLM is widely used in the Industry for subsonic flutter calculations.

2.7.2 Infinite Plate Spline

In the solution of Aeroelasticity problems like flutter, the aerodynamic model has to interact with the structure. To do this, aerodynamic and structural grids are connected by interpolation. This permits the independent selection of grid points of the aerodynamic elements and the structure elements in a manner appropriate to the specific theory (MSC.Software 2009). In the particular case of a wing, the structural model can involve an array of grid points. The aerodynamic theory may be a strip theory or a lifting surface theory. The interpolation method is also called splining, in the case of the simulation developed in the chapter 7, the method applied is denominated Infinite Plate Spline or Surface Spline.

A surface spline is a mathematical method used to calculate a surface function, $w(x, y)$,for all points *(x,y)* when w is known for a discrete set of points, $w_i = w(x_i, y_i)$. The method defines an infinite plate and then it solves for the plate deflections, given its deflections at some known points; in other words, it is the problem of a plate with multiple deflecting supports. The surface spline is a smooth continuous function that will become almost linear

in *y* and *x* at great distances from the points (x_i,y_i). The deflection of the plate is calculated as the sum of deflections due to a set of point loads on the infinite plate(MSC.Software 2009).

2.7.3 PK Method to solve Flutter

Flutter problem can be solved in any airspeed regime through the selection of the suitable aerodynamic theory. In the lineal case assumed by the program Nastran (MSC.Software 2009), the solution takes into account a set of complex eigenvalue solutions; the eigenvalue problem to be solved is determined by the way in which the aerodynamic loads are incorporated in the equations of motion or whether certain damping terms are taken into account.

One of the methods to solve the flutter problem is called "the British Method". It includes the aerodynamic loads into the equations of motion as damping terms and frequency dependent stiffness. In this method it should be observed that the aerodynamic terms are slowly varying functions of the reduced frequency. PK method is a variation of the British method in which the aerodynamic loads are treated as complex springs (MSC.Software 2009). The PK method is applied in the simulation carried out in Nastran that is described in the chapter 7.

The principal advantage of the PK-method is that it produces results directly for given values of velocity. In addition, the damping given by this method is a more realistic estimate of the physical damping than the parameters given by other methods that are only a mathematical artifice without physical interpretation.

PART 1

DELTA WING

Chapter 3

Pre-processing of FSI Simulation

This chapter presents the pre-processing of the FSI simulation of a Delta Wing. Different cases are described as well as the details about the geometry and the configuration of the solvers that participated in the FSI simulation. This chapter focus especially in the setup of the most relevant steps to get a successful FSI simulation for this kind of structures.

3.1 Background of the Delta Wing Design

The delta wing that was studied correspond to an experiment that was carried out in the wind tunnel of the University of Liege in order to investigate its dynamic response (Korbahti, Kagambage et al. 2011). The Wind Tunnel is a closed loop subsonic wind tunnel with two working sections. The Delta Wing was tested in the aeronautical section whose measures are 5m x 15m x 2 m (length x height x width), the maximum airspeed of the wind tunnel is 60 km/h in this section. It was mounted in a turntable that provides the possibility of rotate the wing at different angles of attack.

The delta wing was placed at multiple different steady angles of attack in the range from 0^{o} to 10^{o}. The Airspeed in the experiment was varied between 5 to 40 m/s.

A hammer Testing was also carried out in the same University, the results of this experiment were the modal frequencies for modes 1 – 8 (Korbahti, Kagambage et al. 2011).

3.2 Geometry of Delta Wing

The geometry of the delta wing is illustrated in figure 3.1. The wing has a constant thickness of 1 mm and it is completely clamped at its root through screws. In addition, two accelerometers were installed in the position a_1 and a_2 to sense the oscillation of the wing.

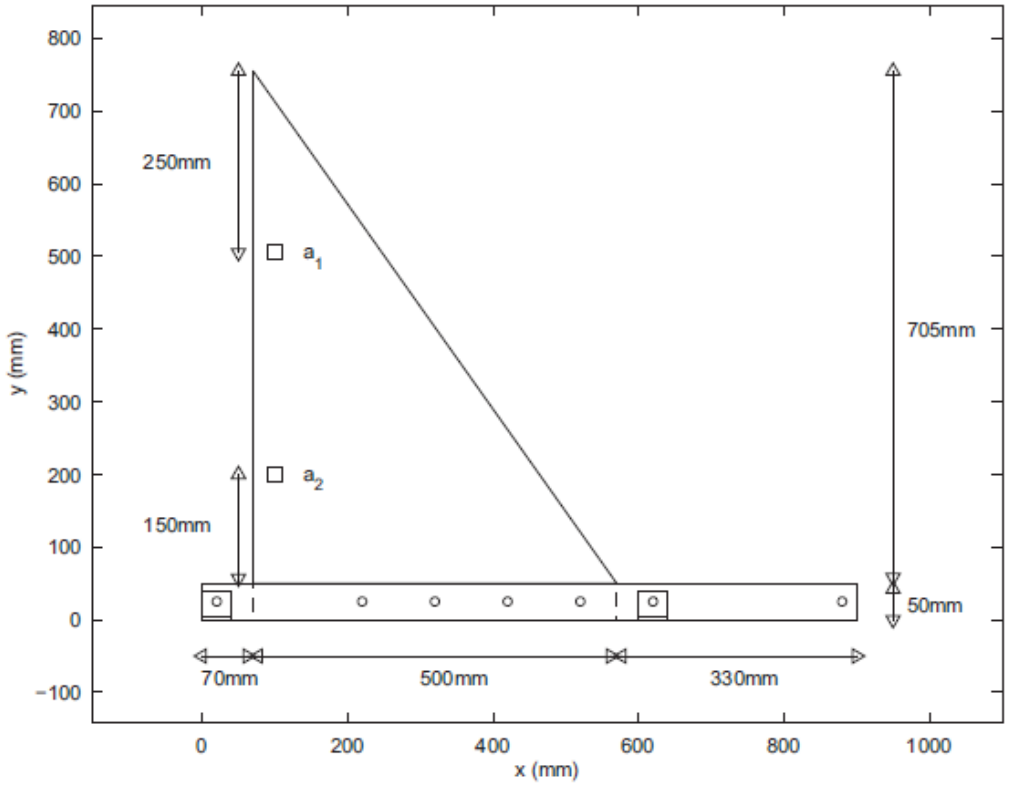

Figure 3. 1: Drawing of the Delta Wing and support. (Korbahti, Kagambage et al. 2011)

The figure 3.2 illustrates the system to attach the wing in the wind tunnel, the base of the wing was clamped between two wooden blocks that were bolted together and screwed solidly to the wind tunnel's turntable. Consequently, the wing was completely clamped at its root. It can be observed in the figure 3.1 that the wooden blocks have a height of 50 mm.

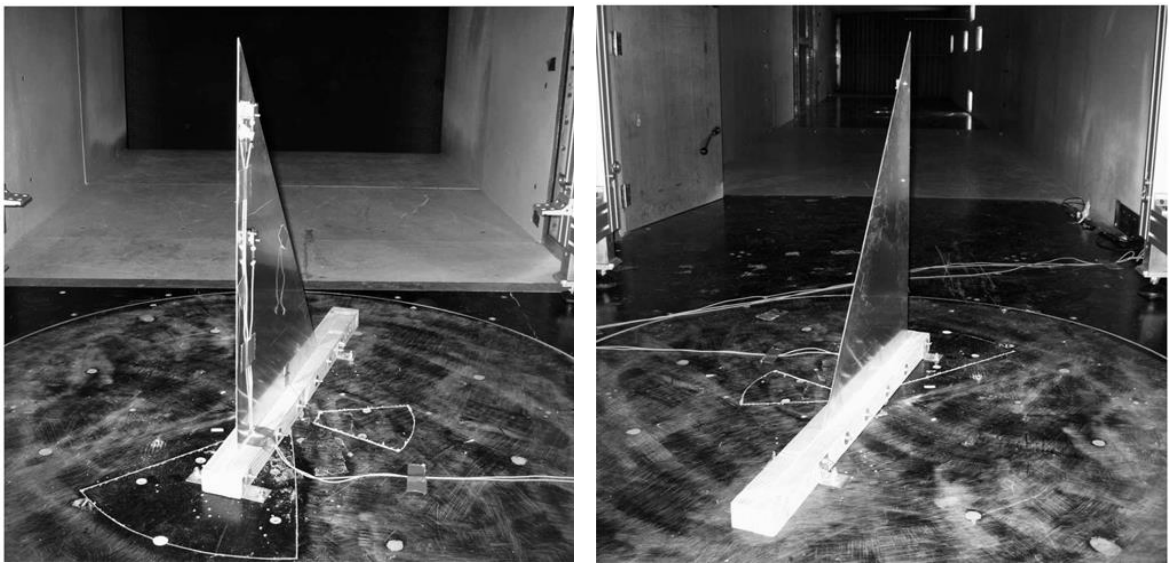

a) b)

Figure 3. 2 :Delta Wing in Wind Tunnel: a) Rear View b) Front view (Korbahti, Kagambage et al. 2011)

3.3 Modal Analysis

A modal Analysis of the Delta Wing was carried out in Ansys. The objectives of this Analysis were the validation of the accuracy of Ansys to calculate the natural frequencies, and the study of the effect of the mesh on the calculation of these frequencies. The results from the simulation were compared with the experimental results obtained by Korbahti, Kagambage et al. (2011).

The modal analysis in Ansys was carried out through the module 'Modal' of Ansys. A Boundary condition of fixed support was imposed in the root of the Delta wing to simulate the experimental conditions.

The table 3.1 shows the values of the natural frequency for the 8th first modes of vibration of the Delta Wing. The experimental and the simulation results for different element size in the mesh are also presented in this table.

It can be appreciated in the table 3.1 that the mesh has some effect in the calculation of the natural frequencies, when the size of the element decreases, which implies that the mesh density increases, the effect is the decrease of the natural frequencies. However, it can be observed that the natural frequencies converge around the frequency values of the element

size 0.006 m. It also can be observed that the results in Ansys match the experimental results in almost all the modes of vibration, the two modes that have a considerable difference with the experimental results are the third mode with around 22% of relative difference, and the eighth mode with around 12% of relative difference. Figure 3.3 illustrates the deformation pattern for the 1st mode with 0.006m as the maximum element size of the mesh.

Table 3. 1: Natural frequencies of the Delta Wing, all the frequencies are in Hz

Mode	Type	Frequency in the Experiment (Hz)	Frequencies in the Simulation: Modal Analysis			
			Maximum Element size of the mesh			
			0.01m	0.008m	0.006m	0.002m
1	1st bending	3.16	3.1727	3.1653	3.1613	3.16
2	2nd bending	12.71	13.302	13.214	13.185	13.175
3	1st torsion	23.43	19.061	18.87	18.784	18.766
4	3rd bending	30.31	32.79	32.456	32.294	32.252
5	2nd torsion	44.72	46.363	45.508	45.217	45.144
6	Bending-torsion	57.61	62.47	61.218	60.704	60.571
7	Bending-torsion	78.32	73.811	72.047	71.42	71.272
8	Bending-torsion	95.19	86.751	84.356	83.84	83.165

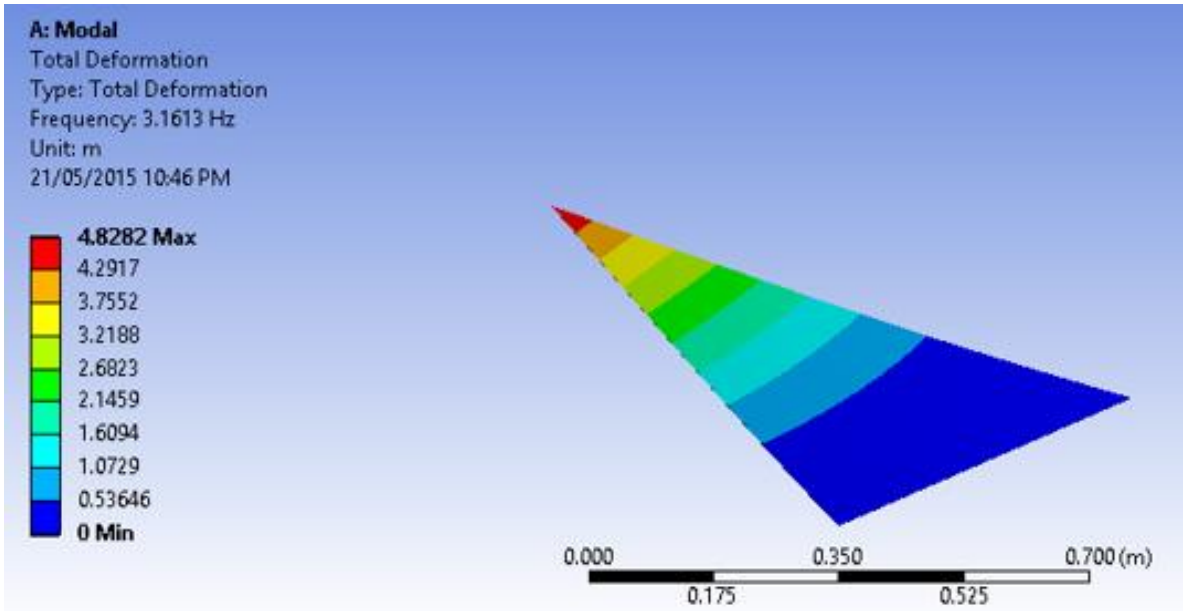

Figure 3. 3: Deformation pattern for the 1st mode with 0.006m as the maximum element size of the mesh.

3.4 FSI Simulation

The results of the experiments carried out revealed that the wing presents strong oscillations in the perpendicular direction to the fluid flow. In this case, the oscillation had a significant amplitude in which means that the deformation of the delta wing is also affecting the fluid flow. Therefore, the appropriate FSI model must be a 2-way coupling simulation. The figure 3.4 shows the general scheme of the FSI simulation applied to the delta wing.

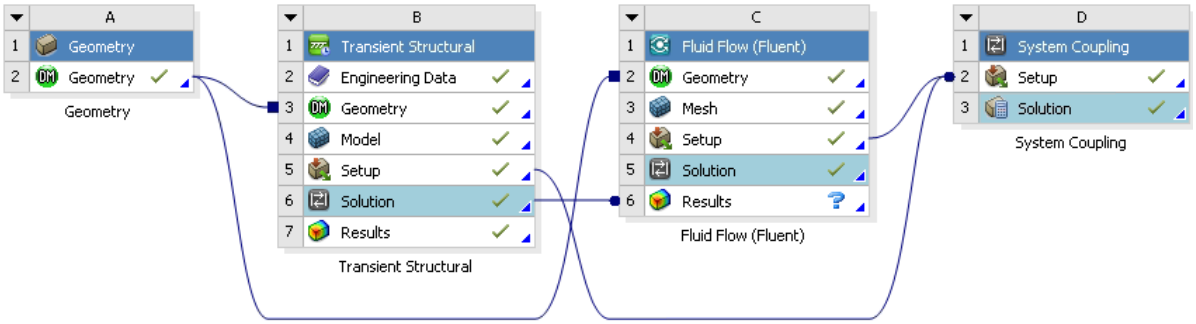

Figure 3. 4: Layout of the Delta Wing FSI simulation in Ansys-Workbench

The figure 3.4 shows that the simulation is composed by the following modules or components.

- **Geometry:** Independent module to model the Wing and the Geometrical domain.
- **Transient Structural :** This module is used to simulate the structural behaviour of the wing structure
- **Fluent:** This module is used to simulate the dynamic of the flow the geometrical domain.
- **System Coupling:** This module allows the coupling between the two solvers. Transient structural and Fluent.

It can be appreciated that each module is identified with a letter. In addition all the tabs are identified by a number. This is a cell system that allows to reference each tab through its cell position, for example the tab “model” in the module “Transient Structural” is the cell B4.

The configuration or each one of these components is explained below.

3.4.1 Geometry Module

The Geometry in FSI simulations has to include two volumes which corresponds to the volume of the structure and the volume of the fluid Domain. To model the geometry in Ansys was used an independent geometry module.

The delta wing was modelled in Solid Edge ST5 according with the specifications of figure 3.1. Figure 3.5 illustrates the dimensions that were considered to define the Geometrical domain. The width and the height of the Geometrical domain were determined by a factor of 11 times the wing chord length, this factor is used to avoid the aerodynamic effect of the geometrical domain walls in the wing. The dimensions of the fluid domain can be appreciated in the figure 3.5. In this figure, the dimensions are identified as F4, T5 and P3. The dimension F4 is 6,742.1 mm, the dimension T5 is 10,000 mm, the dimension P3 is 5,000 mm, and the depth is 2,200 mm.

The procedure to define completely the geometry in the geometric module had the following steps.

1. The Wing was modelled in Solid Edge ST5 and the file was saved on .IGES format.

2. The CAD model of the wing in .IGES format was imported into the DesigModeler module of Ansys which corresponds with the cell A2 in the figure 3.4.

3. The volume with the maximum dimensions of the geometrical domain (fluid domain) was extruded.

4. A Boolean operation was carried out to subtract the volume of the wing from the volume created in the third step. It is necessary to keep or not eliminate the solid bodies after the Boolean operation (subtract) because both solids, the geometrical domain volume and the wing volume, are necessary to perform the FSI simulation.

5. To perform the FSI simulation, it is necessary to define two named surfaces that will allow the coupling between the Transient structural module and the FLUENT module. These surfaces correspond with all the wing surfaces, except the root. They were named as “wall_cfd_coupled” and “wall_fea_coupled”.

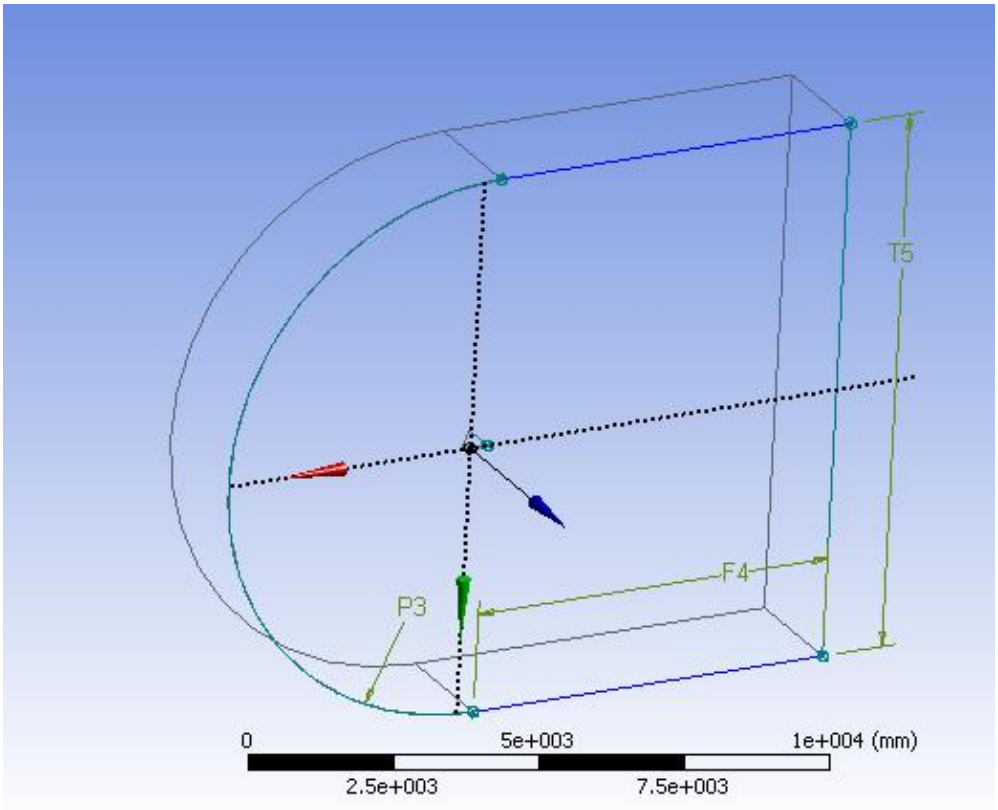

Figure 3. 5: Geometrical domain for the Delta wing

3.4.2 Transient Structural module

The Transient structural module takes the geometry of the wing from the geometry module. The material, which is Aluminium is assigned in the tab "Engineering Data"(cell B2 in the figure 3.4). Ansys has a set of materials defined by default, among them, the Aluminim Alloy NL was selected to be included into the library of materials, and its mechanical properties are described in table 3.2. In addition, this material was assigned to the delta wing geometry in the tab "Model" (cell B4 in the figure 3.4).

Table 3. 2: Mechanical Properties of Aluminium alloy NL

Mechanical Property	Value
Density	2,770 Kg/m^3
Young's Modulus	71 GPa
Poisson's Ratio	0.33
Shear Modulus	26.692 GPa

3.4.2.1 Mesh and Boundary Conditions

The tab 'model' opens the Mesh module of Ansys-Transient Structural. The Mesh for the wing structure is illustrated in the figure 3.6. It can be appreciated that there are two elements along the thickness, this arrangement allows to capture the deformation and stresses due to bending, it also can be appreciated that the leading edge was modified with a sharp edge in order to minimize some of the problems of having a blunt edge facing to the flow, such as the turbulence that a completely vertical wall would provoke in the flow. The mesh of the wing has 55,902 tetrahedral elements and 113,066 nodes. The Appendix A describes more details about the mesh such as the orthogonal quality and the skewness.

The boundary conditions for the structure are defined in this module. A fixed support in the wing root was defined to impose the clamped support of the delta wing as it can be observed in the figure 3.7.

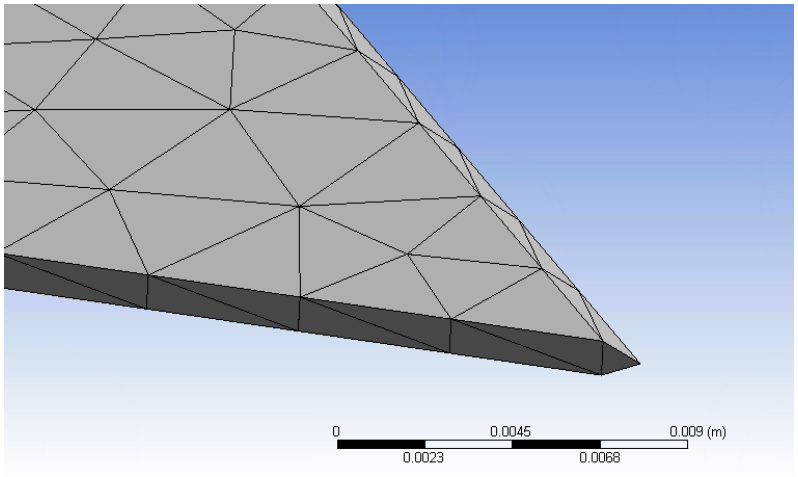

Figure 3. 6: Detail of the Delta Wing mesh

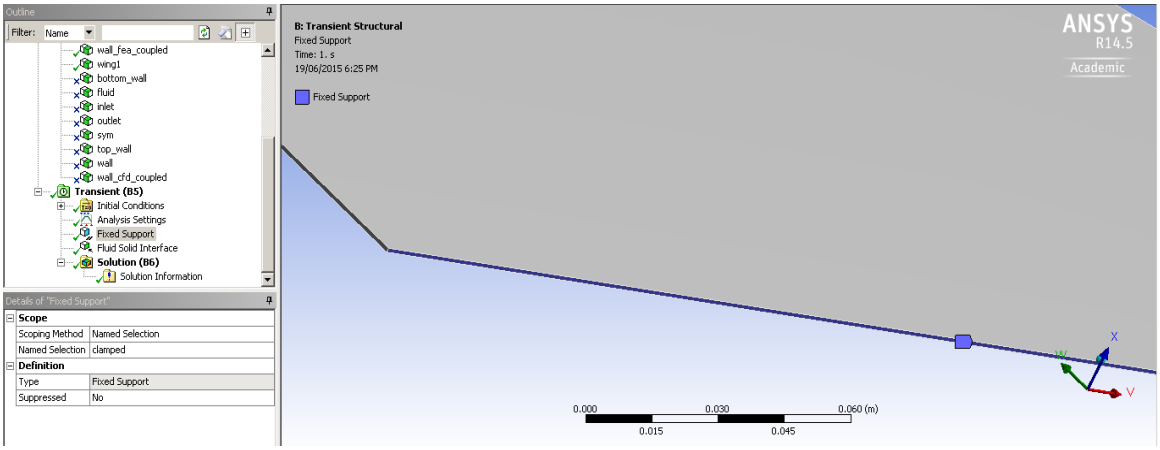

Figure 3. 7: Boundary condition in the delta wing. Fixed support in the base for this case.

3.4.2.2 Solver Configuration

The set-up tab in the Transient Structural Module (cell B5) allows the configuration of parameters for the coupling with the fluid system. The most important aspect in this stage is the definition of the Fluid Solid Interface. This surface is the wetted outer surface in contact with the fluid. System Coupling will map the forces from the CFD computation onto this surface, and transfer back the resulting deformation to Fluent (ANSYS 2013). In this case, the surface called "wall_fea_coupled" was selected to be the Fluid Solid Interface. Figure 3.8 illustrates a detail view of the "Wall_fea_coupled" surface around the leading edge , it can be observed that this surface is effectively the wetted area the delta wing, which means that it include all the surfaces of the wing except the wing root.

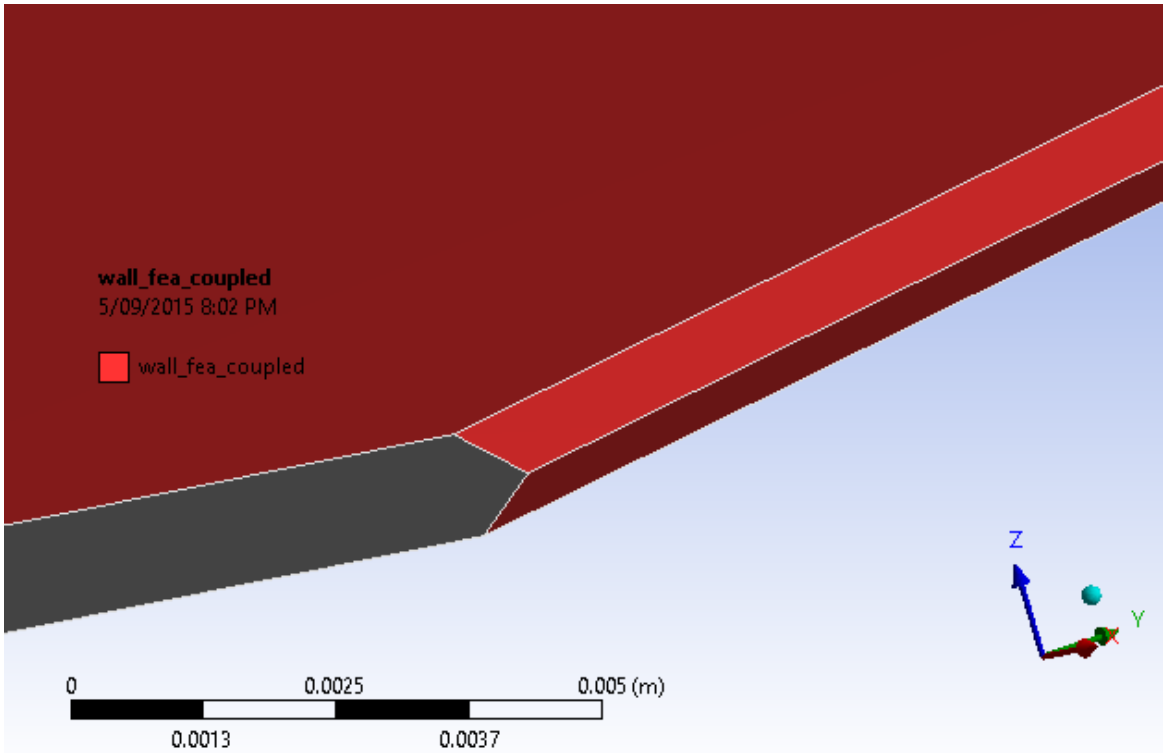

Figure 3. 8: Surface "Wall_fea_coupled".

3.4.3 Fluid Flow Module (Fluent)

Figure 3.4 shows a connection between the cell A2 and the cell C2. This connections means that the Fluent module (module C) takes the geometry of the Geometrical Domain from the Geometry module (module A).

3.4.3.1 Mesh

The mesh of the fluid domain was carried out in the meshing module of Ansys-Fluid Flow (Fluent) which is open through the cell C3 of the workbench space. The main principle that was followed in the mesh was the generation of a high density of elements in the proximity of the wing and low density of elements far away from the wing. In terms of the element size, this principle means small element size in the proximity of the wing and high element size far away from the wing. This principle was followed to reach two goals, the first one is to get a good accuracy of the flow over the wing surface, and the second one was to minimize the number of elements since this is a critical factor to reduce the computational work in the CFD simulation and the subsequent FSI simulation.

To achieve the goals that were mentioned before, six size functions were implemented over the faces of the geometrical domain, these size functions allowed to specify the element size on the six faces. Figure 3.9 illustrates the faces that were used to define the mesh, table 3.3 describes the size of the element that was used in each face, the faces over the wing (face A, B in figure 3.9 b) requires an small element size since it is desirable to obtain a good detail of the fluid flow over the wing.

Besides the size functions, a mesh inflation over the wing surface was implemented. The inflation was applied specifically to the named surface wall_fea coupled which was used as the coupling surface in a subsequent step.

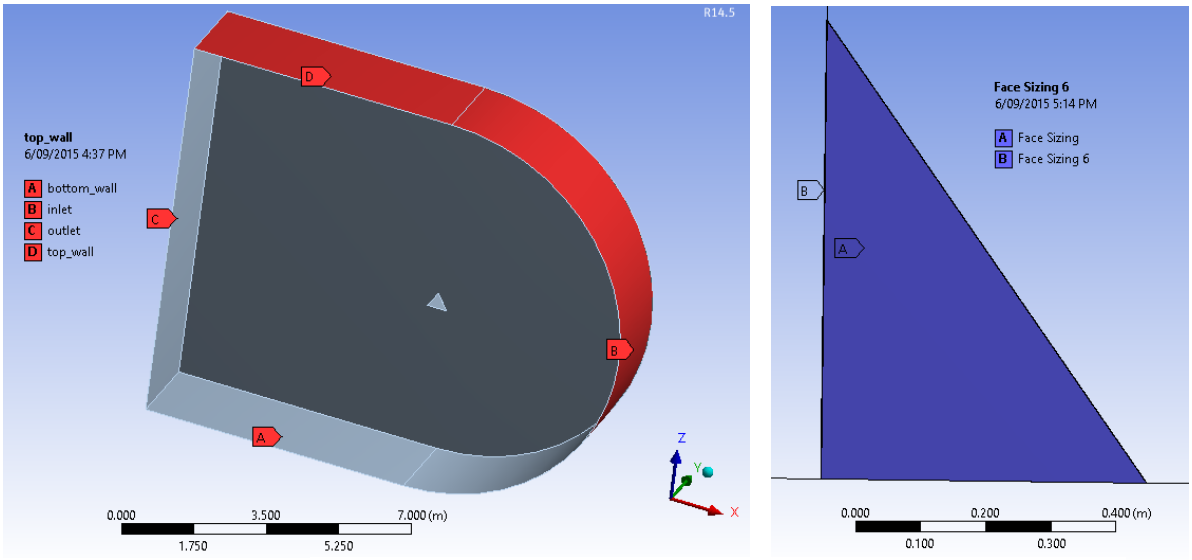

a) b)

Figure 3. 9: Face Sizing used in the meshing of the fluid domain

Table 3. 3: Size function in the Fluid Domain mesh

Surface	Element Size
Bottom_wall	0.4 m
Top_wall	0.4 m
Inlet	0.3 m
Outlet	0.5 m
Wing surface (A)	0.001 m
Wing Surface (B-the trailing edge)	0.001 m

Figure 3.10 illustrates the mesh that was obtained. Figure 3.11 shows the detail of the mesh around the wing root, it can be appreciated that around the airfoil the elements are small and the density of the elements is high. The Mesh of the geometrical domain has 882,169 tetrahedral elements and 225,209 nodes. The orthogonal quality has an average of 0.82, the skewness has an average of 0.29. Other details of the mesh are described in the appendix B.

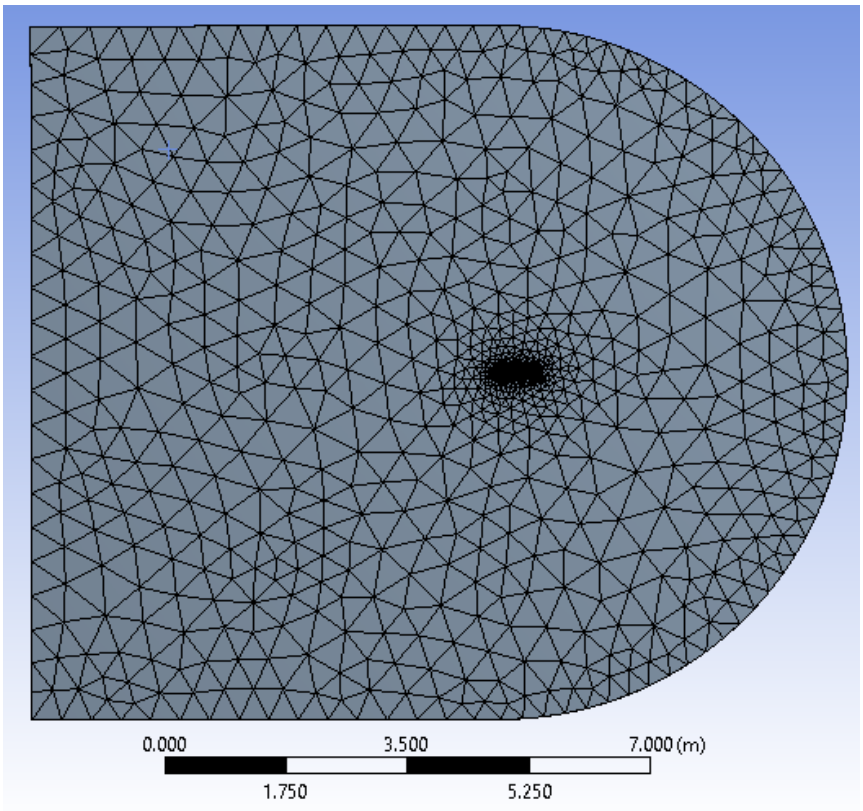

Figure 3. 10: Mesh of Geometrical Domain for the Delta wing

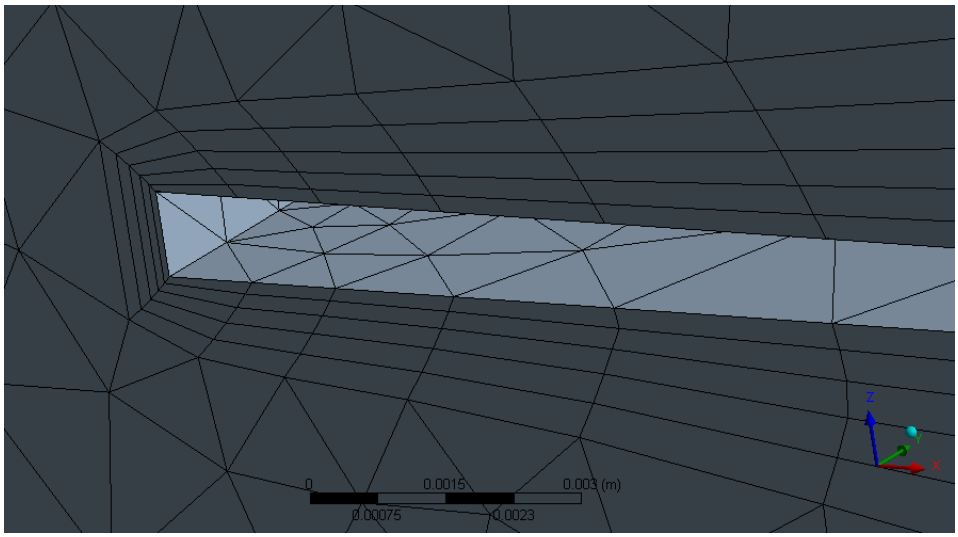

Figure 3. 11 : Detail of the mesh around the wing root –trailing edge

3.4.3.2 Solver configuration

The configuration of the Fluent– Solver which is developed in the tab "Set up" (cell C4). Figure 3.12 illustrates the Graphical User Interface (GUI) of Fluent, the tabs in the left side represents all the steps to complete the configuration, monitor the execution, and post-process the results. In turns, each tab opens a box dialog with multiple options. In this section only the most relevant aspects related with the FSI simulation are described. The full configuration is described in the appendix C.

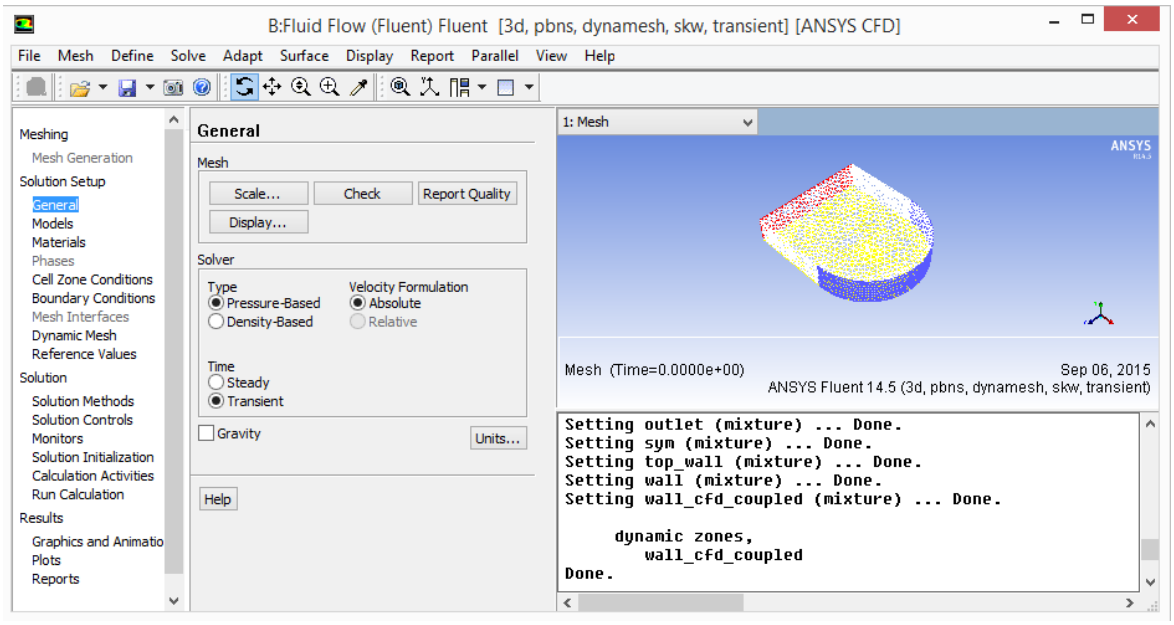

Figure 3. 12: Graphical User Interface (GUI) of Fluent

3.4.3.2.1 Boundary Conditions

The boundary conditions are described in table 3.4. They were defined according with the velocity regime which is subsonic since the airspeed in the experiment and the simulations varied from Mach 0.08 to Mach 0.1 approximately. The velocity values and pressure were selected to match the values of the experiment that was described before.

Table 3. 4: Boundary conditions for the simulation of the Delta wing in Fluent.

Surface	**Boundary Condition**
Inlet	Velocity Inlet
Outlet	Pressure outlet
Wing surfaces	Wall
Wing root surface	Symmetry
Other walls	wall

The values of the turbulence in the inlet and outlet were also taken from the experimental conditions. However this configuration is described in a subsecuent section.

3.4.3.2.2 Dynamic Mesh

To perform an FSI simulation, the mesh of the fluid domain can not be static or permanent. Due to the deformations of the structure, the mesh of the fluid domain has to adapt to the structure motion. In the particular case of this delta wing, the deformations in the perpendicular direction to the fluid flow are large. The most important features of the dynamic mesh are described as follow (ANSYS 2012).

- Smoothing

  The smoothing option was activated. The smoothing is used to adjust the mesh of a zone with a moving and/or deforming boundary, the interior nodes of the mesh move, but their connectivity and the number of nodes does not change. In this way, the interior nodes "absorb" the movement of the boundary.

  The option of smoothing that was used in this simulations was diffusion based on boundary distance. This option allows to control how the boundary motion diffuses into the interior of the domain as a function of boundary distance. Decreasing the diffusivity away from the moving boundary causes those regions to absorb more of the mesh motion, and better preserves the mesh quality near the moving boundary.

This is particularly helpful for a moving boundary that has pronounced geometrical features (such as sharp corners) which corresponds with the geometry of the delta wing that has sharp corners in the tip and root. The value of the diffusion parameter that was used in these simulations was 1.

- Remeshing

The remeshing option was activated. When the boundary displacement is large compared to the local cell sizes, the smoothing methods are not enough to avoid the loss of mesh quality in the zones close to the moving boundaries. In this case, it is necessary to use the remeshing function, as its name indicates, this function carries out a local remeshing in order to maintain a good mesh quality, especially in the vicinity of the moving boundaries. The "CutCell Zone" method was chosen because it works for all cell types.

- Dynamic Mesh Zones

The dynamic Mesh zones are the zones or boundaries that have to move in order to follow the motion of the structure(ANSYS 2014). In this case, the dynamic mesh zone is the surface "Wall_cfd_coupled" because this is the wetted area of the wing,it can be appreciated in figure 3.13. The type of dynamic mesh zone that was selected for the "Wall_cfd_coupled" was "system coupling" because this surface can receive displacements from the System Coupling. In other words, it receives the displacement from the wing.

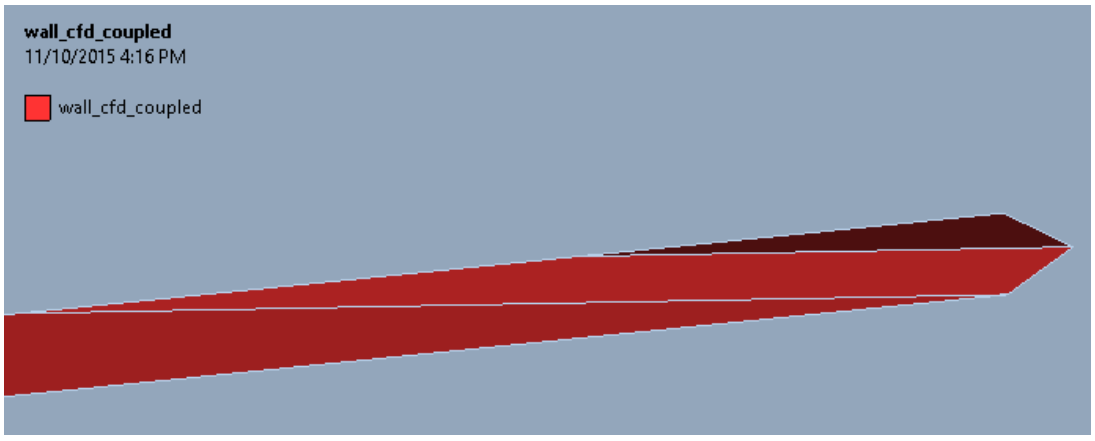

Figure 3. 13: Dynamic mesh Zone (wall_cfd_coupled).

3.4.4 System Coupling

The configuration in this module consisted in the definition of the magnitudes that will be transferred between the solvers (Ansys modules), the time step, and the duration of the simulation.

The system coupling module (module D figure 3.4) carried out the transfer of displacements from the structural simulation (the transient structural module) to the dynamic fluid module (FLUENT), and the transfer of the aerodynamic forces over the wing from the dynamic fluid module (FLUENT) to the structural simulation module (Transient Structural Module). The table 3.5 describe the configuration that was used for this first simulation.

Table 3. 5: Configuration of the System Coupling

Transfer 1	Transfer Variable:	Force
	From:	Fluent
	To	Transient Structural
Transfer 2	Transfer Variable:	Incremental Displacement
	From:	Transient Structural
	To	Fluent
Time Step	0.004 s	
End Time	0.884 s	

The selection of the time step and the end time is determined mainly by the natural frequencies of the wing that were calculated in the modal analysis. The time step should be small enough to capture the behaviour of the natural frequencies of the wing or at least to capture the behaviour of the first vibration mode.

The end time should be long enough to cover one period of the first vibration mode. However, it is also desirable an end time that allows the visualization of the relevant dynamic behaviours. In this case, the end time was extended until the appearance of LCOs that are captured in the experiment (Korbahti, Kagambage et al. 2011).

Therefore, the Time step was defined following the following procedure.

1. Calculation of the period of the first vibration mode. From the table 3.1.

Frequency first mode

$$f = 3.16\ Hz$$
$$T = \frac{1}{f} = \frac{1}{3.16\,Hz} = 0.3164s \tag{3.1}$$

2. To get enough points to describe the dynamic behaviour is recommended to have at least 20 point in the period of the first vibration mode.

$$Time\ step = \frac{T}{20} = \frac{0.3164s}{20} = 0.0158s \tag{3.2}$$

Therefore, a time step less than 0.0158 s is appropriate for the simulation.

3. In order to capture the behaviour of more vibration modes, the steps 1 and 2 were repeated with the frequency of the second mode of vibration which yield a time step of 0.0039 s. Therefore a time step of 0.004 s was selected to the simulation.

The selection of the time step and the End Time also must consider the available computational resources. The reduction of the time step also signifies more time steps to reach the same end time. In consequence, the size of the files in the hard disk memory increases. In addition the running time could increase dramatically if the time step is reduced. A good balance between computation performance and high level of accuracy in the results should be reached in this kind of simulations. The specification of the computational resources used to perform the simulations and the specification of the files is described in the appendix D.

Chapter 4:

Post-processing of FSI Simulation and Results

This Chapter presents the results and analysis of the FSI simulations that were carried out with the Delta Wing. A mesh independence analysis and a turbulence analysis are also presented. The results of the simulations were compared against the experiment described in the chapter 3 in order to validate the FEA models.

4.1 POST-PROCESSING PROCEDURE

The accelerations were collected and analysed in the Post-processing. These results were selected because they are the physical magnitudes that were measured in the experiment, therefore it is possible to compare directly the experimental results against the simulation results.

The points that were selected to collect the acceleration correspond to the same points where the accelerometers were located in the experiment (Korbahti, Kagambage et al. 2011), they are located in the trailing edge as it was illustrated in figure 3.1. The acceleration was measured in the perpendicular direction to the wing plane. Therefore, the post-processing collected the acceleration of both points in that direction.

The procedure to collect the results consisted in the following steps, this procedure was applied to all the simulations of the delta wing. All the results and graphs that are illustrated in this section corresponds to the parameter described in table 4.1.

Table 4. 1: Delta wing simulation parameters:

Angle of Attack	0º
Air speed	34 m/s
Number of element in wing mesh	55902
Number of elements in fluid flow mesh	882,237
Turbulence Model	Realizable K-epsilon, enhanced wall treatment
Turbulence in the boundary conditions(inlet-outlet)	Turbulence Intensity: 5% Hydraulic Diameter: 0.2 m

Step 1: **Verification of Convergence**

The convergence was verified in the system coupling report that shows the convergence state of each solver (Fluent and Transient Structural) in all the iterations and all the time steps. Figure 4.1 illustrates one section of the report where it can be appreciated that the iterations 2 and 3 of the time step 136 converged. In some iterations, especially at the initial time steps, the solvers did not converge, this behaviour occurs because the simulation is the beginning of a transient state where the real response could be far away from the initialization data. However, it is expected that, with the progress of the simulation towards a steady state, all the iterations within the time steps converge.

TIME STEP = 136	SIMULATION TIME = 5.44000E-001	
Solver Data Transfer Diagnostics	Solution Status Source Side	Target Side
COUPLING ITERATION = 1		
Transient Structural	Converged	
Data Transfer Change:RMS	5.56546e-004	6.48708e-004
Fluid Flow (Fluent)	Converged	
Data Transfer 2 Change:RMS	1.90708e-001	2.84923e-001
COUPLING ITERATION = 2		
Transient Structural	Converged	
Data Transfer Change:RMS	6.70193e-002	3.35175e-002
Fluid Flow (Fluent)	Converged	
Data Transfer 2 Change:RMS	1.00440e-002	1.31702e-002

Figure 4. 1: Section of the report execution in the Coupling Module

Step 2: **Definition of local system coordinates and local planes.**

To get the value of the accelerations and displacements in Ansys is necessary to define a local coordinate system in the position where accelerometers were located in the experiment. Then, planes are defined based on these coordinate systems. Figure 4.2 shows the local coordinate systems and the local planes. The plane and coordinate systems close to the tip are denominated plane A1 and coordinate system A1 because they match with the position of the accelerometer a_1 in the experiment. In a similar manner, the plane and coordinate system located close to the root were called plane A2 and coordinate system A2. The global coordinate system is represented in the low-left corner of figure 4.2.

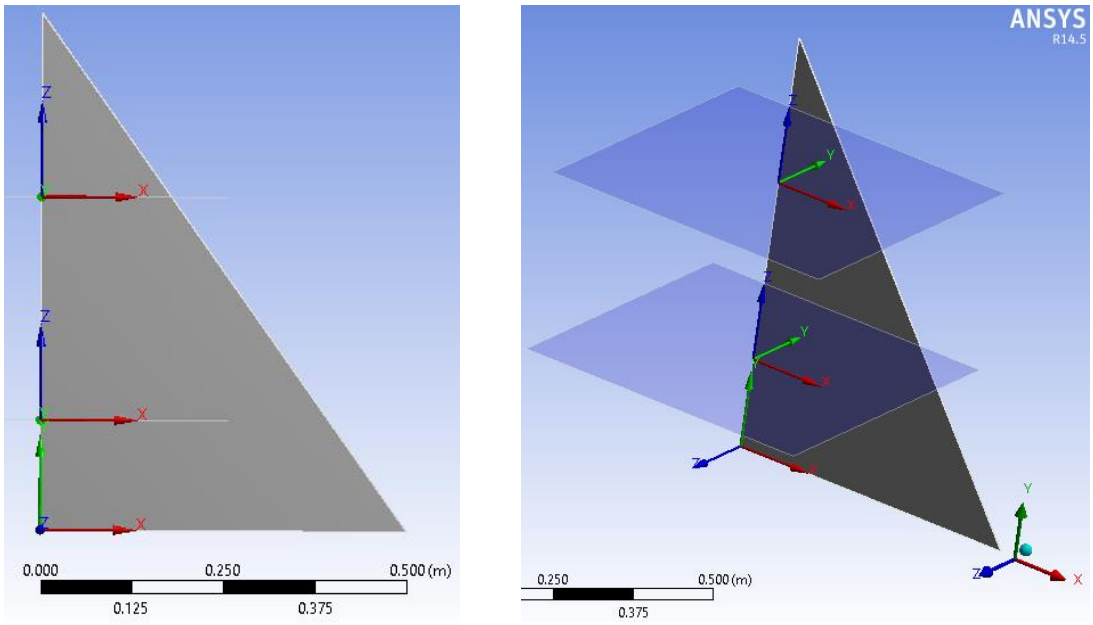

Figure 4. 2: Local coordinate systems and local planes in the Delta Wing

3. Calculate the relevant information in the local planes

The relevant results can be calculated in the local planes. In these simulations the accelerations and displacements in the local planes were calculated. These magnitudes were calculated in the global Z direction which correspond with the perpendicular direction to the wing plane. These calculations allow the creation of graphs where the maximum and minimum values can be identified. For example, figure 4.3 illustrates the graphs that are obtained, they are the maximum (green) acceleration and minimum (red) acceleration in the cross section defined by the local plane A1 in each time step. For example, it can be appreciated in the table that the time 0.752 s is highlighted, for this time, the maximum acceleration (green) is 55.697 m/s^2 and the minimum acceleration is 4.05 m/s^2. Figure 4.4 shows the values of the accelerations in the local plane A1 at the time 0.748 s.

Figure 4.3 also illustrates that the maximum value of the maximum accelerations is 56.49 m/s^2, and the minimum value of the minimum accelerations is -56.39 $m/^s$, the animation also shows that these minimum and maximum acceleration values are reached in the trailing edge at some specific times as it is illustrated in figure 4.4, where the trailing edge reach its maximum acceleration value at 0.748 s according with the color scale. Therefore, the maximum and minimum accelerations at the position of the accelerometer a_1 are 56.49 m/s^2 and -56.39 $m/^s$.

The acceleration of the position a_2 and the displacements of the position a_1 and a_2 were calculated in the post-processing following a similar process. A summary of these information is presented in table 4.2.

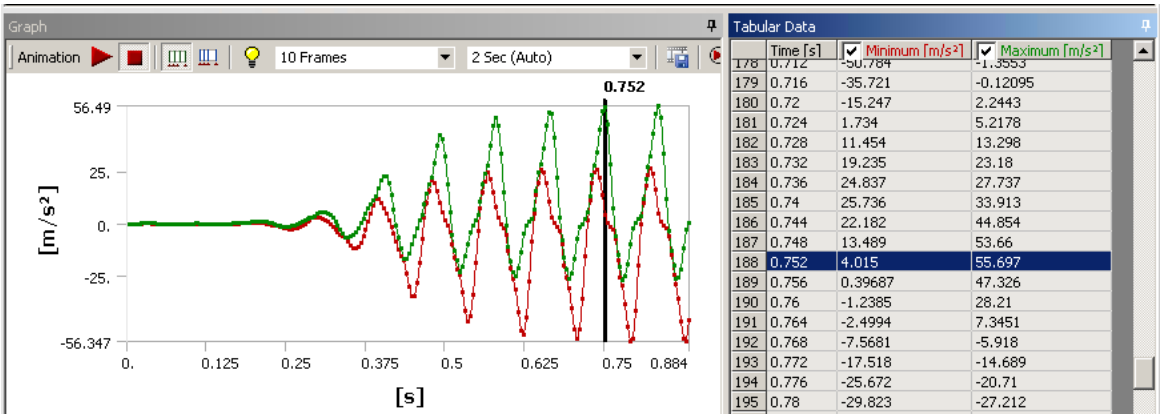

Figure 4. 3: Maximum and minimum acceleration in the plane A1 (accelerometer a1)

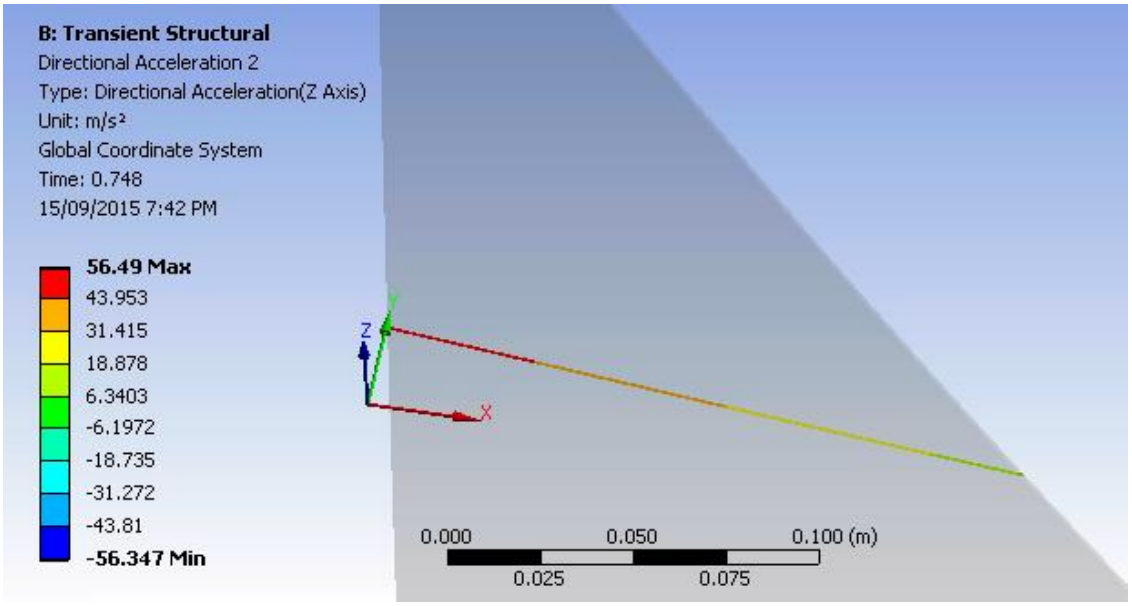

Figure 4. 4: Acceleration in the Plane A1 at 0.748 s

Figure 4.5 illustrates the displacement that results from the oscillation of the wing. The wing is represented from the trailing edge point of view or rear view. It can be appreciated that the minimum displacement of the trailing edge is about 9 mm in the negative Z direction of the Global Coordinate System.

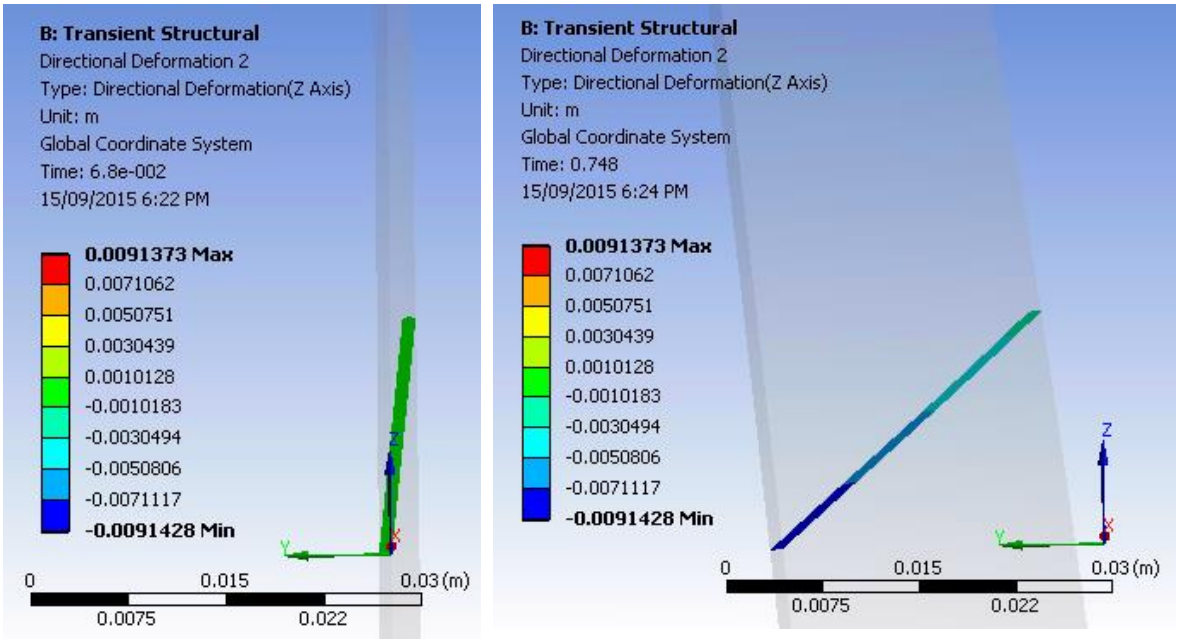

Figure 4. 5: Displacement in the plane A1 at 0.068 s (left) and 0.758 s (right).

Table 4. 2: Results of the simulation

Magnitude	**Acceleration**		**Displacement**	
Location	A1 (m/s^2)	A2 (m/s^2)	A1 mm	A2 mm
Maximum	56.49	15.045	9.1373	1.4348
Minimum	-56.34	-14.821	-9.428	-1.4155

4.2 Mesh Independence Analysis

Three simulations with different mesh resolution were carried out in order to perform a mesh convergence study. The parameters of the simulations are described in table 4.1. Since the fluid flow and the structure are interacting, it was necessary to vary the mesh in both systems.

The methodology to perform the analysis consisted in defining a rough mesh with the smaller amount of elements in the mesh in both domains. Then, the medium and fine mesh were defined by doubling the amount of elements. In this way, the medium mesh has almost the

double of the elements than the rough mesh, and the fine mesh has also the double of the elements of the medium mesh.

The results that were obtained for each mesh are described in table 4.3

Table 4. 3: Results of the Mesh Independence Analysis

Simulations	**Magnitude**	**Acceleration**		**Displacement**	
Number of Elements in the mesh		**a_1** (m/s^2)	**a_2** (m/s^2)	**a_1** (mm)	**a_2** (mm)
Rough Mesh Fluid: 436,345 Wing: 55.902	Maximum	54.524	13.438	9.382	1.366
	Minimum	-57.523	-15.818	-8.771	-1.401
Medium Mesh Fluid: 882,237 Wing: 55,902	Maximum	56.49	15.045	9.1373	1.4348
	Minimum	-56.34	-14.821	-9.428	-1.4155
Fine Mesh Fluid: 1,712,960 Wing: 99,374	Maximum	56.767	14.911	9.3204	1.45
	Minimum	-57.719	-15.41	-9.1098	-1.4522
Maximum Relative differences among meshes	Maximum	3.95%	10.68%	2.6%	5.79%
	Minimum	2.38%	6.3%	6.96%	3.52%

Table 4.3 shows the maximum relative differences between the three meshes. The maximum relative differences occur usually between the rough mesh and the fine mesh, and the maximum value was 10.68%. In addition, the values of the medium mesh and the fine mesh are close. Therefore, it can be concluded, from the relative differences, that the results are reasonably independent of the mesh resolution.

4.3 Turbulence Analysis

Four simulations were carried out in order to investigate the effects of different turbulence models. These simulation covered two aspects of the turbulence effects in this particular aeroelastic case. The first aspect is the effect of applying three different turbulence models in the fluid flow close to the wing structure. The second aspect is the effect of turbulence intensity in the boundaries, specifically in the inlet and outlet of the fluid domain.

Three simulations were carried out to study the first aspect of the turbulence analysis. Each simulation ran a different turbulence model. Realizable k-epsilon, Standard k–ω, and SST k–ω model were the turbulence models to be implemented in the simulations. These models were selected because, as was explained in the chapter 2, Around 2/3 of all the simulations reported use some variation of the 1 or 2 equations turbulence model, which mean that they use the k-epsilon family, and the k- ω family.

All the simulations to test the turbulence models have the parameters described in the table 4.1, except for the turbulence model that varies in each case. The mesh with medium resolution in the fluid flow and the wing structure was selected to perform these simulations because the mesh independence has been demonstrated in the previous section. In addition, the medium size resolution was suitable for the available computational resources. The results of these simulations are described in table 4.4.

Table 4. 4: Results of the Turbulence Analysis

Turbulence Model	**Acceleration**		**Displacement**	
	a_1 (m/s^2)	**a_2** (m/s^2)	**a_1** (mm)	**a_2** (mm)
K-epsilon model Fluid mesh: 882,237	Max: 56.49 Min:-56.34	Max:15.045 Min:-14.821	Max:9.382 Min:-8.771	Max:1.366 Min:-1.401
Standard K-omega model Fluid mesh: 882,169	Max:57.818 Min:-58.64	Max:15.926 Min:-16.678	Max:9.6874 Min:-9.4688	Max:1.4733 Min:-1.4638
SST K-omega model Fluid mesh: 882,169	Max: 58.127 Min: -57.784	Max:15.927 Min:-16.353	Max: 9.4164 Min: -9.4174	Max:1.4239 Min: -1.4071
Maximum Relative difference	4.08%	12.5%	7.9%	7.28%

One simulation was carried out to study the second aspect of the turbulence analysis, which is the turbulence in the boundaries of the fluid domain. Ansys-Fluent has multiple options to model the turbulence in the inlet and outlet of the fluid flow domain. The option that was selected for this simulation was the definition of the turbulence intensity and the turbulence viscosity ratio. Since the simulation is intended to imitate the experiment described in the chapter 3, the turbulence intensity of the wind tunnel in the University of Liege was applied in the simulation, this value is 0.2 %. For the viscosity ratio, a value of 10 % was employed because it is typically a good value for external flows (Ansys 2011). Table 4.5 describes the results of this simulation and the comparison with the simulation without the suitable turbulence magnitudes in the boundaries. Both simulations have the parameters described in table 4.1 except for the turbulence parameters in the inlet and outlet which vary in each case, it is important to note that both simulations in table 4.5 have a medium mesh definition

Table 4. 5: Results of turbulence Analysis in the boundaries of the fluid –flow domain

Simulations	**Acceleration**		**Displacement**	
	a_1 (m/s^2)	**a_2** (m/s^2)	**a_1** (mm)	**a_2** (mm)
Fluid mesh: 882,237 Inlet and Outlet Turbulence intensity: 5% Hydraulic Diameter: 0.2m	Max: 56.49 Min:-56.34	Max:15.045 Min:-14.821	Max:9.382 Min:-8.771	Max:1.366 Min:-1.401
Fluid mesh: 882,169 Inlet and outlet: Turbulence intensity: 0.2% Turbulence viscosity ratio 10%	Max:57.714 Min: -57.488	Max:15.359 Min:-15.294	Max:9.268 Min:-9.2043	Max:1.4485 Min:-1.4294
Maximum Relative Differences	2.16%	3.19%	4.9%	6.03%

4.4 Results and Validation for Angle of attack 0°

For 0º in the angle of attack (AOA), three simulations were performed, each one at three different air speeds to quantify the accuracy of the FSI solver. The post-processing that was described in the previous sections was applied in all the simulations. The results are the

accelerations in the perpendicular direction to the wing plane (Z direction in the Global Coordinate System). These results are compared against the experimental results in table 4.6 and figure 4.6 that represent the acceleration in terms of the gravity acceleration g, taking 1g = 9.81 m/s^2. Some graphs of acceleration and displacement are presented in figure 4.7 and the appendix E.

The three simulations have the k-epsilon (2 equation) Realizable Model with enhanced wall treatment on the wing surfaces. In the inlet and outlet boundaries, the turbulence was defined with a turbulence intensity of 0.2 % and a Turbulence Viscosity Ratio of 10.

Table 4. 6: Results of the Simulation (Sim) at 0º AOA and comparison against experimental results (Exp)

Air Speed (m/s)		**Acceleration a_1 (g)**			**Acceleration a_2 (g)**		
		Sim	**Exp**	**Relative difference**	**SIM**	**Exp**	**Relative Difference**
U=29 (LCO)	Max	1.5714	1.9421	19.08 %	0.281	1.1401	75.35
	Min	-1.571	-2.5934	39.2 %	-0.2628	-1.1957	78.02
U=34 (LCO)	Max	5.75	5.22	-10.1 %	1.565	3.3954	53.9
	Min	-5.74	-9.57153	40.03 %	-1.559	-4.3893	64.48
U=36 (LCO)	Max	8.96	10.52	14.82 %	2.51	9.9788	74.84
	Min	-8.95	-19.1882	53.35 %	-2.54	-12.4209	79.55

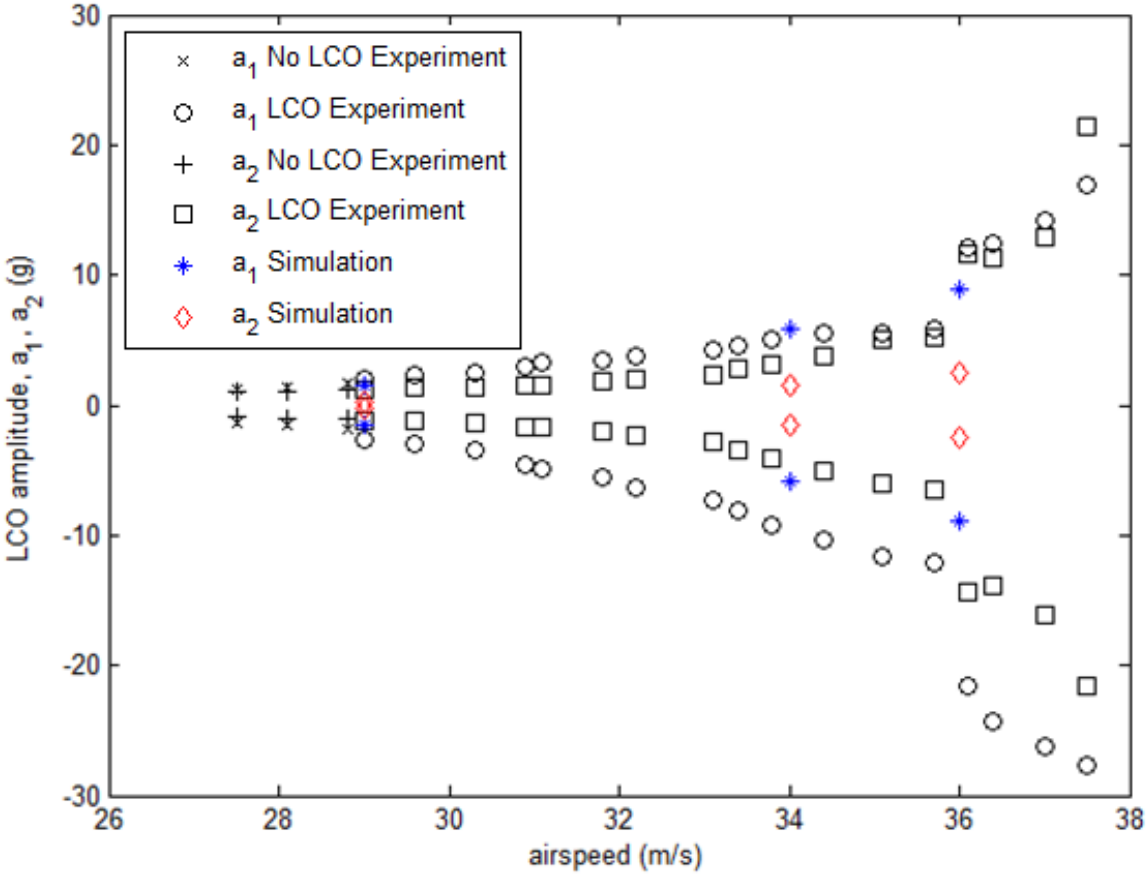

Figure 4. 6: Results of the Simulation at 0º AOA and comparison against experimental results (Korbahti, Kagambage et al. 2011)

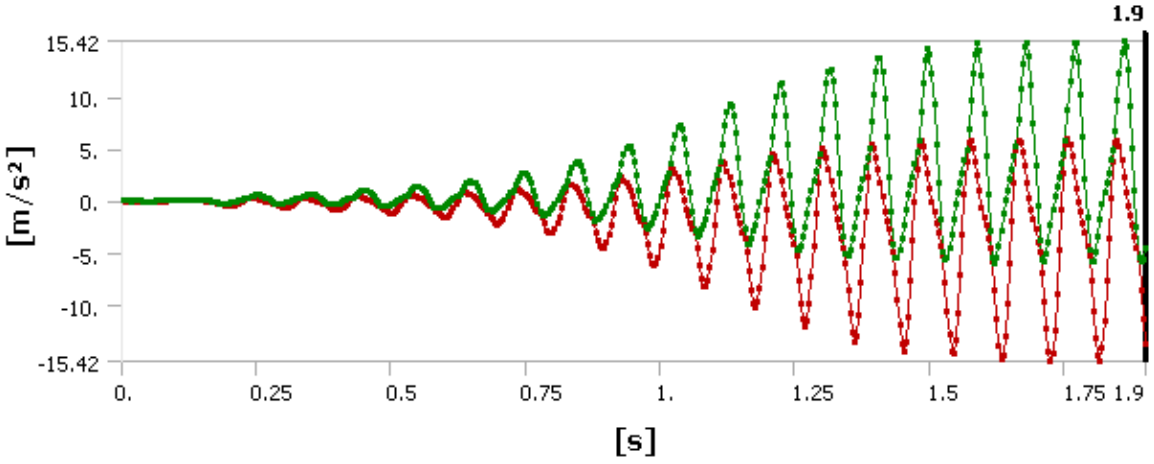

Figure 4. 7: Simulation result, acceleration a_1 for airspeed 29 m/s and 0° in AOA

There are three aspects that are relevant in the validation of the simulation results which is done by a comparison with the experimental results. The first aspect is the appearance of the LCOs in the simulations at all airspeeds (29,33 and 36 m/s) as it is described in the table 4.6 (first column) and illustrated in figure 4.6. In addition, it can be appreciated in figure 4.7 that the type of dynamic response correspond to LCOs behaviour. This matches the

experimental results that also registered the LCO behaviour for the range of airspeeds between 29 m/s and 38 m/s.

The second aspect is the symmetry between the negative accelerations and the positive accelerations. As observed in figure 4.6, the experimental results are asymmetric while the simulation results are symmetric. It also can be appreciated in table 4.6 and figure 4.6 that the degree of asymmetry in the experimental results grows with the speed since the asymmetry of the acceleration a1 at 29 m/s is around 33.5 % while the asymmetry at 36 m/s is around 82.3 %, these values are calculated according with the equations 4.1 and 4.2. It also can be observed that the degree of asymmetry in acceleration a_1 is higher in comparison with the acceleration a_2.

At U=29 m/s. Acceleration a_1

$$Assymetry = \frac{|-2.5934| - 1.9421}{1.9421} \times 100 = 33.5\% \tag{4.1}$$

At U=36 m/s Acceleration a_1

$$Assymetry = \frac{|-19.1882| - 10.52}{10.52} \times 100 = 82.3\% \tag{4.2}$$

The third aspect is related with values of the acceleration. Overall, the positive values of the acceleration a_1 calculated by the simulation match the experimental results, the relative differences are not higher than 20 %, being 34 m/s the airspeed that matches better with the experimental results with 10.1 % of relative difference. In contrast, the values of acceleration a_2 calculated by the simulation do not match the experimental results, being 53 % the lowest relative difference. For both cases, a_1 and a_2, their negative values do not match very well with the experimental results, this is in part a consequence of the asymmetry that was explained before.

4.5 Results and Validation for Angle of Attack 1°

Similarly to the simulations at 0º in the angle of attack, three simulations were performed for 1º in AOA, each one at three different airspeeds to quantify the accuracy of the FSI solver. The post-processing was also the same that was explained before. The table 4.7 and the figure 4.8 describe the simulation results, the experimental results and the comparison

between them. The acceleration a_1 for each airspeed is illustrated in the figures 4.9, 4.10 and 4.11. Other graphs of acceleration and displacement are presented in the appendix F.

Table 4. 7: Results of the Simulation (Sim) at 1° AOA and comparison against experimental (Exp) results .

Air Speed (m/s)		**Acceleration a_1 (g)**			**Acceleration a_2 (g)**		
		Sim	**Exp**	**Relative difference**	**Sim**	**Exp**	**Relative Difference**
U=28.6 (No LCO)	Max	2.2809	6.3557	64.1 %	0.8541	2.8799	70.3 %
	Min	-2.0582	-7.3442	71.9 %	-0.5731	-4.6292	87.6 %
U=31.1 (No LCO)	Max	2.999	9.0345	66.8 %	1.0133	6.0598	83.2 %
	Min	-3.085	-9.8905	68.8 %	-0.7215	-3.9155	81. %
U=33.9 (LCO)	Max	5.9835	19.8735	69.8 %	1.2833	19.271	93.3 %
	Min	-4.4823	-19.9502	77.5 %	-1.7758	-12.4937	85.7 %

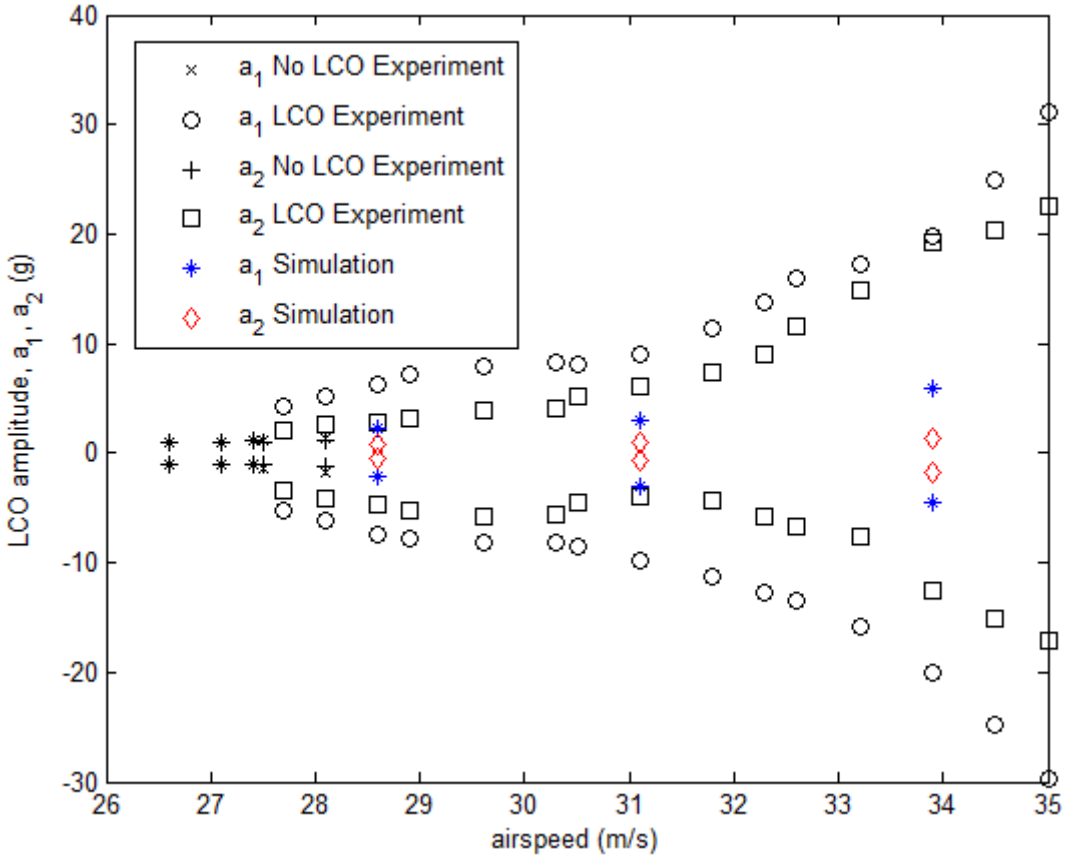

Figure 4.8: Results of the Simulation at 1° AOA and comparison against experimental results (Korbahti, Kagambage et al. 2011)

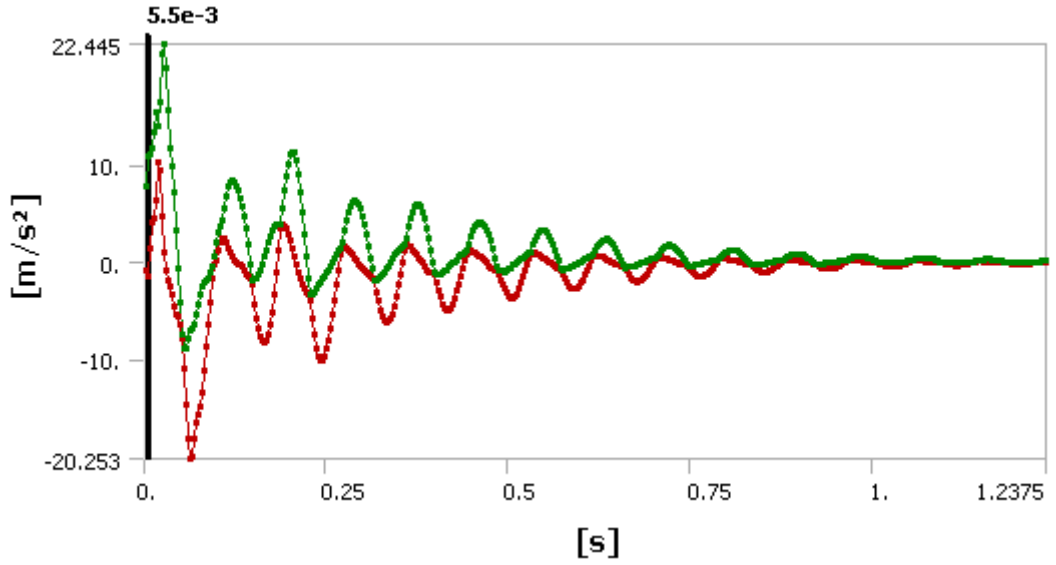

Figure 4. 9: Simulation result, acceleration a1 for airspeed 28.6 m/s and 1° in AOA

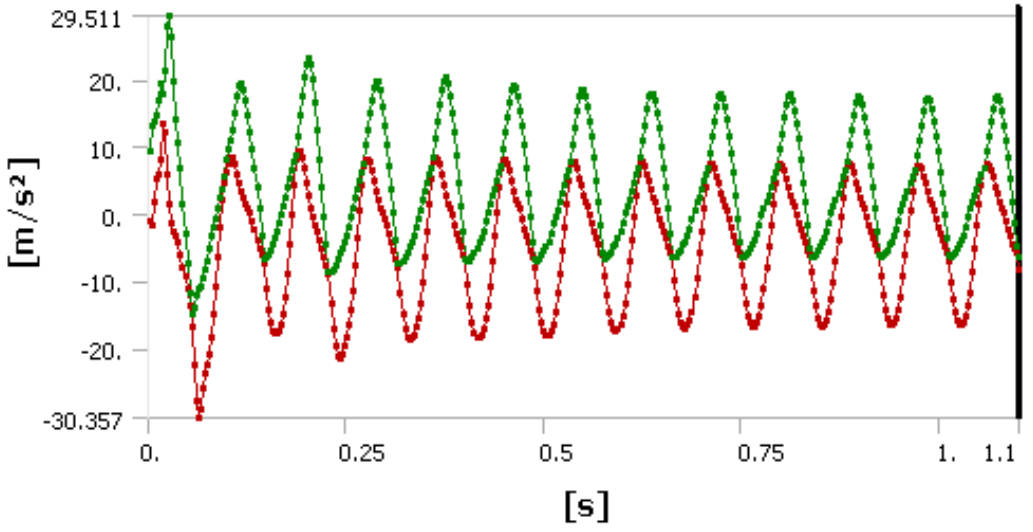

Figure 4. 10: Simulation result, acceleration a1 for airspeed 33.1 m/s and 1° in AOA

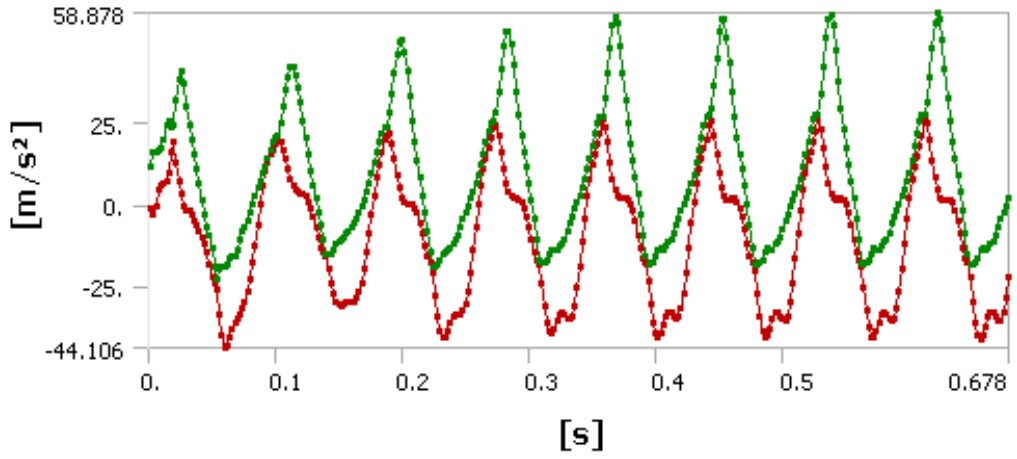

Figure 4. 11: Simulation result, acceleration a1 for airspeed 33.9 m/s and 1° in AOA

Similarly to the simulation results at 0 AOA, the simulation results at 1° AOA and the comparison with the experimental data reveals three important aspects. The first one is about the appearance of LCOs, figure 4.8 shows that the experiment registered LCOs behaviour for three analyzed airspeeds. In contrast, figures 4.9 and 4.10 show that, at 28.6 m/s and 31.3 m/s, the simulations produced a dynamic response that begins with a strong oscillations that are attenuated until reach a steady state, the peak of the oscillations at the beginning is the value that is registered in the figure 4.8. The only airspeed that presents a LCOs behaviour in the simulations is the highest one which is 33.9 m/s. The experiment also shows steady state behaviour with zero acceleration but in the range of 26 m/s to 28.5 m/s, particularly, at airspeed between 27.5 and 28.5 m/s the wing displayed either steady or LCO behaviour, if the wing is static and no external excitation is applied, then it remain static in this airspeed range. Conversely, if an external excitation is applied, it will undergo LCOs, this particular behaviour is demonstrated by the data at 28.1 m/s (Korbahti, Kagambage et al. 2011).

The second aspect is the symmetry between the negative accelerations and the positive accelerations. It can be seen in figure 4.8 that the experimental accelerations, a_1 and a_2, are much more symmetrical in comparison with the accelerations at 0° AOA illustrated in figure 4.6. On the other hand, the simulation results are less symmetric in comparison with the results of the simulation at 0° AOA, this difference is particularly demonstrated by the simulation results at 33.9 m/s (figure 4.11) where it can be appreciated that the peaks of positive accelerations are higher than the peaks of negative accelerations, this difference is derived from the angle of attack since the fluid flow has a small component in the perpendicular direction of the wing. Therefore, despite the fact that the wing is oscillating, it is pushed by the fluid flow in the positive Z direction of the Global Coordinate system. Overall, at 1° AOA, the simulation and the experiment results match in terms of symmetry because both of them show a significant level of symmetric behaviour in the accelerations a_1 and a_2.

The third aspect is related with the values of the acceleration. Overall, the values of the accelerations a_1 and a_2 calculated by the simulation do not match the experimental results, being 93.3% the maximum relative difference, and 64.1 % the minimum relative difference according with the equations 4.3 and 4.4. A comparison between the relative differences of the accelerations a_1 and a_2 shows that a_1 has lower values of relative difference than a_2, which is similar to the trend presented at 0° AOA.

$$\frac{19.271-1.2833}{19.271}\times 100 = 93.3\% \quad (4.3)$$

$$\frac{6.3557-2.2809}{6.3557}\times 100 = 64.1\% \quad (4.4)$$

4.6 Discussion of the Results

The oscillation of the delta wing is caused by the simple stall of a flat plate. When the flow comes around, the sharp edge generates stall almost immediately, pushing the wing to one side, then the wing reaches quickly an angle of attack that provokes the stall again and is pushed to the opposite side, then the phenomenon is repeated again, and the wing remains oscillating between two angles of attack. It is also important to note that the flat plate is characterized by a flow separation that begins at low AOA (around 3°). In consequence, the flat plate also begins to stall at these low AOA, or in other words, the stall occurs very quickly. The thickness of the wing also has some effect in these oscillations. Due to the low thickness, the wing has a low bending stiffness. As a consequence, the deflection is high, generating a reaction of the wing to recover its original shape. Similar experiments that have been carried out in the wind tunnel at the University of Sydney have shown that these oscillation are not presented when the thickness is 3 mm, this demonstrates the significant effect of the structural stiffness in this type of phenomenon.

Table 4.4 describes the results of the turbulence analysis, it shows that the implementation of different turbulence models in the wing surface does not affect significantly the results of the simulation since the maximum relative difference is 12.5 %. Table 4.5 describes the results of the turbulence analysis in the fluid flow domain, it also shows that the implementation of the real turbulence magnitudes in the boundaries does not affect significantly the results. This behaviour could be explained by the low airspeed of the test , which was 34 m/s, and by low turbulence intensity of the Wind tunnel at the University of Liege which is 0.2 % , taking into account that a turbulence intensity of 1% or less is generally considered low and turbulence intensities greater than 10% are considered high (ANSYS 2014).

Regarding the simulations at 0° and 1° angles of attack. The results of the simulation showed a limited consistency with the experimental results in the aspects of appearance of LCOs,

symmetry and acceleration values. However, there also significant differences between them. Some of the possible causes of these differences are exposed below.

Regarding to the differences in the symmetry of the results, especially at 0° AOA could be the normal imperfections in the geometrical shape of the real wing. The main imperfection is that the real wing is not a perfect flat plate. The causes could be multiple, including thin thickness and defects in the manufacturing processes. These imperfections could cause a difference in the flow between the both sides of the wing that could result in a small lift force that begins the oscillations even at 0° AOA and produces the asymmetry in the accelerations. In contrast, the geometry in Ansys is a perfect flat plate. Therefore, there is not differences in the flow on both sides of the wing in the simulation. Errors in the location of the wing also could have some effect in the asymmetry of the results, for example, if the wing is not perfectly centered in the wind tunnel, the effect of the tunnel walls on the wing produces an unbalanced force on the wing.

The highest degree of asymmetry in the experiment is present at 0º AOA, which was the only aerodynamically symmetric configuration. The buckling of the plate due to in-plane forces in the wind direction is also a possible explanation for this behaviour. However, it is not possible to verify this hypothesis due to the absence of strain measurements in this direction (Korbahti, Kagambage et al. 2011).

Regarding the values of the accelerations, one of the possible causes of the differences, especially at 1° AOA where the differences are significant, is the sharp edge located at the leading edge that was described in the chapter 3, this sharp edge was included in the geometry to minimize some of the problems of having a blunt edge facing to the flow. This geometrical feature might mitigate too much the actual stress of the flow at these angles of attack, reducing in turns the acceleration amplitude of the oscillations. However, it is also important to note that the inclusion of the sharp edge can not explain completely the big differences between the simulation and the experiment since the attachment length of the flow over the wing varies very little with the inclusion of the sharp edge.

PART 2

Onera M6 Wing

Chapter 5

CFD Simulation

This chapter presents the CFD simulation of the Onera M6 in steady state. This simulation considers that the Onera M6 is a fully rigid body, thus there is not deformation of the wing and in turns there is not an aeroelastic behaviour. However, this simulation is necessary to ensure that the setup of the CFD solver is appropriate to be used in the FSI simulation that is presented in the next chapter. The validation of the simulation was carried out by the comparison with experimental results.

5.1 Pre-Processing

The CFD simulation of the ONERA M6 wing was carried out in the Package Fluent of Ansys 14.5. All the steps of the pre-processing were completed before the execution of the simulation in Fluent, they are described as follow.

5.1.1 Geometry

The Onera M6 is a wing developed by ONERA (Office National d'Etudes et Recherches Aérospatiales). The experiments that were carried out with this wing are usually taken as reference studies to validate CFD models. The geometry of the wing is illustrated in figure 5.1. All the features of the geometry were described by Schmitt and Charpin (1979). The geometry of the section wing was taken from Slater (2008) in txt format.

A particular characteristic of the geometry is that the airfoil profile is located perpendicular to the 40.18 percent of the chord line. According with Babel (2008), this percentage was taken from the leading edge. The wing tip was modelled as the half of a revolution body in a similar way as it was modelled by Babel (2008).

In figure 5.1 also can be appreciated seven chord lines that are located at specific positions given by the ratio y/b. These chord lines correspond with the sections where the pressure distributions were taken in the experiment described by Schmitt and Charpin (1979).

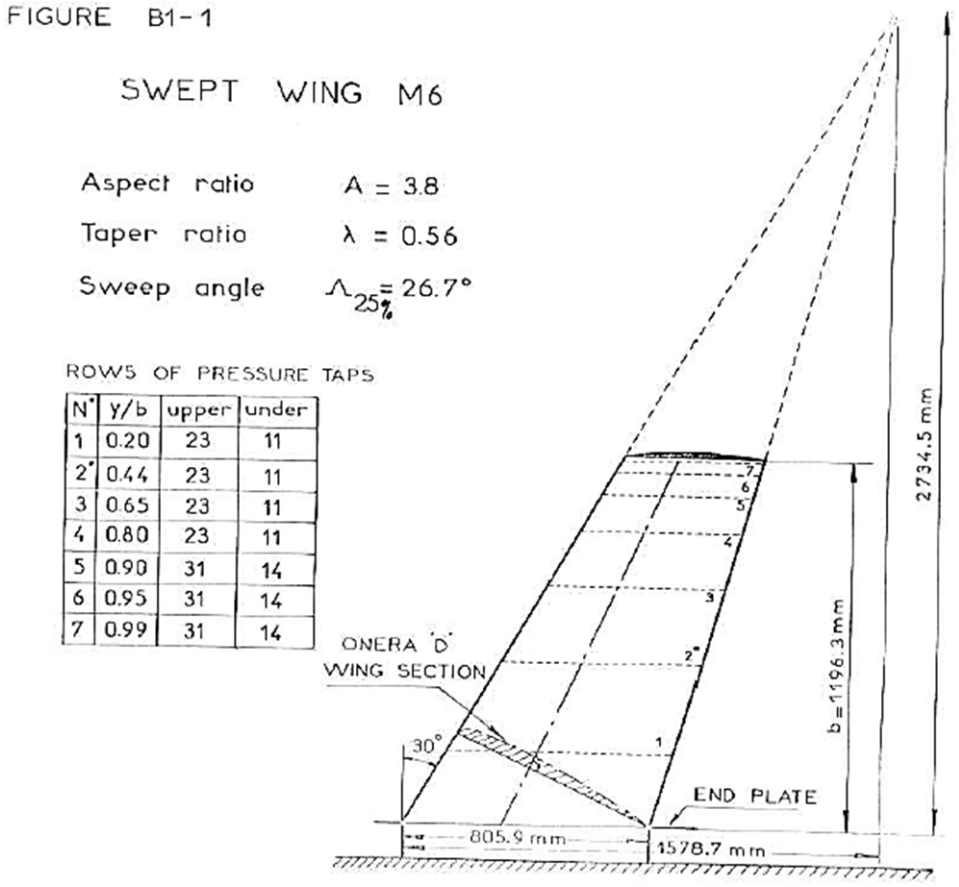

Figure 5. 1: Geometry of the Onera M6 wing, (Schmitt and Charpin 1979)

The Onera M6 was modelled in the CAD software Solid Edge ST5, and it was imported to Ansys as IGES file format. The figure 5.2 illustrates the CAD model of the wing, it can be observed that the wing is a complete solid body since no internal structure is considered in a CFD steady state simulation.

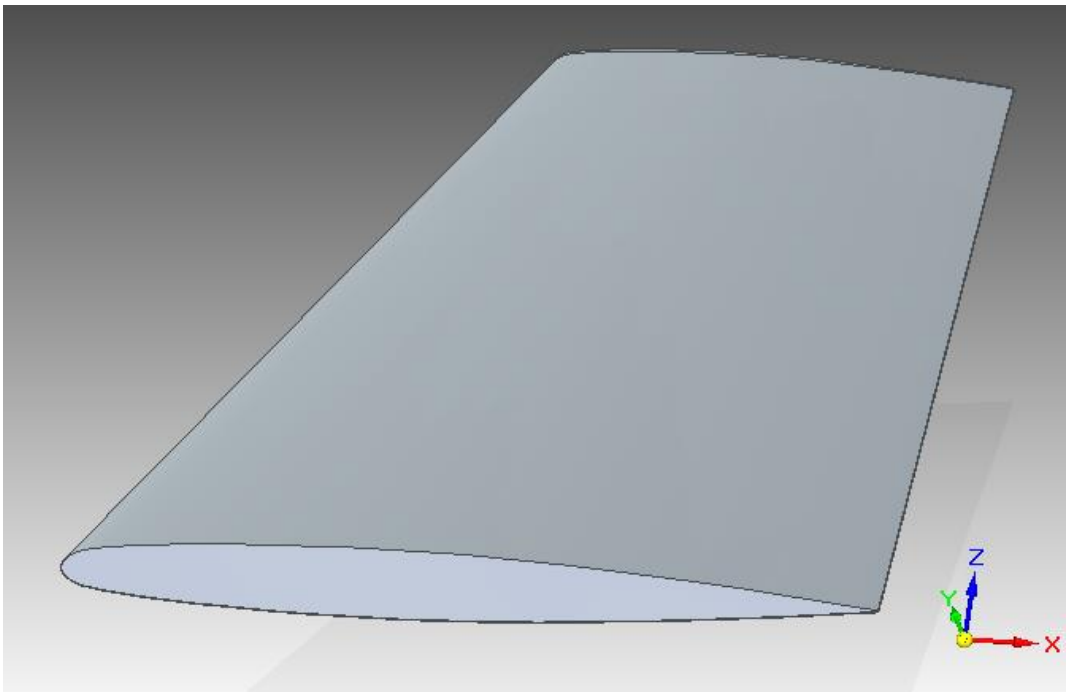

Figure 5. 2: CADModel of the Onera M6 wing

5.1.2 Geometrical Domain

The geometrical domain, also called fluid domain, was modelled as a box that represents the volume that is occupied by the flow. This signifies that the volume of the wing is subtracted from the box volume. The Geometrical domain requires a set of minimum dimensions to avoid the disturbance of the flow over the wing due to the presence of the walls that define the Geometrical domain. The figure 5.3 illustrates the dimensions that were considered to define the Geometrical Domain. Based on the dimensions defined by Abobaker, Toumi et al. (2014), the wide and height of the Geometrical domain were determined by a factor of 11 times the wing chord length at the root of the wing. The dimensions can be appreciated in the figure 5.3. The dimension H4 is 22,000 mm, the dimension V3 is 11,000 mm, and the depth is 3,500 mm.

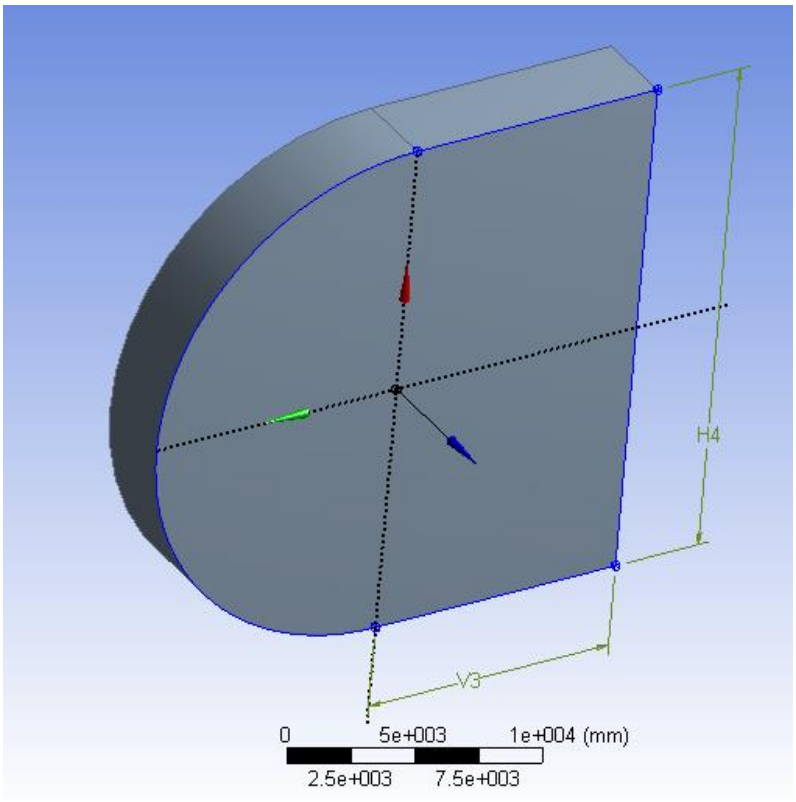

Figure 5. 3: Fluid domain for the Onera M6 wing

The geometrical Domain was modelled in the DesigModeler module of Ansys. First, the model of the wing in .IGES format was imported, then a volume with the maximum dimensions of the geometrical domain was extruded, the last step was the Boolean operation to subtract the volume of the wing from the volume created in the second step. In this case, it is not necessary to preserve the body of the wing, therefore, the option to preserve tool bodies was set up as negative.

Multiple attempts to create the geometrical domain directly in Solid Edge were carried out but they failed because, later on, there was a significant problem to do the mesh of the volume. The problem consisted in the lack of recognition of the void created by the subtraction of the wing volume. As a result, Ansys generated a mesh inside the wing volume. The causes of this problem were not found. The only solution was the procedure that was described before.

5.1.3 Meshing

The mesh of the geometrical domain was carried out in the meshing module of Ansys. The main principle that was applied in this case is the same that was applied for the Delta Wing. As explained in the chapter 3, six size functions were implemented over the faces of the fluid domain, these size functions allowed the definition of the element size in the six faces. Figure 5.4 illustrates the faces that were used to define the mesh, the table 5.1 describes the size of the element that was used in each face, it can be observed that the faces over the wing (face A, B ,C, and D in figure 5.4b) require a small element size since it is desirable to obtain a good detail of the fluid flow over the wing. It is important to note that the faces A and B in figure 5.4 b correspond with the half upper and the half lower of the wing respectively, this partition was necessary to facilitate the production of graphs in the post-processing.

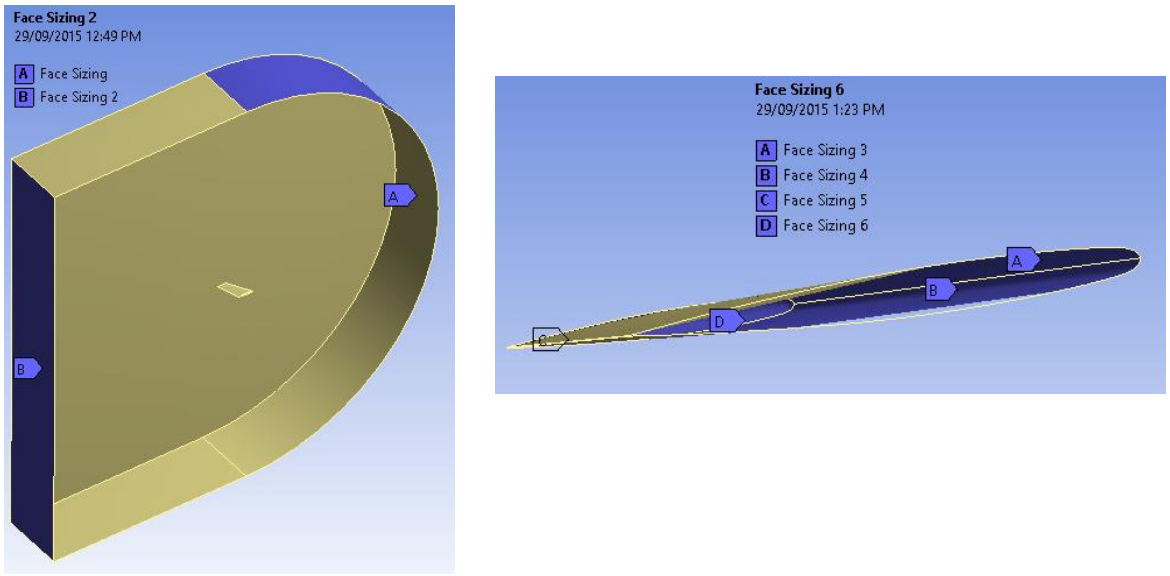

a) b)

Figure 5. 4: Faces used in the Size Functions

Table 5. 1: Size functions in the Fluid Domain mesh

Surface	Element Size
Inlet (Face A figure 5.4 a)	700 mm
Outlet (Face B figure 5.4 a)	500 mm
Upper Face Wing (face A figure 5.4b)	9 mm
Lower Face Wing (face b figure 5.4 b)	9 mm
Wing tip (face D figure 5.4 b)	10 mm
Trailing edge (face D figure 5.4 b)	10 mm

The figure 5.5 illustrates the mesh that was obtained. The figure 5.6 shows the detail of the mesh around the wing root, it can be appreciated that around the airfoil the elements are small and the density of the elements is high. The Mesh has 453,550 tetrahedral elements and 87,259 nodes. The orthogonal quality has an average of 0.84, the skewness has an average of 0.25.

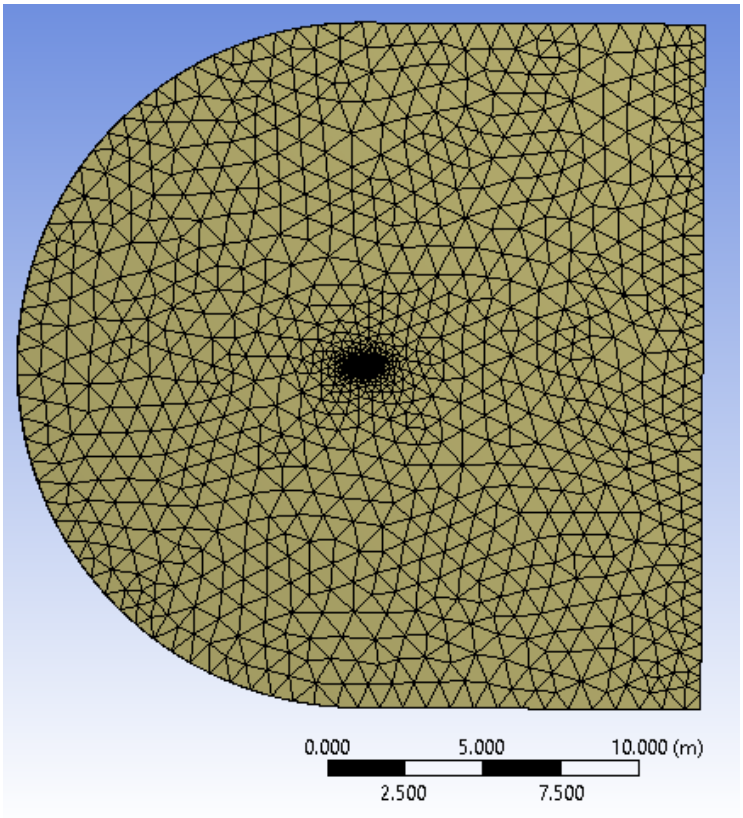

Figure 5. 5: Mesh obtained for Onera M6 wing

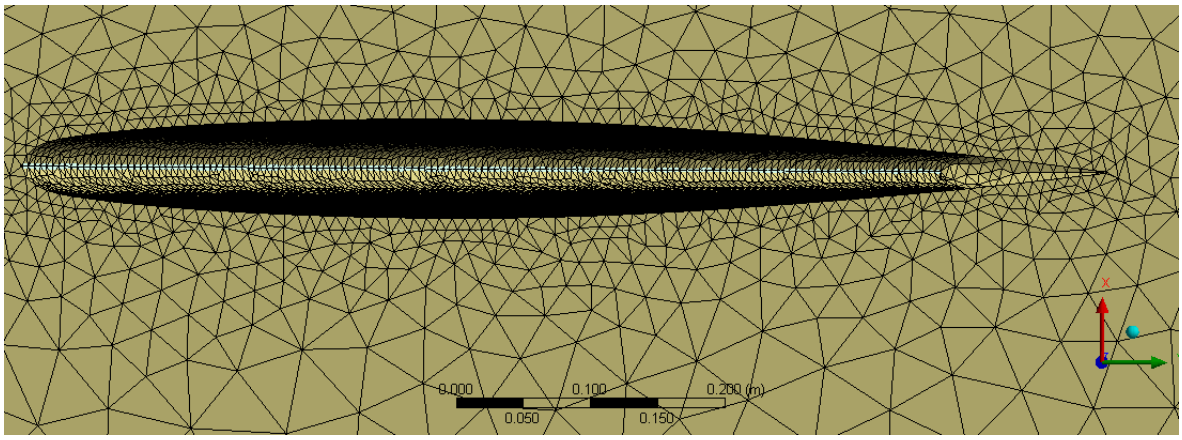

Figure 5. 6: Mesh in the proximity of the wing profile at the wing root

5.2 Configuration of the Solver

In order to compare the simulation with the experimental results. The physical parameters that were implemented in the simulation correspond with one of the experimental points that is described by Schmitt and Charpin (1979), the values of the parameters are described in the table 5.1. It can be appreciated that the operating pressure is 83900 Pa which corresponds to the atmospheric pressure of the place where the experiment was carried out.

Table 5. 2: Physical parameters of the CFD simulation

Air speed	0.8395
Angle of Attack	3.06
Operating Pressure	83,900 Pa

The pre-processing also included the boundary conditions which are described in the table 5.3. The boundary conditions were defined according with the velocity regime which is transonic since the Mach number is 0.8395.

Table 5. 3: Boundary Conditions of the simulation

Surface	Boundary Condition
Inlet	Pressure far field
Outlet	Pressure outlet
Wing surfaces	Wall
Wing root surface	Symmetry
Other walls	Pressure far field

Considering that the objective of this simulations is the validation of the CFD model. The steady step option was selected and the dynamic mesh was omitted.

5.3 Post-Processing ,results and validation

The simulation ran and converged successfully. The convergence graphs can be appreciated in the appendix G. The post-processing consisted in getting the graphs of the pressure coefficients in the sections whose locations are indicated in figure 5.1. Figure 5.7 illustrates the data that was obtained from the simulation, they are graphs of the pressure coefficients in the upper surface and the lower surface of the wing. The reference of the position in the

chordwise direction is the leading edge of each cross section along the wing span. It also can be observed that the position along the chordwise is normalized (x/c) being c the chord length at the corresponding cross section. A post-processing was carried out in Excel to compare the simulation results with the experimental data which were taken from Slater (2008) .

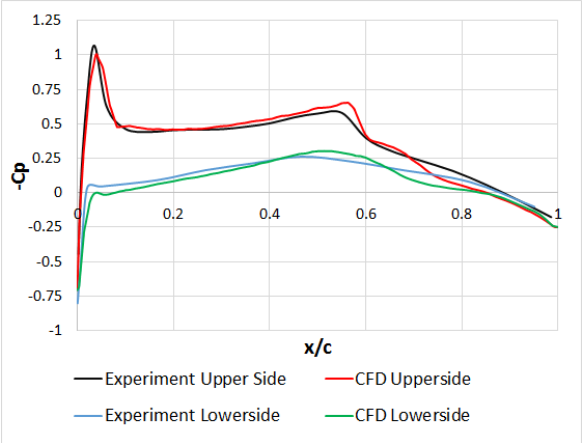

a) y/b= 0.2

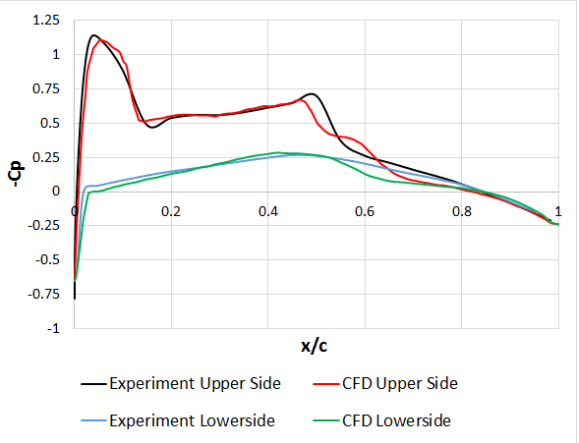

b) y/b=0.44

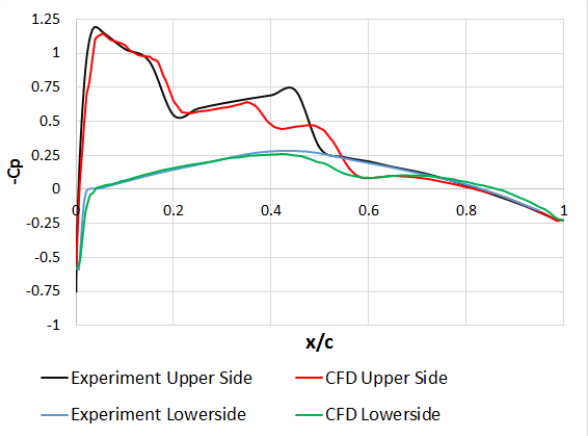

c) y/b=0.65

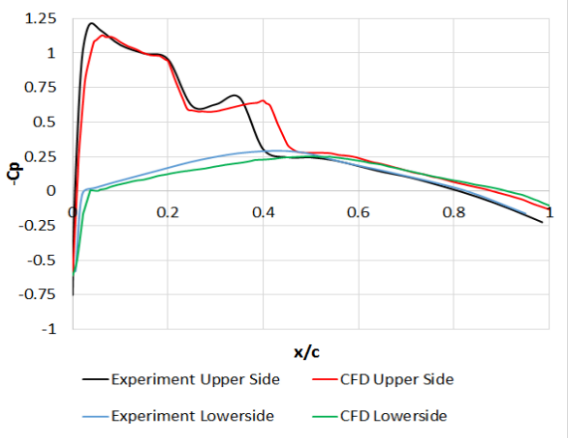

d) y/b= 0.8

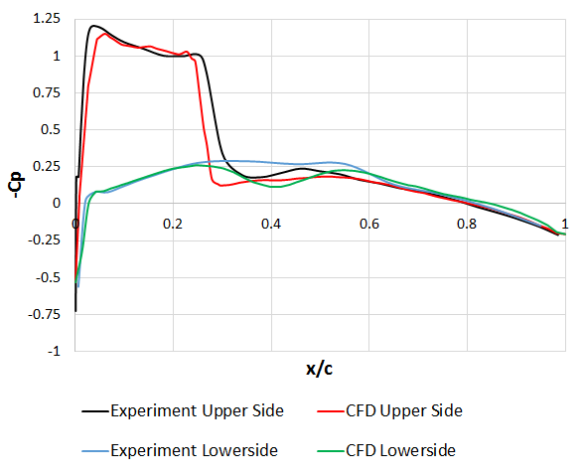

e) y/b= 0.9

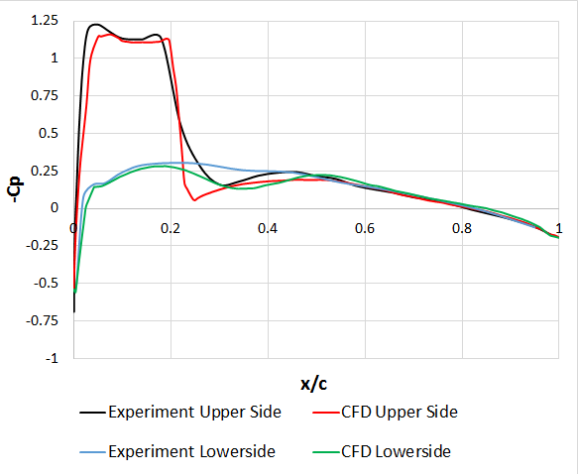

f) y/b = 0.95

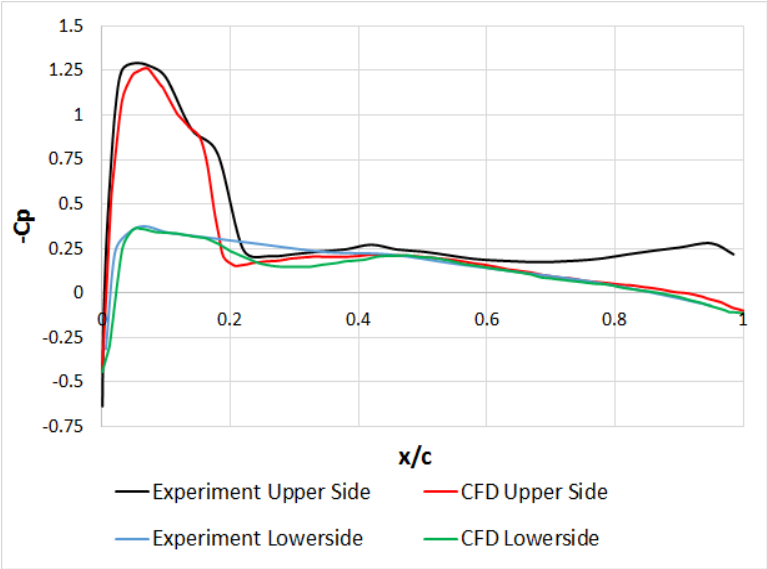

h) y/b = 0.99

Figure 5. 7: Graphs of pressure coefficients at different cross sections (y/b) along the wing span

The graphs in figure 5.7 show that the results from the CFD simulation match the experimental results with good precision. However, the graphs at the sections y/b=0.65 and y/b=0.8 of the wing span show a difference between the simulation and the experiment in the medium part of the chord wise. It seems that there are shock waves in this area that the simulation does not capture. To determinate the causes of the differences between the experiment and the simulation are necessary sensitivity studies with respect to aspects such as the turbulence model, the algorithms and the grid. Other measures that could help to improve the matching. For example, refining the resolution of the boundary layer to y+ of 1, and further stream wise refinement of the mesh may contribute to capture the shock waves on the upper surface (Slater 2008). However, since the conclusion is that the comparison is good overall, additional refinements were not considered necessary to perform the FSI simulations in the next stage of the project.

5.4 Mesh Independence Analysis

Another simulation with a higher resolution grid was performed in order to perform a mesh convergence analysis. This simulation has a mesh with 896,776 tetrahedral elements, it has almost two times the number of elements of the simulation presented previously which has

a mesh with 453,550 tetrahedral elements. The analysis consisted in the comparison of the pressure coefficients in one of the cross sections whose locations are indicated in figure 5.1.

Figure 5.8 illustrates the comparison of results. The mesh with 896,776 elements was called "fine mesh", while the mesh with 423,550 elements was called rough mesh. It can be seen that differences between the results of the fine mesh and the rough mesh is very small. Even, the difference between the pressure coefficients for the lower side can not be identified because the graphs are practically overlapped. This graph, and the fact that the simulation results match the experiment, point out that the results are reasonably independent of the mesh resolution.

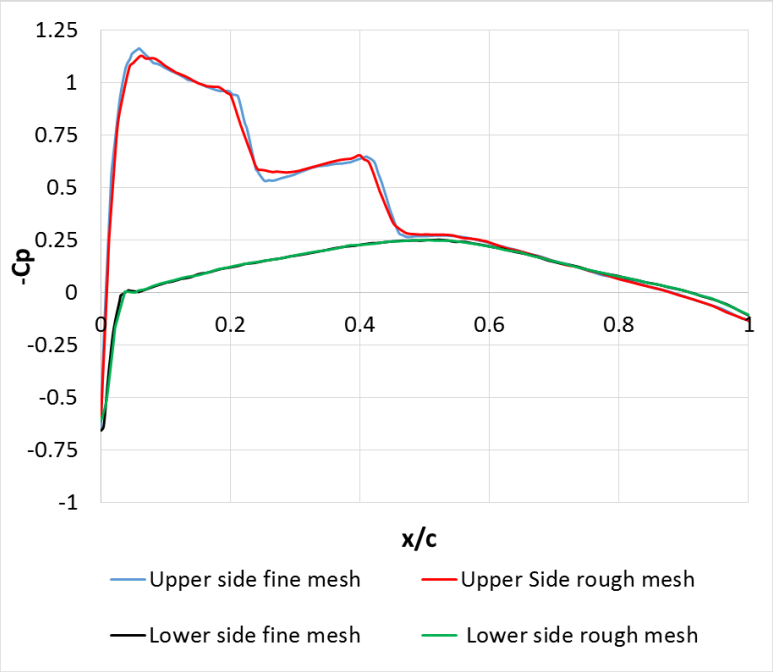

Figure 5. 8: Comparison between fine and rough mesh

5.5 Conclusion of the steady state simulation

The validation of the steady state simulation, and the results of the mesh independence analysis have shown that the values of the CFD simulation parameters provide reliable results. These parameters provide solid bases to undertake the FSI simulation, they are especially useful because a big part of these mesh parameters and simulation parameters are implemented in the configuration of the Fluent module in the FSI simulation that is described in the next chapter.

CHAPTER 6

Pre-processing of FSI Simulation

This chapter presents the pre-processing of the FSI simulation of a wing with the external shape of the ONERA M6 wing. The details of the internal structure of the wing are described here as well as the details about the configuration of the solvers that participated in the FSI simulation. This chapter focus especially in the setup of the most relevant steps to get a successful FSI simulation for this kind of structures.

6.1 Structure of the Wing

The Wing that was simulated has the external shape of the Onera M6 wing that was described in the chapter 5. In contrast with the wing that was modelled to do the CFD, this wing has an internal structure that is composed of two spars, and three ribs. These internal components are covered by the skin that has the shape of the Onera M6 wing in its external face. Figure 6.1 illustrates the components of the internal structure. The dimensions of the internal structure can be observed in the appendix H.

The wing was modelled in the CAD software Solid Edge ST5 in the Part module, the file was exported to parasolid format (.x_t) in order to open the model in Ansys.

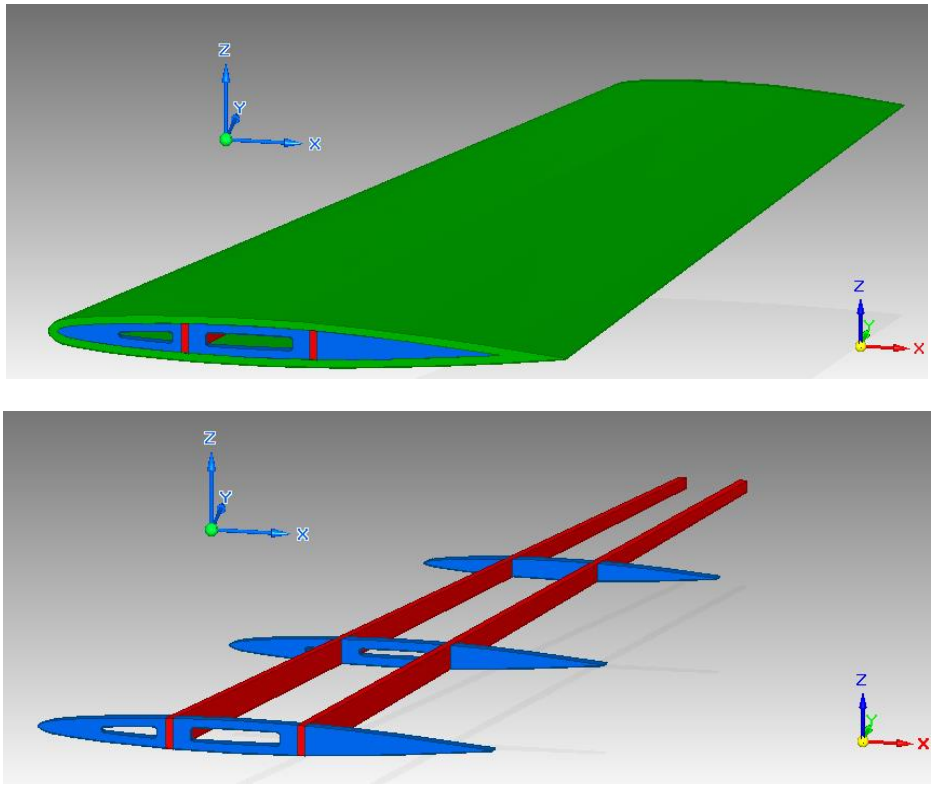

Figure 6. 1: External and internal structure of the wing based on the Onera M6 wing

6.2 Material

The Material that was used in this simulation is an orthotropic material whose properties are described in the table 6.1(Yates). These properties correspond to a type of wood that is denominated mahogany.

Table 6. 1: Material Properties

Property	Value
Density	381.98 Kg/m^3
Young's Modulus X direction	3.1511 X 10^9 Pa
Young's Modulus Y and Z directions	4.1622 X 10^8 Pa
Poisson's Ratio XY, YZ,XZ Planes	0.31
Shear Modulus XY,YZ,XZ Planes	4.3922 X 10^8 Pa
Thickness	0.012 m

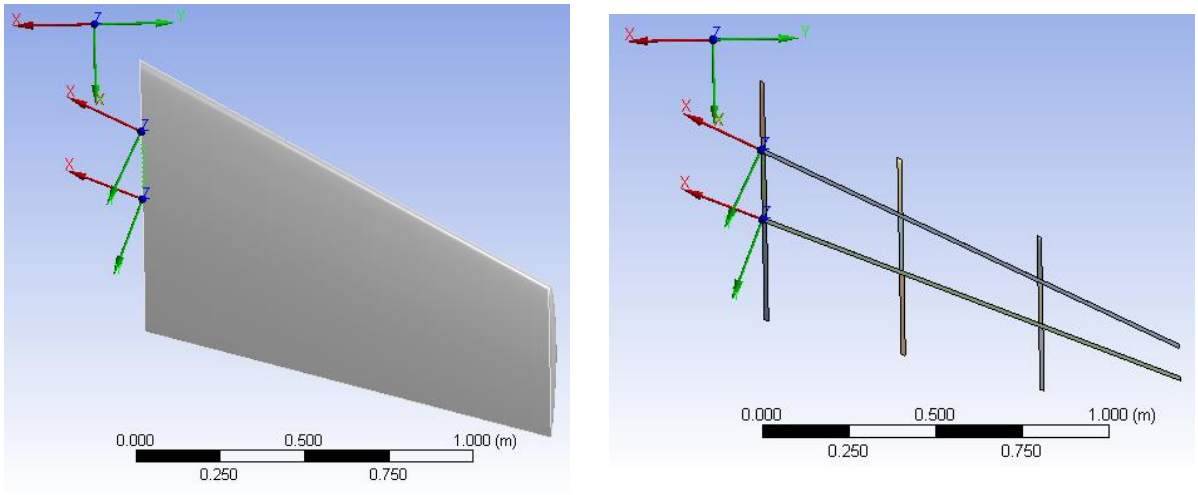

Figure 6. 2: Assigning properties to structural elements

To assign the material properties to the structural elements is necessary to define the direction of the main fibre in each component. To do this, it is necessary to define local coordinate systems taking into account that, according with the table 6.1, the direction of the fibre is in the X axis of the coordinate system. Then, the coordinate systems must be oriented according with the desirable direction of the fibre in each element. Figure 5.2 illustrates the local coordinate systems that were defined. It can be seen, for example, that there is a coordinate system located in the frontal spar whose X axis is oriented along the spar. Therefore, to assign the material properties to each components, it is necessary to point out which is the appropriate coordinate system.

6.3 Modal Analysis

A modal analysis of the wing was carried out in Ansys. The objective of this Analysis was the identification of the natural frequencies that in turns are necessary to determine the appropriate time step and the end time in the subsequent FSI simulation.

The modal analysis in Ansys was carried out through the module 'Modal' of Ansys. A Boundary condition of fixed support was imposed in the root of the wing to simulate the join of a clamped wing. Ansys recognized automatically the contact surfaces between the structural components, this is an important feature to simulate the joins that exist between the structural parts since they affect significantly the frequency response. The figure 6.3 illustrates one of the contact surfaces that was identified by Ansys, in this case, this is the contact surface between one of the ribs and the internal face of the skin.

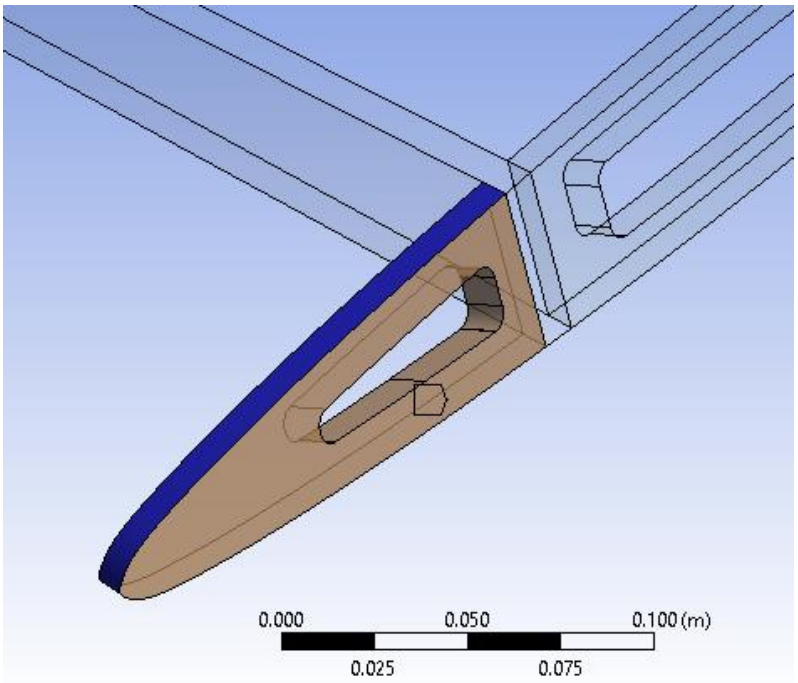

Figure 6. 3: Surface contact between a rib and the skin

Similarly to the Delta Wing Case, the table 6.2 points out that the mesh has some effect in the calculation of the natural frequencies. However, the effect of the mesh in this case in negligible since the difference due to the mesh are less than 0.07 % in terms of relative difference. The figure 6.4 illustrates the deformation pattern for the 1st mode with 96,973 elements in the mesh.

Table 6. 2: Natural Frequencies of the wing

Mode	**Type**	**Frequencies in the Simulation: Modal Analysis**		
		Number of Elements		
		48,959	**96,973**	**189.262**
1	1st bending	17.139 Hz	17.131 Hz	17.127 Hz
2	2nd bending	63.129 Hz	63.064 Hz	63.026 Hz
3	1st torsion	79.009 Hz	78.918 Hz	78.878 Hz
4	3rd bending	134.76 Hz	134.55 Hz	134.41 Hz
5	2nd torsion	141.99 Hz	141.94 Hz	141.92 Hz
6	Bending-torsion	170.95 Hz	170.57 Hz	170.38 Hz

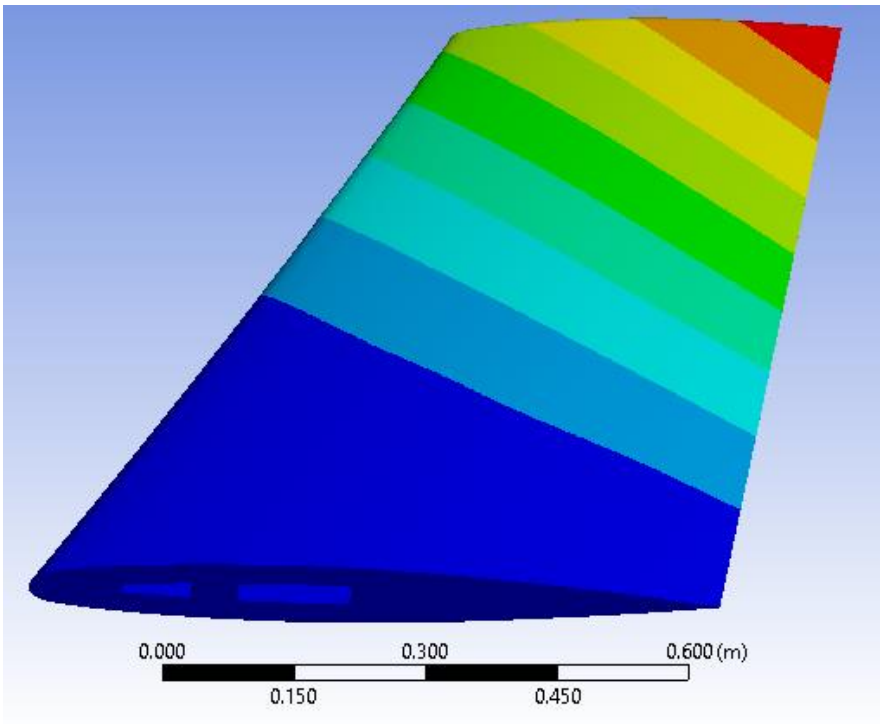

Figure 6. 4: Deformation pattern for the 1st mode with 96,973 elements

6.4 FSI Simulation Pre-processing

The configuration of the FSI simulation of the Delta Wing and the Onera M6 wing have a lot of aspects in common. Therefore, only the aspects that differentiate this simulation from the delta wing simulation are explained in this section.

Similarly to the delta Wing, a 2-way coupling simulation was used to model the behaviour of the ONERA M6 wing that was described before. Figure 6.5 illustrates the general layout of the FSI simulation applied in this case.

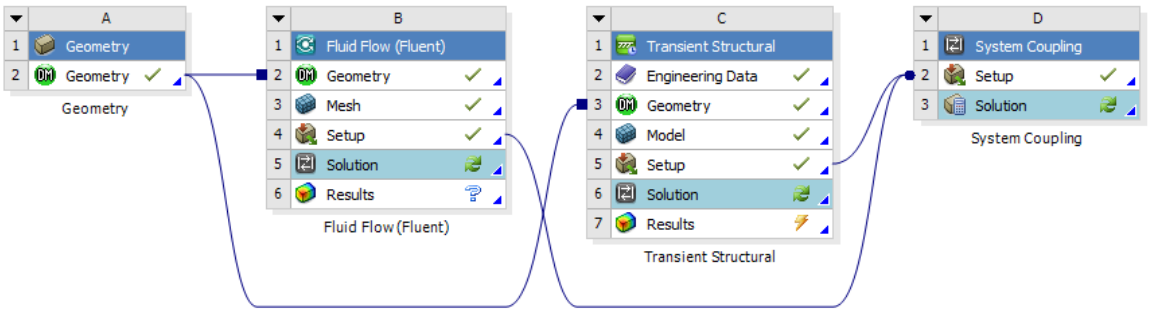

Figure 6. 5: Layout of the Delta Wing FSI simulation in Ansys-Workbench

It is important to note that many of the parameters used in this simulation were defined through a process of trial-and-error in order to achieve the completion of the simulation avoiding errors during the execution. This trial-and-error process was especially necessary in the FLUENT (module B) solver and the System Coupling (module D).

6.4.1 Geometry Module

The Geometry in FSI simulations has to include two volumes which corresponds to the volume of the structure and the volume of the fluid Domain. To model the geometry in Ansys was used an independent geometry module.

The process to model the geometry of the fluid domain and the wing structure was explained in the chapter 3 and 5. However, in this case was necessary to export the CAD model of the wing from Solid Edge ST5 using the parasolid format (.x_t) . It is important to verify in Ansys that the CAD model is make up of solid bodies in all its components, otherwise, if the software recognizes surfaces instead of bodies, there would be many problems to get a suitable mesh. The parasolid format was the only format that allowed the recognition of solid bodies in all the structural components.

The fluid domain has the same dimensions of the fluid domain in the CFD steady state simulation that was described in the chapter 5. Similarly to the Delta wing. It is necessary to preserve the body of the wing, therefore, the option to preserve tool bodies was set up as Positive. To perform the FSI simulation, it is also necessary to define two named surfaces that will allow the coupling between the Transient structural module and the Fluent module. These surfaces correspond with all the wing surfaces, except the root. They were named as “wall_cfd_coupled” and “wall_fea_coupled”.

6.4.2 Fluid Flow Module (Fluent)

The figure 6.5 shows a connection between the cell A2 and the cell B2. This connection means that the Fluent module (module B) takes the geometry of the geometrical domain from the Geometry module (module A).

6.4.2.1 Mesh

The mesh of the fluid domain was carried out in the meshing module of Ansys-Fluid Flow (Fluent) which is open through the cell B3 of the workbench space. The Mesh applied in this simulation has the same parameters and principles of the mesh used in the CFD steady state simulation described in the chapter 5. However, a mesh inflation over the wing surface was also implemented, the inflation was applied specifically to the named surface "wall_fea coupled" which was used as the coupling surface in a subsequent step. The inflation was applied mainly to help the remeshing operation that is essential in a FSI simulation, the inflation also contributes to capture better the boundary layer. The figure 6.6 illustrates part of the inflation mesh at the root of the wing.

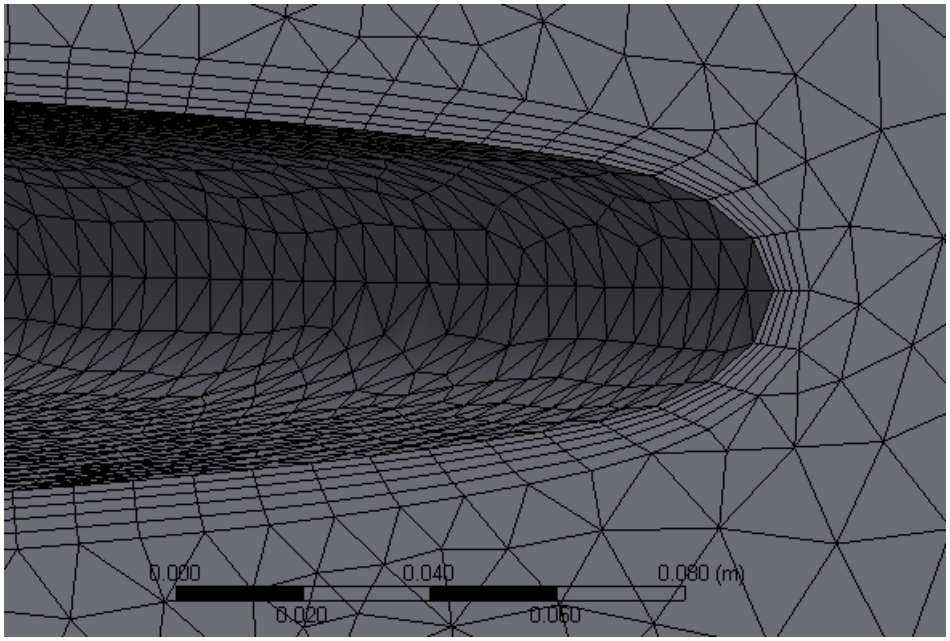

Figure 6. 6: Mesh Inflation at the wing root

The Mesh of the geometrical domain has 588,769 tetrahedral elements and 176,201 nodes. The orthogonal quality has an average of 0.87, the skewness has an average of 0.23. Other details of the mesh are described in the appendix I.

6.4.2.2 Solver Configuration

The configuration of the FLUENT– Solver is developed in the tab "Set up" (cell B4). A big part of the configuration was taken from the CFD steady state simulation that was described

in the chapter 5. For example, the boundary condition are the same. The main difference in the FSI configuration is the Dynamic Mesh that is indispensable to complete the simulation and avoid errors during the execution.

6.4.2.2.1 Dynamic Mesh

The main parameters of the dynamic mesh were explained in the chapter three. The values for the parameters used in this simulation were defined by a process of trial-and-error and they are described as follow.

- Smoothing.

  The option of smoothing that was used in this simulations was diffusion based on boundary distance. The value of the diffusion parameter that was used in these simulations was 1.5 which is considered as a high value for this parameter. The effect of this parameter value was the increment in the absorption of the mesh motion due to the moving boundary, this effect is present especially in the zones away from the moving boundary. Thus, there is also an increment in the capacity to preserve the mesh quality near to wing surface

- Remeshig

  The remeshing was not applied in this simulation because this function consumes a lot to computational resources and time which in these case was critical because the available computational resources were used at the limit of their capacity.

- Dynamic Mesh Zones

  The dynamic mesh zone is the surface called “Wall_cfd_coupled” .This surface was selected because it is the wetted area of the wing. The type of dynamic mesh zone that was selected for the surface “Wall_cfd_coupled” was the option “system coupling” because this surface can receive displacements from the System Coupling. In other words, it receives the displacement from the wing.

6.4.3 Transient Structural module

The Transient structural module takes the geometry of the wing from the geometry module. The material and the process to assign the material properties to each structural component are the same that were described in the section 6.2.

6.4.3.1 Mesh and Boundary Conditions

The tab 'model' opens the Mesh module of Ansys-Transient Structural. The first step in this module is the verification of the contact regions that Ansys usually recognizes automatically. Similarly to the Modal Analysis, these contact zones are essential to model correctly the behaviour of the wing.

To mesh the wing were applied two size functions. They were applied to the trailing edge at the root and at the tip as it is illustrated in the figure 6.7. The Boundary condition was applied through a fixed support in the wing root surface as it is illustrated in the figure 6.8.

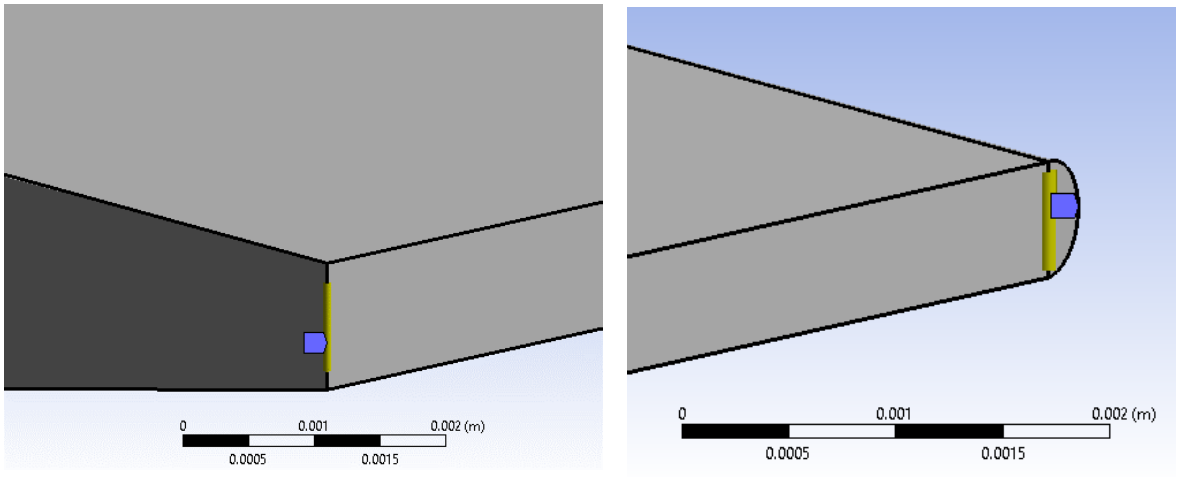

Figure 6. 7: Size functions applied to the mesh

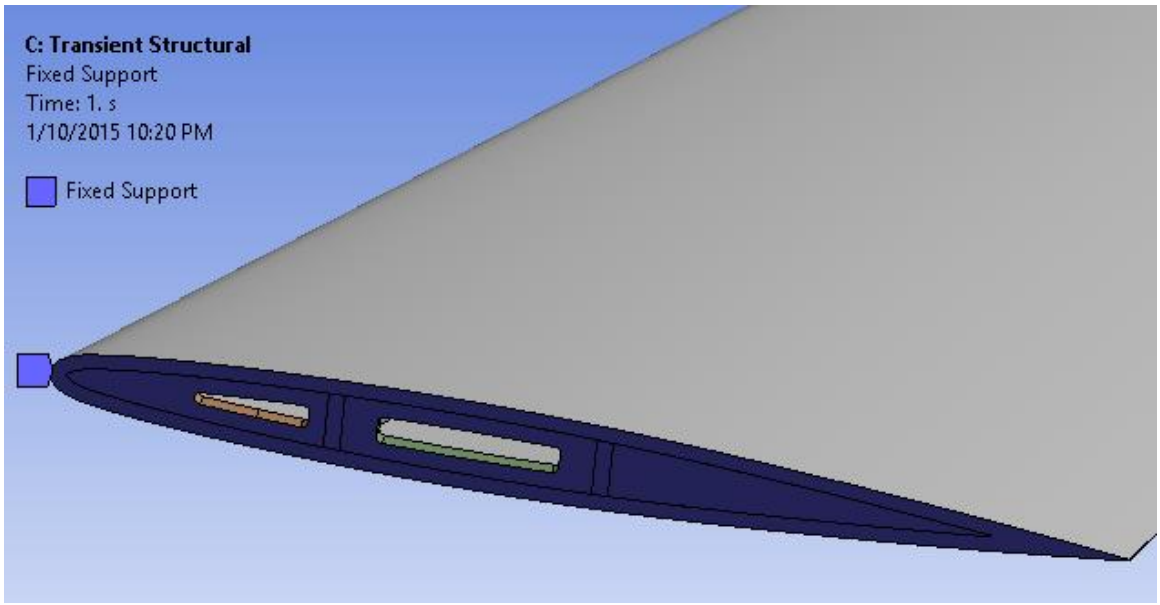

Figure 6. 8: Boundary Condition: Fixed support in the wing root face

The mesh of the wing structure is illustrated in the figure 6.9. It can be appreciated the effect of the size functions, which is getting elements with small thickness in the trailing edge to fit the original geometry. The mesh of the wing has 48,766 tetrahedral elements and 107,933 nodes. The orthogonal quality has an average of 0.8, the skewness has an average of 0.33. Other details of the mesh are described in the appendix J.

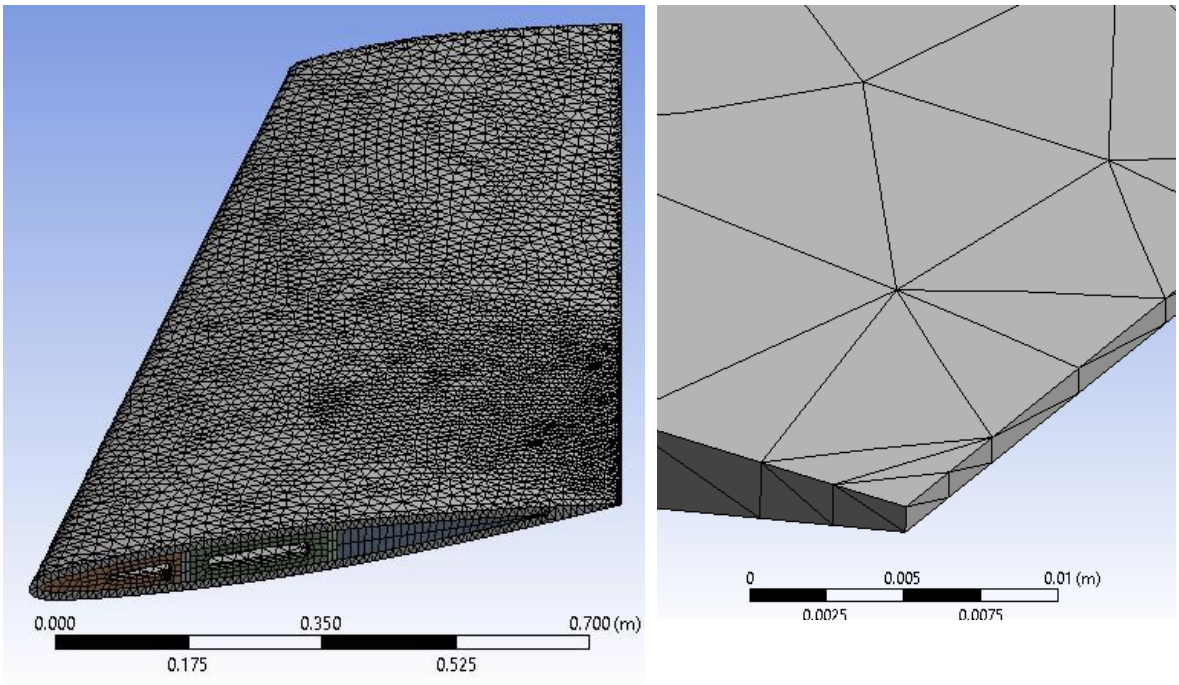

Figure 6. 9: Mesh of the wing structure

6.4.3.2 Solver Configuration

The set-up tab in the Transient Structural Module (cell C5) allows the configuration of parameters for the coupling with the fluid system. As explained in the chapter 3, the most important aspect in this stage is the definition of the Fluid Solid Interface. The surface called "wall_fea_coupled" was selected to be the Fluid Solid Interface. It can be observed in figure 6.10 that this surface is the wetted area the wing, which means that it include all the external surfaces of the wing except the surfaces on wing root.

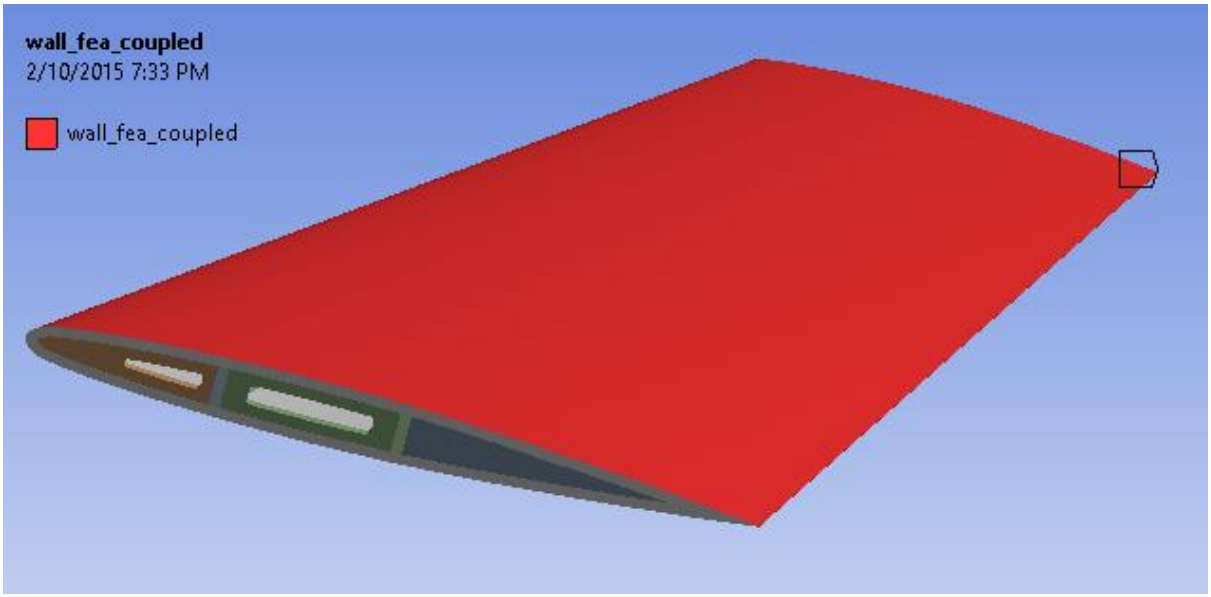

Figure 6. 10: Fluid Solid Interface in the Transient Structural Model

6.4.4 System Coupling

The configuration of the System Coupling Module (module D figure 6.5) is very similar to the configuration used in the Delta Wing Simulation. The main difference consisted in the time step and the end time that were used. Table 6.3 illustrates the parameters and transfer operations used in this simulation.

Table 6. 3: Configuration of the System Coupling

Transfer 1	Transfer Variable:	Force
	From:	Fluent
	To	Transient Structural
Transfer 2	Transfer Variable:	Incremental Displacement
	From:	Transient Structural
	To	Fluent
Time Step	0.0001 s	
End Time	0.5 s	

The selection of the time step and the end time is determined mainly by the natural frequencies of the wing that were calculated in the modal analysis. As was mentioned in the chapter 3, the time step should be small enough to capture the behaviour of the vibrations modes of the wing or at least to capture the behaviour of the first vibration mode. The end

time should be long enough to cover one period of the first vibration mode, and also long enough to allow the visualization of the relevant dynamic behaviours.

Therefore, the Time step was defined by the following procedure.

1. Calculation of the period of the first vibration mode. The frequency was taken from the table 6.2. Considering the mesh with 48,959 elements because it is the closest mesh resolution to the mesh used in this simulation.

Frequency first mode

$f = 17.139\ Hz$

$$T = \frac{1}{f} = \frac{1}{17.139\ Hz} = 0.05834s$$

2. To get enough points to describe the dynamic behaviour is recommended to have at least 20 point in the period of the first vibration mode.

$$Time\ step = \frac{T}{20} = \frac{0.05834s}{20} = 0.002919s$$

Therefore, a time step less than 0.002919 s is appropriate for the simulation.

Multiple values of the time step were tested in the simulation, beginning with 0.0029 s and decreasing the time step, however the simulations were not successful since errors appeared and interrupted the execution in the first time steps. Then it was necessary to reduce the time step until 0.0001 s to get a simulation working beyond the first time steps. The end time was selected to be 0.5 s in order to appreciate relevant dynamic behaviours.

The reduction of the time step increased significantly the amount of memory in the hard disk used by the simulation and the time to perform the simulation. The size of the files was in the order of hundreds of Gigabytes and the execution time was in the order of weeks. The specification of the computational resources used to perform the simulations and the specification of the files is described in the appendix K.

Chapter 7

Post-processing of FSI Simulation and Results

This Chapter presents the results and analysis of the FSI simulations in Ansys-Fluent that were described in the chapters 6. In addition, it also presents a simulation of the Onera M6 wing in Patran-Nastran that was carried out in order to validate the results obtained in Ansys.

This Chapter also presents a simulation in Patran-Nastran that was also carried out in order to validate the results obtained in Ansys. This program uses an aeroelasticity solver based on the Doublet-Lattice method to solve flutter problems. The relevant details of the configuration in Patran-Nastran, the results of this simulation, and the comparison with the results obtained in Ansys are described in the second half of this chapter.

7.1 Results of FSI simulations

Three FSI simulations in Ansys-Fluent with different dynamic pressures were performed in order to find the dynamic response of the wing structure. These simulations required a

different post-processing in comparison with the delta wing because they were executed from the command line and not from the workbench as it was in the delta wing Simulations.

7.1.1 Execution and Post-Processing from the Command Line

First, it is important to note that these simulations required better computational resources than the simulations of the delta wing described in the chapters three and four. The complexity of the wing structure is the main cause of the growing demand of computational resources since the wing based on the Onera M6 wing has an internal structure while the Delta wing is a simple flat plate.

The complexity of structure also caused the increment in the space of hard disk memory employed by the result files. The results files used hundreds of gigabytes of the storage capacity. As a consequence, only three simulations were conducted to avoid running out of memory space in the hard disk.

In addition to the use of a better computer, these simulations also required a different method of execution and post-processing. The traditional method, which is the use of workbench, is the easier method to run the simulation and generate the relevant results, but it is also more expensive in term of computational resources employed. There is an alternative method to run the simulation and conduct the post-processing, it is the execution using the command line (Miller 2012), this method is more difficult to use but it demands less computational resources during the execution. The difference between the two methods is considerable in terms of execution time since the execution form the workbench could be 3 or 4 times longer than the execution from the command line using the same hardware.

7.1.2 Post-Processing Procedure

The post-process in this case consisted in the calculation of the accelerations in the wing, especially, the accelerations in the tip, since this is the part of the wing that is supposed to undergo the highest accelerations due to the bending deformation. The procedure to collect the results was applied to all the simulations of the Onera M6 wing. All the results and graphs that are illustrated in this section corresponds to the parameter described in the table 4.1.

Table 7. 1: FSI simulation parameter of the Onera M6 wing

Angle of Attack	3.03 º
Air speed	34 m/s
Number of element in wing mesh	48,766
Number of elements in fluid flow mesh	588,769
Solver	Density-Based
Model	Viscous-SST K-omega

The procedure to collect the results consisted in the following steps:

Step 1: **Verification of Convergence**

Similarly to the FSI simulation of the delta wing, the convergence was verified in the system coupling report. The figure 7.1 illustrates one section of the solution report where it can be appreciated the coupling iteration 1 and 2 of the time step 665 that corresponds with the time 0.0665 s. The Fluid Flow (Fluent) solver did not converged in the iteration 1. In the iteration 2, both solvers and both transfer operations converged. Then, the simulation moved on to the next time step.

COUPLING STEP = 665	SIMULATION TIME = 6.65000e-02	
Solver	Solution Status	
Data Transfer		
Diagnostics	Source Side	Target Side
COUPLING ITERATION = 1		
Transient Structural	Converged	
Data Transfer	Converged	
Change:RMS	1.71330e-04	1.36671e-04
Fluid Flow (Fluent)	Not yet converged...	
Data Transfer 2	Converged	
Change:RMS	5.17999e-03	5.31539e-03
COUPLING ITERATION = 2		
Transient Structural	Converged	
Data Transfer	Converged	
Change:RMS	1.18160e-02	9.90701e-03
Fluid Flow (Fluent)	Converged	
Data Transfer 2	Converged	
Change:RMS	5.96966e-05	6.09298e-05

Figure 7. 1: Solution Report of the System Coupling

Step 2: Calculation of the relevant information in the Wing Tip.

The accelerations and displacements in the tip were collected, but only the leading edge and the trailing edge at this section were considered. These magnitudes were calculated in the global Z direction which correspond with the perpendicular direction to the wing plane. Figure 7.2 illustrates an example of the information collected at this stage.

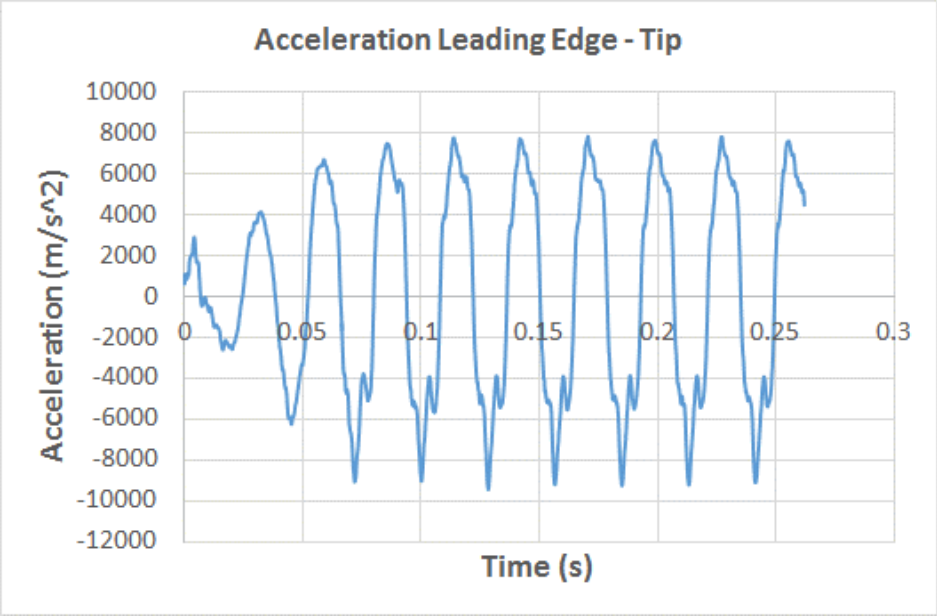

Figure 7. 2: Acceleration in the Leading Edge

7.1.3 Results

As mentioned before, three simulations were carried out. A different dynamic pressure was used in each simulation. The dynamic pressure was defined through the operating pressure in Fluent, the following values were implemented.

Table 7. 2: FSI Simulations of the Onera M6 Wing

Simulation	**Operational Pressure**
Simulation 1	67,120 Pa
Simulation 2	83,900 Pa
Simulation 3	100,680 Pa

The results of each simulation are described below

7.1.3.1 Simulation 1.

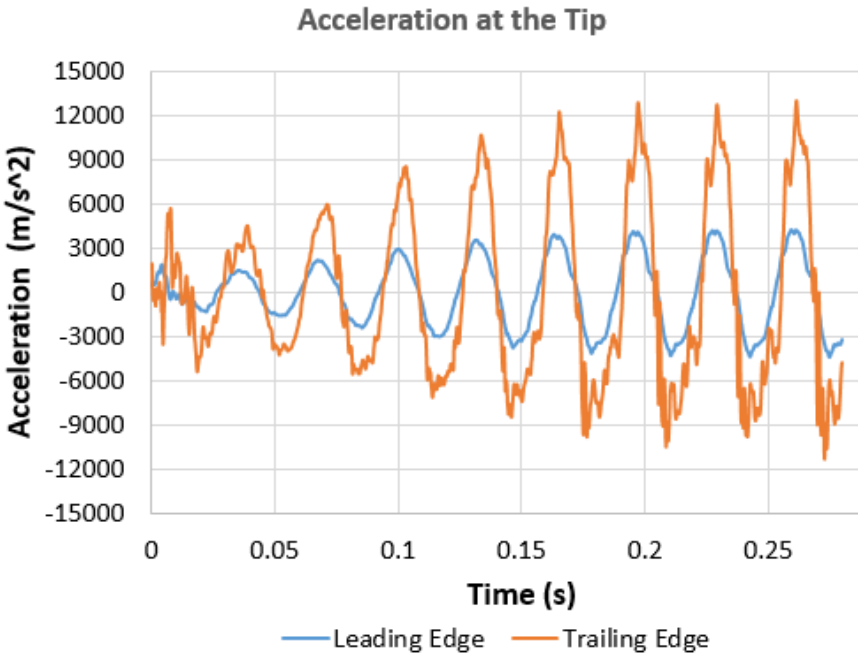

Figure 7. 3: Acceleration at the tip in simulation 1

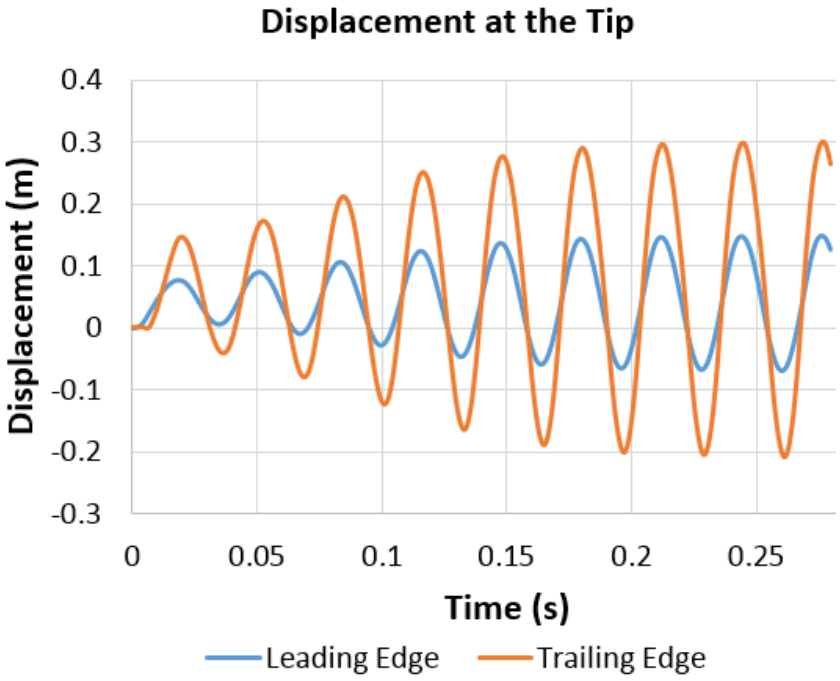

Figure 7. 4: Displacement at the tip in simulation 1

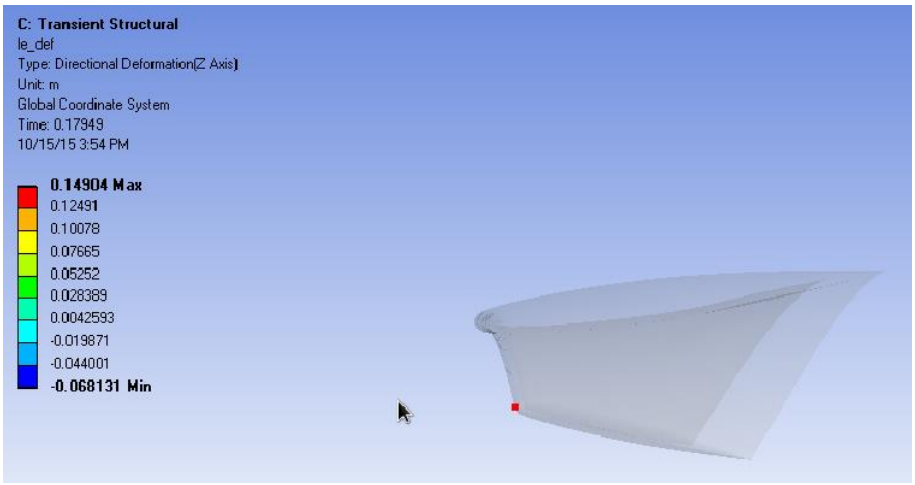

Figure 7. 5: Side View of the wing in simulation 1 at 0.17949 s

7.1.3.2 Simulation 2

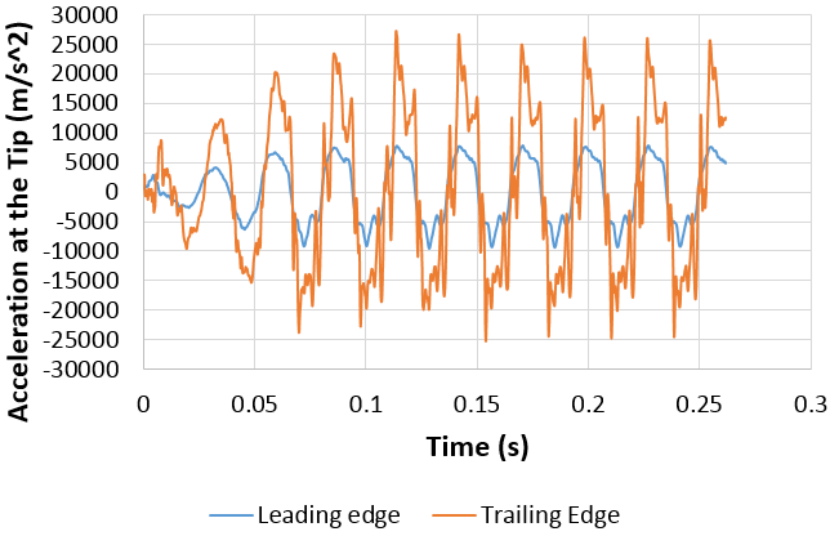

Figure 7. 6: Acceleration at the tip in simulation 2

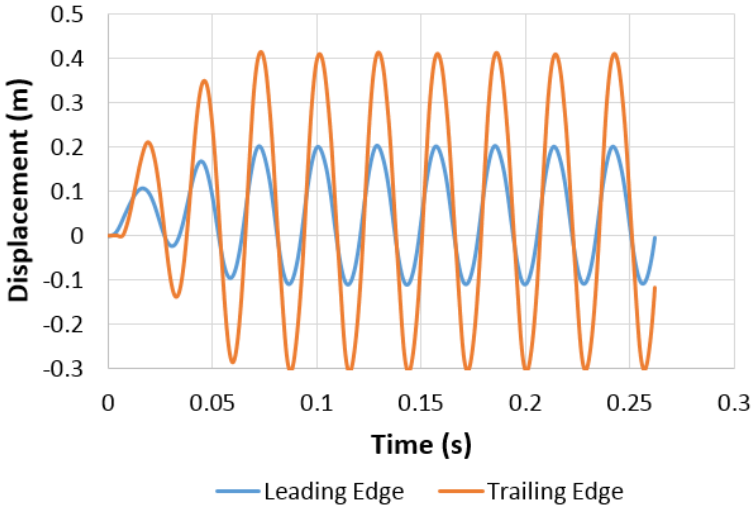

Figure 7. 7: Displacement at the tip in simulation 2

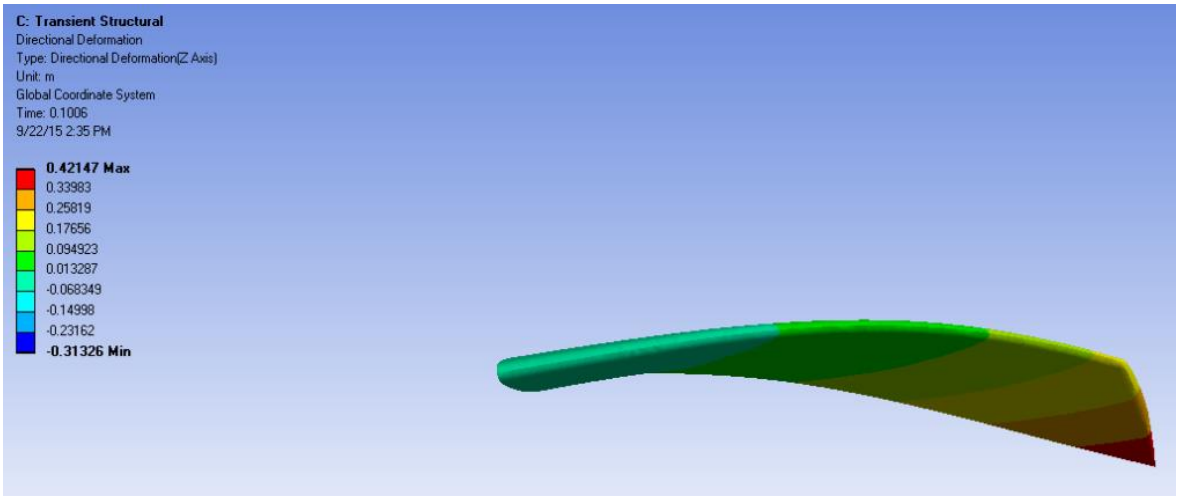

Figure 7. 8: Directional Deformation (Z axis) in simulation 2 at 0.1006 s

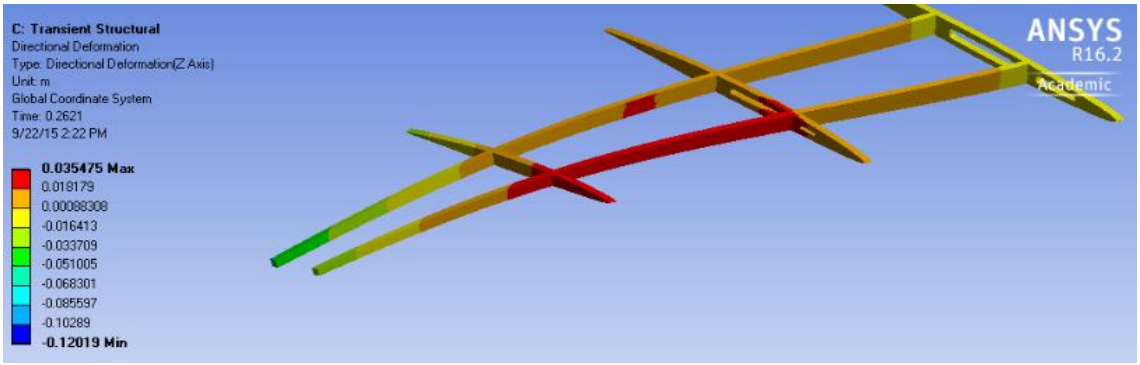

Figure 7. 9: Directional Deformation (Z axis) of the internal structure in the simulation 2 at 0.2621 s

7.1.3.3 Simulation 3

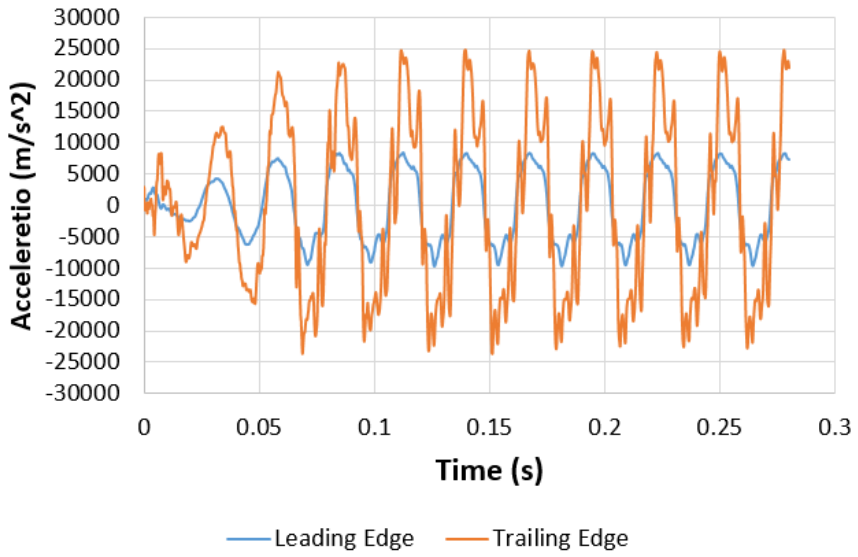

Figure 7. 10: Acceleration at the tip in simulation 3

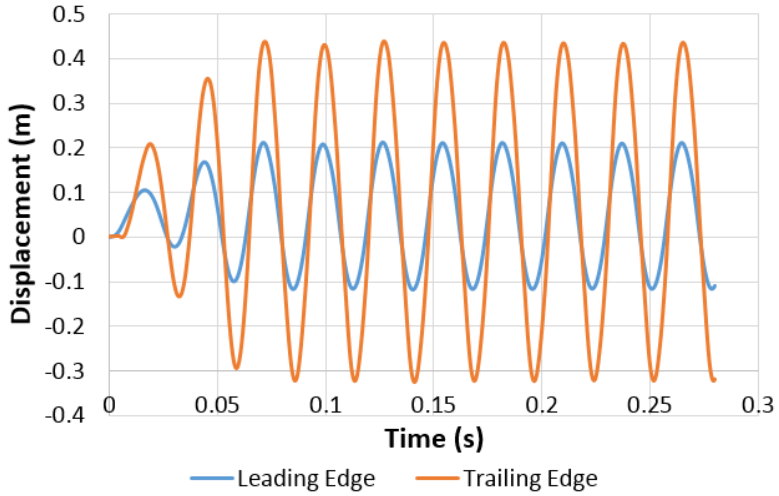

Figure 7. 11: Displacement at the tip in simulation 3

7.1.4 Analysis of Results

Overall, the results of the three simulations show a significant deformation of the wing that occurs under the effect of very high acceleration values. The following physical aspects stand out in the results.

First, the dynamical response in all the simulations is a Limit Cycle Oscillation, which is considered as a stable flutter condition. In addition, in all the cases, the maximum amplitude is reached in few cycles.

Second, the displacements and accelerations of the trailing edge are significantly higher than the accelerations and displacements of the leading edge. This suggest than, in addition to the bending deformation, the twisting of the wing is also present. However, the motions of the leading edge and the trailing edge seem to be synchronized since the graphs of acceleration and displacement seem to be in phase, which means that both points are moving in the same direction all the time.

Third, all the graphs of accelerations and displacements are asymmetric, in other words the maximum values and minimum values are different. The asymmetry in the displacement graphs is higher than in the acceleration graphs. This asymmetry could be explained by the angle of attack, that is 3.03° for all the simulations. Due to this angle of attack, the fluid flow has a small component in the perpendicular direction of the wing. Therefore, despite the fact that the wing is oscillating, it is pushed by the fluid flow in the positive Z direction

of the Global Coordinate System. A similar behaviour was observed in the delta wing at 1° in the angle of attack.

Fourth, the increment in the dynamic pressure provokes the increment in the maximum amplitude of the accelerations and the displacements. This phenomenon can be noted especially when the simulation 1 and 3 are compared. This behaviour could be explained by the fact that the aerodynamic loads on the wing are directly proportional to the dynamic pressure (NASA 2015).

7.2 Simulation in Patran - Nastran

Patran - Nastran is a commercial software of Finite Element Methods that is widely recognized by the engineering and research community. It has two environments, Patran, which is a pre-processing and post-processing software, and Nastran, which is primarily a solver for the finite elements analysis.

Nastran can perform different type of analysis, each type of analysis is called a solution sequence code. One of them is the solution sequence 145 - Flutter / Aeroservoelastic analysis which was used in this project. This program also uses the Doublet-Lattice method to solve the aerodynamics and the Infinite Plate Spline method to connect the aerodynamic and structural grids.

As any finite elements Software, it needs a pre-processing that is described below.

7.2.1 Geometry

Similarly to the process followed in Ansys. The Geometry of the Onera M6 wing, which was modelled in Solid Edge ST5, was exported or saved in parasolid format (.x_t). It is very important to verify that the CAD model has the correct units in Patran to ensure the use of a consistent system of units. It is also important to verify that the CAD model is composed by solid bodies. Other CAD entities, such as surfaces, could provoke problems in later stages of the analysis process.

7.2.2 Mesh

The meshing is composed of tetrahedral elements with a global edge length of 10 mm. The initial mesh had 328,857 nodes and 189,523 elements. This mesh is illustrated in figure 7.12.

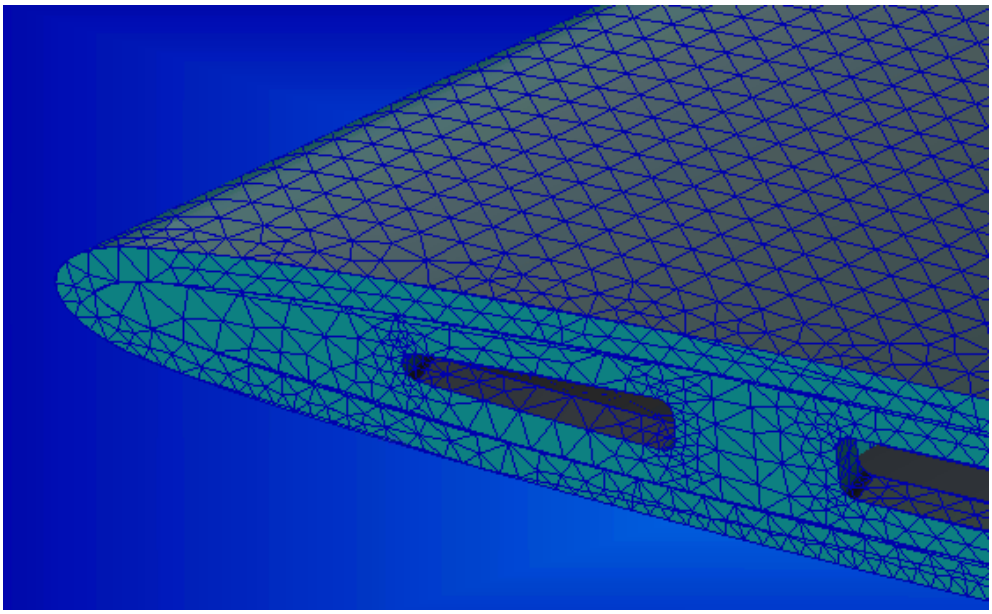

Figure 7. 12: Mesh of the Onera M6 wing in Patran

An additional step is necessary to ensure that the mesh of each structural component of the wing is attached to the adjacent components, this step is important because it represents the joins that exist between the components of the real structure. In Patran, this step is called Equivalence, and it has a similar effect to the contact relations between surfaces in Ansys.

As a result of the Equivalence operation, some nodes are deleted in the mesh. Figure 7.13 shows some of the nodes that were eliminated by the equivalence operation. 121 nodes were deleted. Therefore, the final mesh has 328,736 nodes.

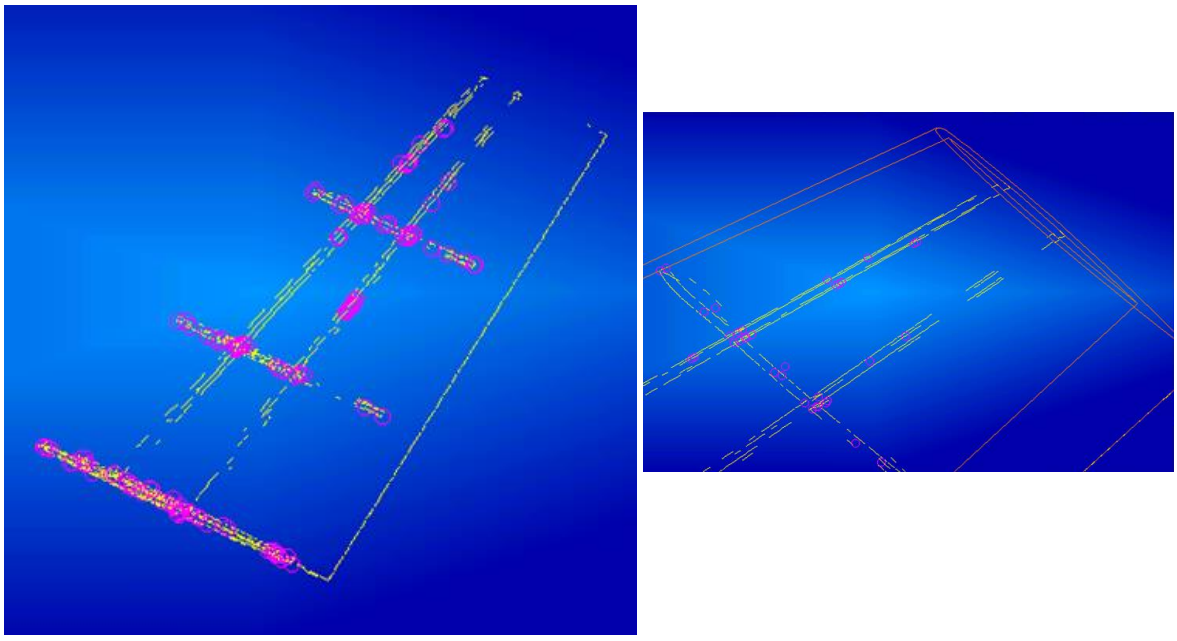

Figure 7. 13: Nodes that were deleted by the Equivalence operation

7.2.3 Material Properties

Similarly to the pre-processing in Ansys that was described in the chapter 6, the assignation of material properties to the structural elements requires the definition of the main fibre in each component, to do this, it is necessary the definition of local coordinates systems. Figure 7.14 illustrates the local coordinate systems defined in Patran, it can be seen that they are analogue to the coordinate systems illustrated in figure 6.2.

The properties of the material are the same that were defined in table 6.1.

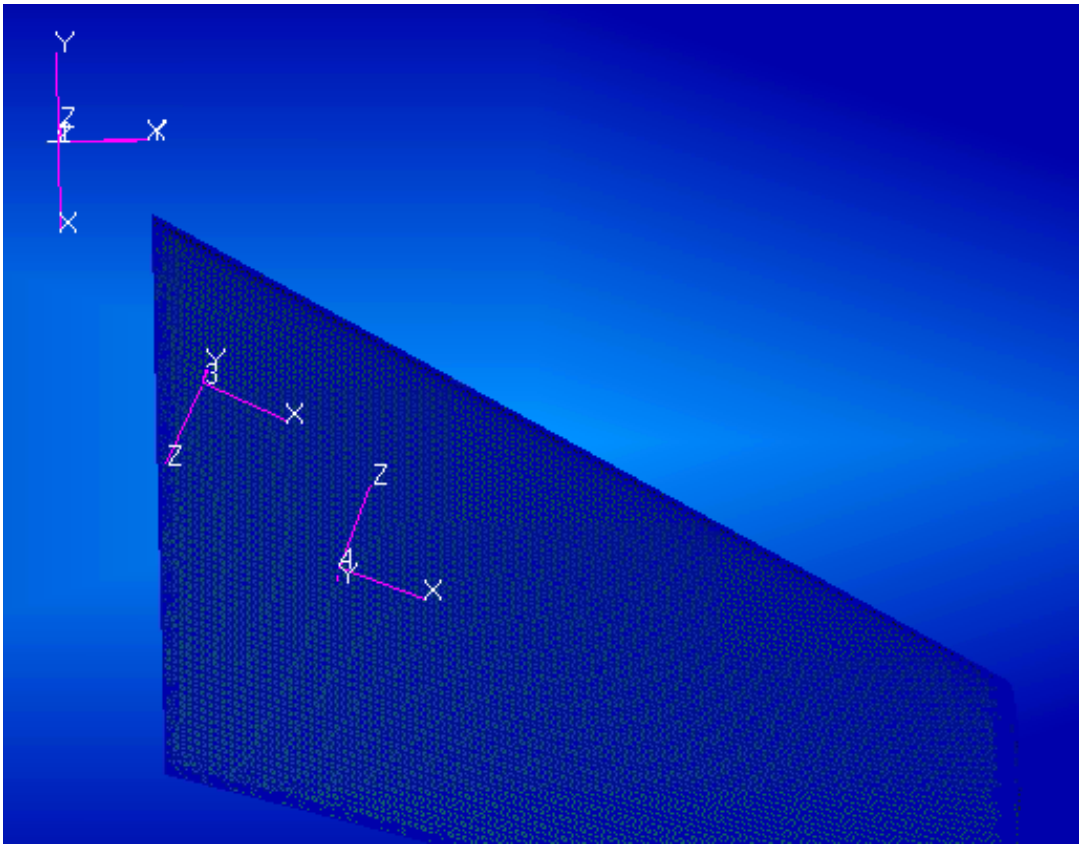

Figure 7. 14: Local Coordinate Systems in Patran

7.2.4 Boundary Conditions

Similarly to the process followed in Ansys, the boundary conditions were imposed in Patran through the definition of displacement equal to zero at the nodes that are located on the wing root surface, this restriction is equivalent to a wing clamped at its root. Figure 7.15 illustrates the definition of the boundary conditions in the wing.

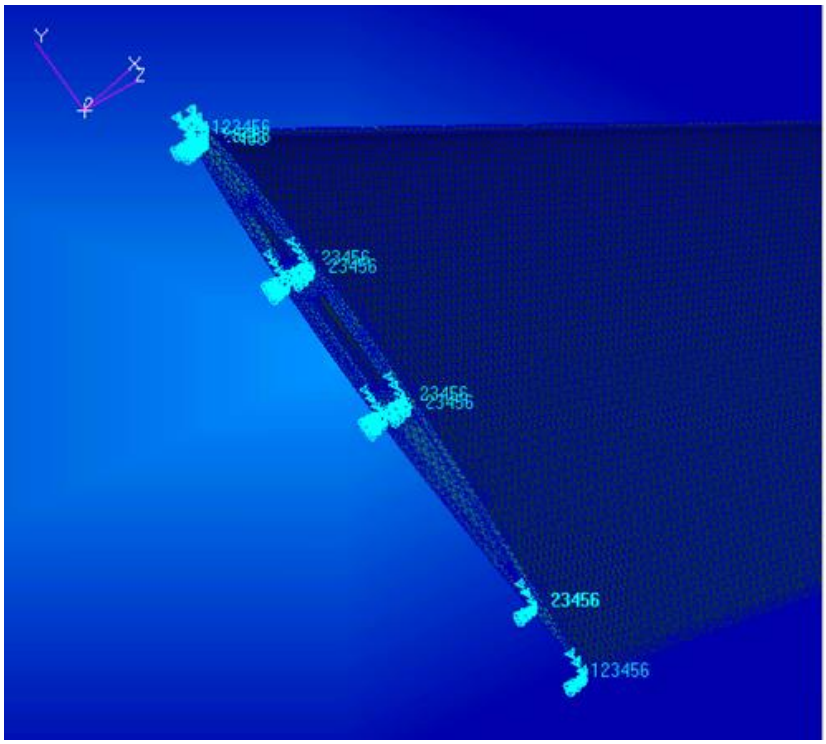

Figure 7. 15: Boundary Conditions applied in Patran

7.2.5 Configuration of the solution sequence 145

To run the simulation in Nastran is also necessary to prepare some files to introduce input data and the configuration of the solution sequence 145. These files are described briefly below.

aero.dat

This file contains the basic parameters for unsteady aerodynamics (MSC.Software 2009), the dimensions of the Onera M6 wing that are necessary to apply the doublet lattice method (DLM), and the data to perform the flutter analysis including the flutter method and the mach numbers to be used in the flutter analysis. In this simulation, the method PKNL was used, this method is a variation of the PK method with no looping.

It is important to note that wing profile of the Onera M6 wing and the angle of attack are not necessary in the solution sequence 145 because this simulation is based on doublet-lattice method (DLM) that only uses the platform geometry (top view) of the wing, and because this method uses the small angle approximation which is appropriate in this case since the angle of attack 3.03°.

set2.dat

This file contains the list of structural grid points in terms of aerodynamic macro elements (MSC.Software 2009).

./fine_mesh_oneraM6v1_struct.pdf'

This file contains the mesh of the wing structure, the boundary conditions and the coordinate systems that were described in the previous sections.

7.2.6 Results

The results of the flutter simulation in Nastran yield the damping coefficient for the range of speeds and Mach numbers that were defined in the setup of the solver 145. This information is provided for all the modes of motion which are called POINTS in Nastran.

The damping column for all the modes of motion can be scanned to see if a branch is going unstable, once a crossing is observed , the flutter velocity can be interpolated from the data that brackets the crossing (MSC.Software 2009), the velocities that correspond with the range of negative values of damping are stable, the velocities that correspond with the range of positive values of damping are unstable. Figure 7.16 illustrates sections of the solution file where it can be appreciated the column damping for the modes 1 and 2. The units of the velocities are mm/s.

The POINTS or modes of motion are presented in the ascending order of the frequencies associated with them. Therefore, the stability is usually determined by the first modes of motion because they have the lowest frequencies.

The figures 7.16 and 7.17 show that the critical flutter speed is defined by the cross point of the mode 1 and it corresponds with a value between 150 m/s and 200 m/s. In this case, the velocities higher than the flutter speed belongs to a stable regime.

MACH NO.	VELOCITY	DAMPING
1.47100E-01	5.00000E+04	4.10872E-01
2.94100E-01	1.00000E+05	6.64145E-02
4.40000E-01	1.50000E+05	8.03086E-02
5.80000E-01	2.00000E+05	-6.59298E-02
7.30000E-01	2.50000E+05	-2.54615E-01
8.00000E-01	2.75000E+05	-2.56974E-01
9.50000E-01	3.00000E+05	-1.98129E-01
1.02000E+00	3.25000E+05	-8.62610E-02
1.10000E+00	3.50000E+05	-9.54473E-02
1.17000E+00	3.75000E+05	-1.01568E-01
1.25000E+00	4.00000E+05	-1.06118E-01
1.32000E+00	4.25000E+05	-1.09665E-01
1.39000E+00	4.50000E+05	-1.12510E-01
1.47000E+00	4.75000E+05	-1.14841E-01

MACH NO.	VELOCITY	DAMPING
1.47100E-01	5.00000E+04	1.23704E+00
2.94100E-01	1.00000E+05	6.11348E-01
4.40000E-01	1.50000E+05	6.66188E-01
5.80000E-01	2.00000E+05	4.03537E-02
7.30000E-01	2.50000E+05	-1.77259E-01
8.00000E-01	2.75000E+05	-1.83372E-01
9.50000E-01	3.00000E+05	3.53258E-02
1.02000E+00	3.25000E+05	-6.12103E-02
1.10000E+00	3.50000E+05	-5.65170E-02
1.17000E+00	3.75000E+05	-5.37916E-02
1.25000E+00	4.00000E+05	-5.18861E-02
1.32000E+00	4.25000E+05	-5.04506E-02
1.39000E+00	4.50000E+05	-4.93232E-02
1.47000E+00	4.75000E+05	-4.84136E-02

Figure 7. 16: Results of the Simulation in Patran-Nastran

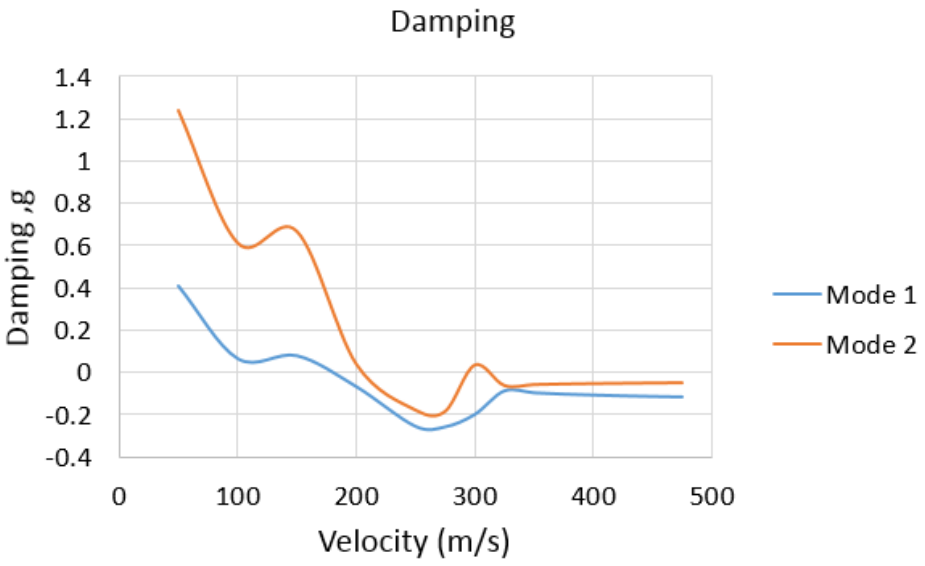

Figure 7. 17: Velocity vs Damping for Onera M6 Wing

7.3 Validation of Results obtained in Ansys

The validation of the results obtained in Ansys can be done through a comparison with the results obtained from the simulation in Patran-Nastran. It is important to note that these simulations have significant differences in terms of the theories that they applied, especially in the aerodynamics. For instance, the simulations in Ansys are based on computational fluid dynamics while the simulation in Nastran is based on the doublet lattice method.

The results from the simulations in Patran-Nastran and Ansys can not be compared directly because they yield different types of results. Ansys produces the complete behaviour of the

structure and the fluid flow in a period of time, while Nastran yields the velocity ranges where the system is stable or unstable. Therefore, the comparison only can be done in terms of the dynamic response that was obtained.

In addition, due to the difference in the essence of the simulations, the comparison should be done in terms of the dynamic pressure, since the aerodynamic forces acting in the wing are directly proportional to the dynamic pressure (NASA 2015).

The dynamic pressure of the simulation in Ansys is calculated below. The air density and the airspeed were taken from the free stream of the fluid domain in the simulation 2 that has an operational pressure of 83,900 Pa according with the table 7.2.

$$\rho = 1.13\ kg/m^3$$
$$V = 347 m/s \qquad (7.1)$$
$$q = \frac{1}{2}\rho V^2 = \frac{1}{2}\left(1.13\, kg/m^3\right)\left(347 m/s\right) = 68{,}302 Pa$$

The simulation in Nastran has an air density of 1.225 kg/m^3 which is the density at standard sea level conditions. Therefore, the airspeed that corresponds with the dynamic pressure of the simulation in Ansys is 333.9 m/s. According with the figure 7.16 and 7.17, this airspeed is in the range of flutter stability. This result matches with the type of dynamic response that was obtained in Ansys which is a Limit Cycle Oscillation (LCO) as it is illustrated in the figures 7.6 and 7.7. As explained in the chapter 2, LCOs are considered as a stable response.

Chapter 8

Conclusions and Future Work

As was described in the chapter 1, the purposes of this project were the evaluation of the capabilities of Ansys to perform FSI simulations and the exploration of the parameters that produce the more reliable results. To achieve these objectives, two aeroelastic cases were studied, they were: the delta wing, and the Onera M6 wing. The details of the conclusions that are presented below are fully described in the chapters 4 and 7 that contain the results of the simulations and discussions about them.

The two Aeroelastic cases or FSI problems that were studied are different in three aspects which are: the airspeed regime, the complexity of the structure, and the reference point to evaluate the results. The delta wing simulation is subsonic, the structure is a simple flat plate made out of aluminium, and the point of reference is an experiment. The Onera M6 wing simulation is transonic, the wing structure has multiple components that are made out of a composite material, and the reference point is a simulation performed in the software Patran-Nastran that is considered the standard software of the industry.

The following conclusions can be made about the delta wing case.

- The main conclusion is that Ansys has shown limited capability to simulate the fluid-structure interaction in this case. The simulations have shown that Ansys has acceptable FSI capabilities because the dynamic behaviour and some results match the experiment with reasonable accuracy. However, it also has shown its limitations

because other experimental results are not accurate and some dynamic responses do not occur in the correct regime of airspeeds. In addition, it also has been shown that the simulations are not able to replicate some particular behaviours of the problem like the asymmetry at 0° AOA.

- The use of different turbulence models over the wing, and the use of different turbulence intensities in the boundaries of the fluid domain do not show significant effects in the results. However, this fact could be related more with the characteristics of the experiment than with the capabilities of Ansys.

The following conclusions can be made about the Onera M6 wing case.

- Ansys is able to reproduce correctly the results of Nastran. However, due to the significant differences in the theories that are used in both programs, it was not possible to perform the comparison in the same terms of the simulations carried out with the delta wing, which means that it was not possible to compare accelerations and displacements.

- The reduction in the time step is essential to achieve the successful completion of the simulation. However, the reduction in the time step also implies the significant increment of the hard disk memory used by the computer and the time to perform the simulations.

- Similarly to the reduction in the time step, the dynamic mesh has shown a major importance to achieve a successful completion of the simulation. In particular, the increment in the diffusion parameter solves many problems during the execution that are related to the distortion of the mesh during the remeshing.

The main conclusion that arise from the comparison of the two problems is that the increment of the complexity in the wing structure requires a better tuning of the time step and dynamic mesh parameters to achieve successful completion of the simulation. The simulation of the delta wing required little work to tune the time step and the dynamic mesh. In contrast, the Onera M6 wing simulations required a lot work to find the appropriate time step and the parameters of dynamic mesh.

Although the evaluation of the computational performance is not part of this project, the problems related with this aspect arose frequently due to the high specifications of computational resources that are required to perform FSI simulations in Ansys. A comparison between both aeroelastic problems in terms of computation resources shows that the increment in the complexity of the geometry and the mesh resolution can increase significantly the demands of computation performance.

Based on the previous conclusions, it is possible to state that the main contribution of this project is the demonstration of the acceptable capabilities of Ansys-Fluent to perform FSI simulations. However, it also has been demonstrated the limitations of the software, especially in relation with the lack of accuracy in some Aeroelastic cases. This research is also part of a learning process in the school of of Aerospace, Mechanical & Mechatronic Engineering about how to take full advantage the capabilities of Ansys, in this particular case, to study Aeroelastic problems, which is one of the areas of interests in the departement of Aeronautical and Aerospace Engineering.

This work provides a strong basis for a range of future tasks to explore the FSI capabilities of Ansys, including:

- Investigate the effects of dynamic mesh parameters on the accuracy of the FSI simulations. As was explained before, the dynamic parameters seem to have a major importance to avoid execution errors. They also could have some effect in the accuracy of the results obtained such as the accelerations that were studied in the Delta wing simulation.

- Perform simulations for all the experimental points that were presented in the chapter four (Korbahti, Kagambage et al. 2011) in order to have a complete comparison between the simulation and the experimental results. This task will allow to determine if Ansys can replicate other interesting behaviours that were described in that experiment.

- Perform simulations with a flat face in the leading edge of the delta wing in order to compare their results against the results that were obtained with a sharp edge and that were presented in the chapter four

- Carry out a systematic study of the factors that could improve the computation performance in the FSI simulations in Ansys. The high computation demands were a big problem during the development of this project. Therefore, any improvement in this aspect may lead to a significant growth in the capabilities to study cases with more complexity and at the same time using the computation resources with higher efficiency. For example, the options to save the data during the execution of the simulation have a significant impact in the memory space used by the computer to store the results.

- Exploration of other tools in Ansys to perform FSI simulations. The solver Fluent was used in all the simulations in this projects, but Ansys also has another CFD solver with FSI capabilities that is called CFX. This may allow to take fully advantage of the Ansys capabilities.

Appendices

A Mesh Quality of the delta wing structure

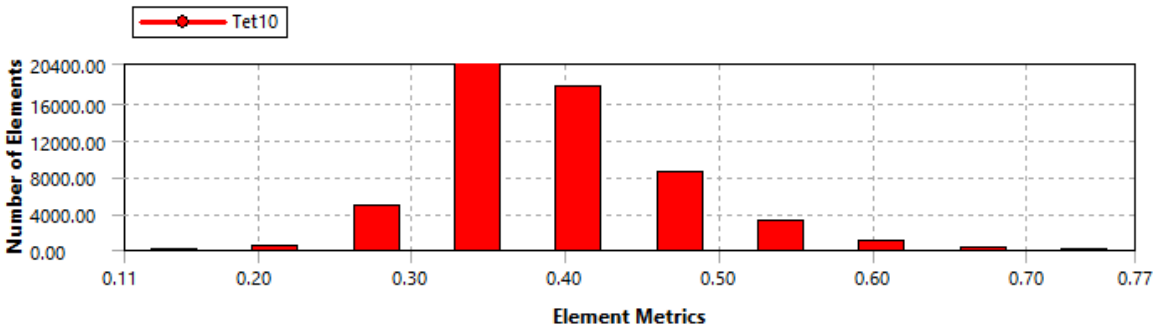

Figure A. 1: Orthogonal Quality

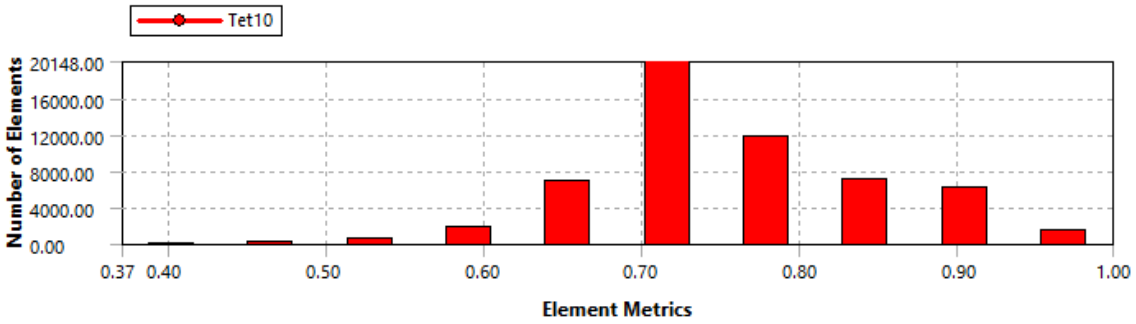

Figure A. 2: Skewness

B Details of Fluid Domain Mesh in Delta Wing

Defaults	
Physics Preference	CFD
Solver Preference	Fluent
Relevance	1
Sizing	
Use Advanced Size Fu...	On: Fixed
Relevance Center	Medium
Initial Size Seed	Active Assembly
Smoothing	Medium
Transition	Slow
Min Size	1.e-003 m
Max Face Size	0.50 m
Max Size	0.50 m
Growth Rate	1.30
Minimum Edge Length	1.e-003 m
Inflation	
Use Automatic Inflation	All Faces in Chosen Named Sele...
Named Selection	wall_cfd_coupled
Inflation Option	Smooth Transition
Transition Ratio	0.272
Maximum Layers	5
Growth Rate	1.2
Inflation Algorithm	Pre
View Advanced Options	No

Figure B. 1: Details of Fluid Domain Mesh in Delta Wing Simulation

C Configuration of Fluent Solver Fluent

Model	Settings
Space	3D
Time	Unsteady, 1st-Order Implicit
Viscous	Realizable k-epsilon turbulence model
Wall Treatment	Enhanced Wall Treatment
Heat Transfer	Disabled
Solidification and Melting	Disabled
Species	Disabled
Coupled Dispersed Phase	Disabled
NOx Pollutants	Disabled
SOx Pollutants	Disabled
Soot	Disabled
Mercury Pollutants	Disabled

Version: 3d, pbns, dynamesh, rke, transient (3d, pressure-based, dynamic mesh, realizable k-epsilon, transient)
Release: 14.5.0
Title:

Solver Settings

Equations

Equation	Solved
Flow	yes
Turbulence	yes

Numerics

Numeric	Enabled
Absolute Velocity Formulation	yes

Unsteady Calculation Parameters

Time Step (s)	0.004
Max. Iterations Per Time Step	20

Relaxation

Variable	Relaxation Factor
Density	1
Body Forces	1
Turbulent Kinetic Energy	0.8
Turbulent Dissipation Rate	0.8
Turbulent Viscosity	1

Linear Solver

Variable	Solver Type	Termination Criterion	Residual Reduction Tolerance
Flow	F-Cycle	0.1	
Turbulent Kinetic Energy	Flexible	0.1	0.7
Turbulent Dissipation Rate	Flexible	0.1	0.7

Pressure-Velocity Coupling

Parameter	Value
Type	Coupled
Pseudo Transient	no
Flow Courant Number	200
Explicit momentum under-relaxation	0.75
Explicit pressure under-relaxation	0.75

Discretization Scheme

Variable	Scheme
Pressure	Standard
Momentum	Second Order Upwind
Turbulent Kinetic Energy	First Order Upwind
Turbulent Dissipation Rate	First Order Upwind

Solution Limits

Quantity	Limit
Minimum Absolute Pressure	1
Maximum Absolute Pressure	5e+10
Minimum Temperature	1
Maximum Temperature	5000
Minimum Turb. Kinetic Energy	1e-14
Minimum Turb. Dissipation Rate	1e-20
Maximum Turb. Viscosity Ratio	100000

D Specifications of Remote Desktop Computer

The simulations of the Delta Wing were carried out in this computer which is a remote desktop located in the University of Sydney.

Processor: Intel® Core ™ i7 CPU 950 @ 3.07 GHz 3.06 GHz
Installed memory (RAM): 12GB
System type: 64-bit Operating System
Pen and Touch: No pen or touch input is available for this display
Operative Syste: Windows 7 Enterprise, service pack 1

Records of memory used for some FSI simulations of the Delta Wing

Table B. 1: Records of Memory used for some simulations of the Delta Wing

Simulation	Hard Disk Space
Rough Mesh	32.5 GB
Medium Mesh	39.9 GB
Fine Mesh	74.5 GB

E Results of Simulations, Delta Wing at 0° AOA

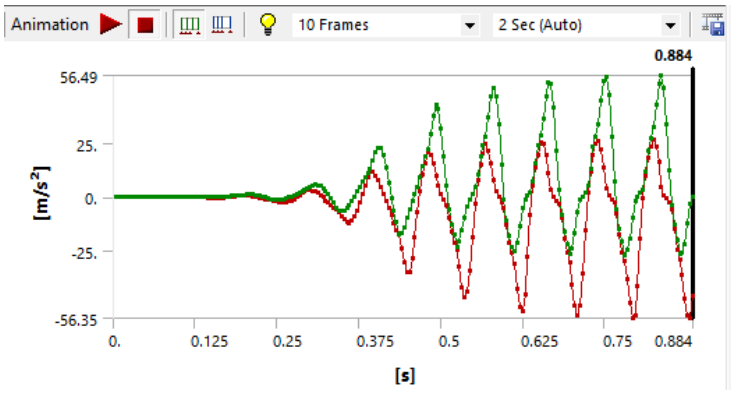

	Time [s]	Minimum [m/s²]	Maximum [m/s²]
1	4.e-003	-6.2669e-002	-4.6931e-002
2	8.e-003	-0.10159	-1.7841e-002
3	1.2e-002	-0.12951	4.2203e-002
4	1.6e-002	-0.10491	1.503e-002
5	2.e-002	-1.399e-003	1.3592e-002
6	2.4e-002	2.0977e-002	0.12841
7	2.8e-002	7.7207e-002	0.16258
8	3.2e-002	0.12404	0.13856
9	3.6e-002	9.9101e-002	0.13215
10	4.e-002	3.4862e-002	0.13887
11	4.4e-002	2.608e-002	8.3574e-002
12	4.8e-002	2.4097e-004	3.9789e-002
13	5.2e-002	-5.0515e-002	5.662e-002
14	5.6e-002	-7.8348e-002	6.0851e-002
15	6.e-002	-6.7286e-002	-7.8173e-003

Figure E. 1: Acceleration a1 at U=34 m/s

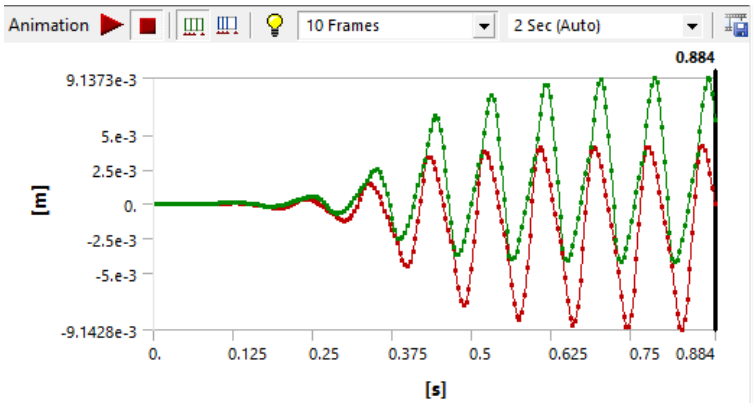

	Time [s]	Minimum [m]	Maximum [m]
1	4.e-003	-5.0553e-007	-3.7858e-007
2	8.e-003	-1.9849e-006	-1.6452e-006
3	1.2e-002	-5.4257e-006	-2.5956e-006
4	1.6e-002	-1.0739e-005	-3.0902e-006
5	2.e-002	-1.6778e-005	-3.4393e-006
6	2.4e-002	-2.1684e-005	-3.5972e-006
7	2.8e-002	-2.4266e-005	-2.9674e-006
8	3.2e-002	-2.444e-005	-7.2975e-007
9	3.6e-002	-2.2447e-005	3.2897e-006
10	4.e-002	-1.8286e-005	8.3804e-006
11	4.4e-002	-1.2349e-005	1.3963e-005
12	4.8e-002	-5.4218e-006	1.9752e-005
13	5.2e-002	2.2784e-006	2.5139e-005
14	5.6e-002	1.0916e-005	2.9497e-005
15	6.e-002	1.9975e-005	3.2692e-005

Figure E. 2: Displacement of a1 at U=34 m/s

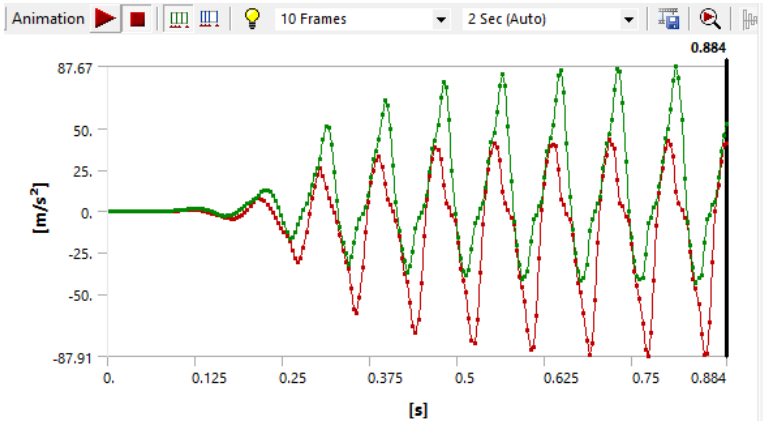

	Time [s]	Minimum [m/s²]	Maximum [m/s²]
1	4.e-003	-2.805e-002	4.1078e-003
2	8.e-003	-0.13131	3.9239e-002
3	1.2e-002	-0.17588	9.6187e-002
4	1.6e-002	-0.10337	3.3885e-002
5	2.e-002	-1.0631e-002	9.6925e-002
6	2.4e-002	1.9696e-002	0.22585
7	2.8e-002	5.3212e-002	0.22544
8	3.2e-002	0.10662	0.19004
9	3.6e-002	8.7532e-002	0.13158
10	4.e-002	9.9939e-003	9.8156e-002
11	4.4e-002	-3.5234e-002	6.1226e-002
12	4.8e-002	-0.10249	2.4912e-002
13	5.2e-002	-0.19238	-6.3845e-004
14	5.6e-002	-0.26117	-5.5405e-002
15	6.e-002	-0.27183	-0.16733
16	6.4e-002	-0.29957	-0.23387
17	6.8e-002	-0.39154	-0.19637
18	7.2e-002	-0.39265	-0.19016

Figure E. 3: Acceleration a1 at U=36 m/s

F Results of Simulations, Delta Wing at 1° AOA

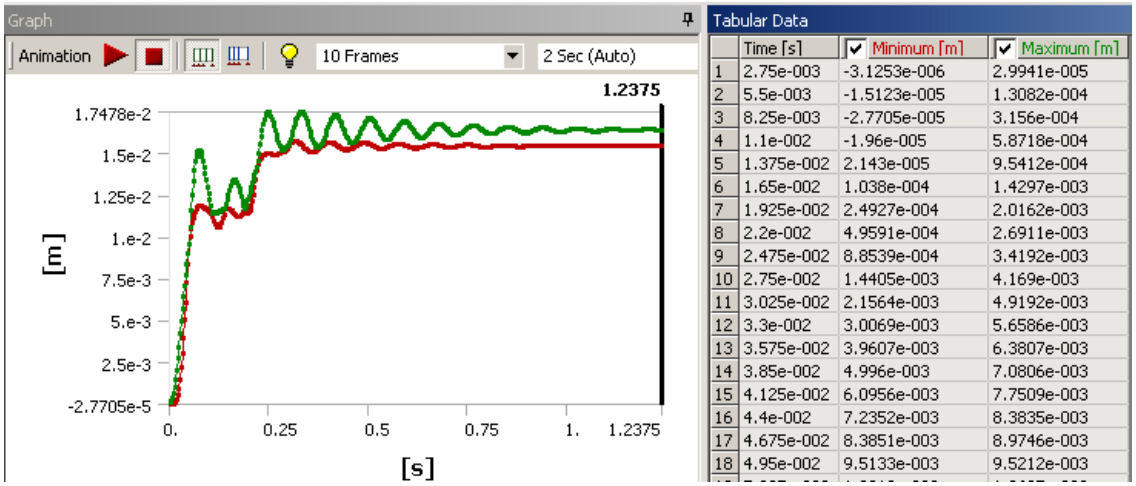

	Time [s]	Minimum [m]	Maximum [m]
1	2.75e-003	-3.1253e-006	2.9941e-005
2	5.5e-003	-1.5123e-005	1.3082e-004
3	8.25e-003	-2.7705e-005	3.156e-004
4	1.1e-002	-1.96e-005	5.8718e-004
5	1.375e-002	2.143e-005	9.5412e-004
6	1.65e-002	1.038e-004	1.4297e-003
7	1.925e-002	2.4927e-004	2.0162e-003
8	2.2e-002	4.9591e-004	2.6911e-003
9	2.475e-002	8.8539e-004	3.4192e-003
10	2.75e-002	1.4405e-003	4.169e-003
11	3.025e-002	2.1564e-003	4.9192e-003
12	3.3e-002	3.0069e-003	5.6586e-003
13	3.575e-002	3.9607e-003	6.3807e-003
14	3.85e-002	4.996e-003	7.0806e-003
15	4.125e-002	6.0956e-003	7.7509e-003
16	4.4e-002	7.2352e-003	8.3835e-003
17	4.675e-002	8.3851e-003	8.9746e-003
18	4.95e-002	9.5133e-003	9.5212e-003

Figure F. 1: Displacement a1 at 28.6 m/s

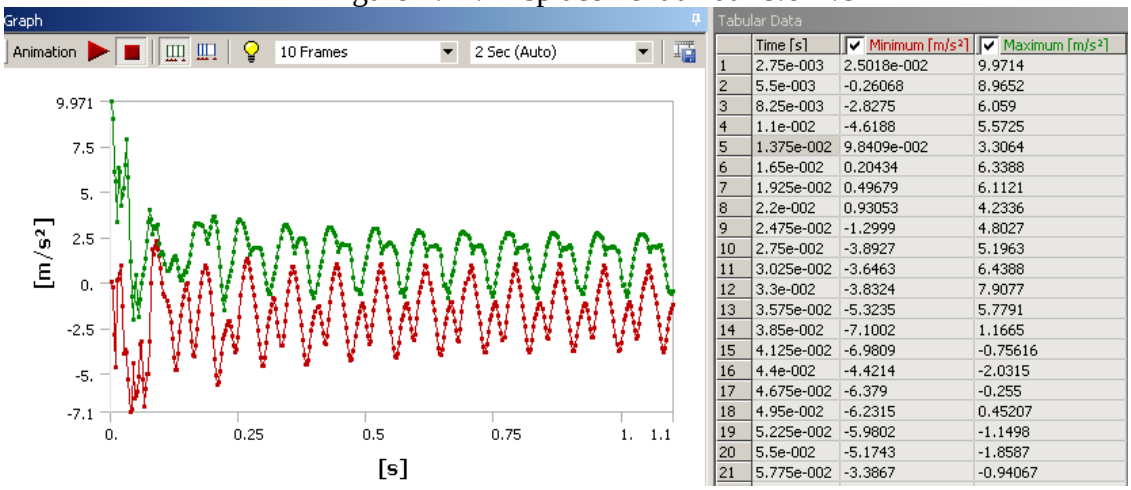

	Time [s]	Minimum [m/s²]	Maximum [m/s²]
1	2.75e-003	2.5018e-002	9.9714
2	5.5e-003	-0.26068	8.9652
3	8.25e-003	-2.8275	6.059
4	1.1e-002	-4.6188	5.5725
5	1.375e-002	9.8409e-002	3.3064
6	1.65e-002	0.20434	6.3388
7	1.925e-002	0.49679	6.1121
8	2.2e-002	0.93053	4.2336
9	2.475e-002	-1.2999	4.8027
10	2.75e-002	-3.8927	5.1963
11	3.025e-002	-3.6463	6.4388
12	3.3e-002	-3.8324	7.9077
13	3.575e-002	-5.3235	5.7791
14	3.85e-002	-7.1002	1.1665
15	4.125e-002	-6.9809	-0.75616
16	4.4e-002	-4.4214	-2.0315
17	4.675e-002	-6.379	-0.255
18	4.95e-002	-6.2315	0.45207
19	5.225e-002	-5.9802	-1.1498
20	5.5e-002	-5.1743	-1.8587
21	5.775e-002	-3.3867	-0.94067

Figure F. 2: Acceleration a2 at 31.1 m/s

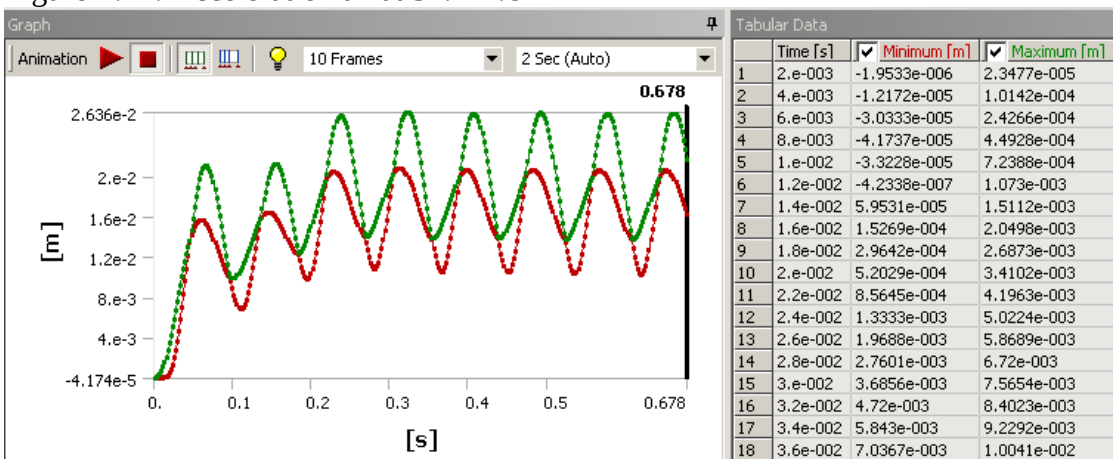

	Time [s]	Minimum [m]	Maximum [m]
1	2.e-003	-1.9533e-006	2.3477e-005
2	4.e-003	-1.2172e-005	1.0142e-004
3	6.e-003	-3.0333e-005	2.4266e-004
4	8.e-003	-4.1737e-005	4.4928e-004
5	1.e-002	-3.3228e-005	7.2388e-004
6	1.2e-002	-4.2338e-007	1.073e-003
7	1.4e-002	5.9531e-005	1.5112e-003
8	1.6e-002	1.5269e-004	2.0498e-003
9	1.8e-002	2.9642e-004	2.6873e-003
10	2.e-002	5.2029e-004	3.4102e-003
11	2.2e-002	8.5645e-004	4.1963e-003
12	2.4e-002	1.3333e-003	5.0224e-003
13	2.6e-002	1.9688e-003	5.8689e-003
14	2.8e-002	2.7601e-003	6.72e-003
15	3.e-002	3.6856e-003	7.5654e-003
16	3.2e-002	4.72e-003	8.4023e-003
17	3.4e-002	5.843e-003	9.2292e-003
18	3.6e-002	7.0367e-003	1.0041e-002

Figure F. 3: Displacement a1 at 33.9

G Convergence Graph of the Steady State CFD simulation Onera M6

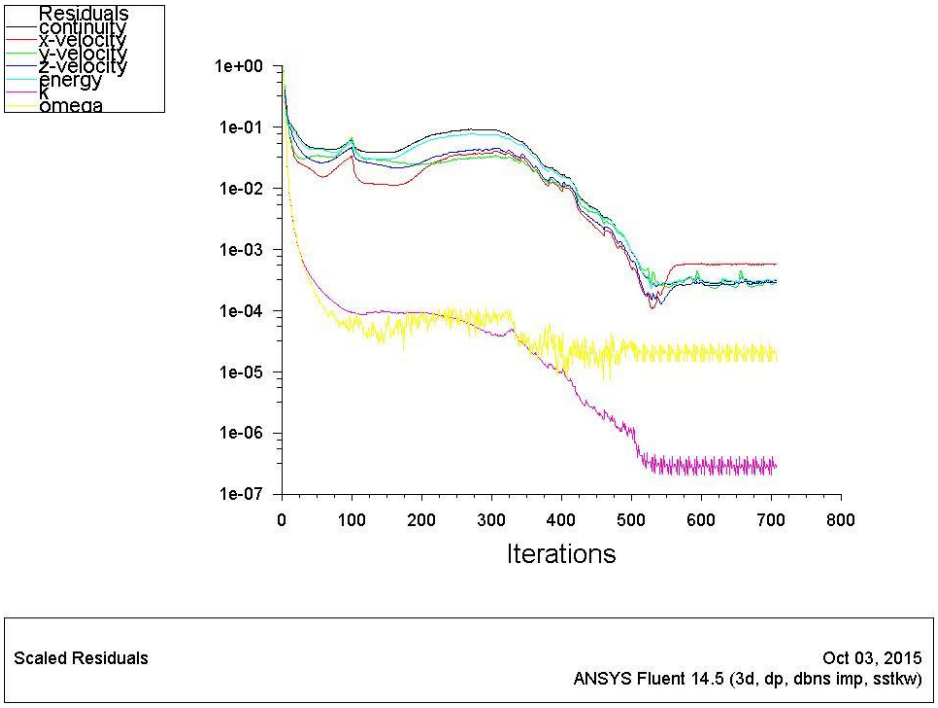

Figure G. 1: Convergence of CFD simulation with rough mesh

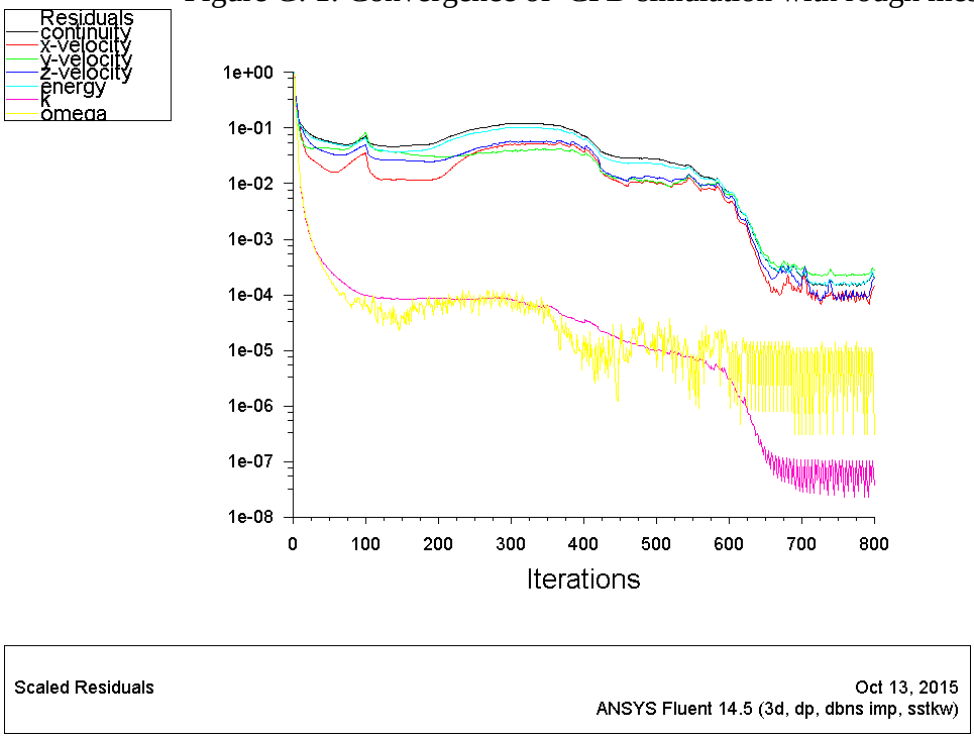

Figure G. 2: Convergence of CFD simulation with fine mesh

H Internal Structure of the Onera M6 Wing

All dimensions in mm

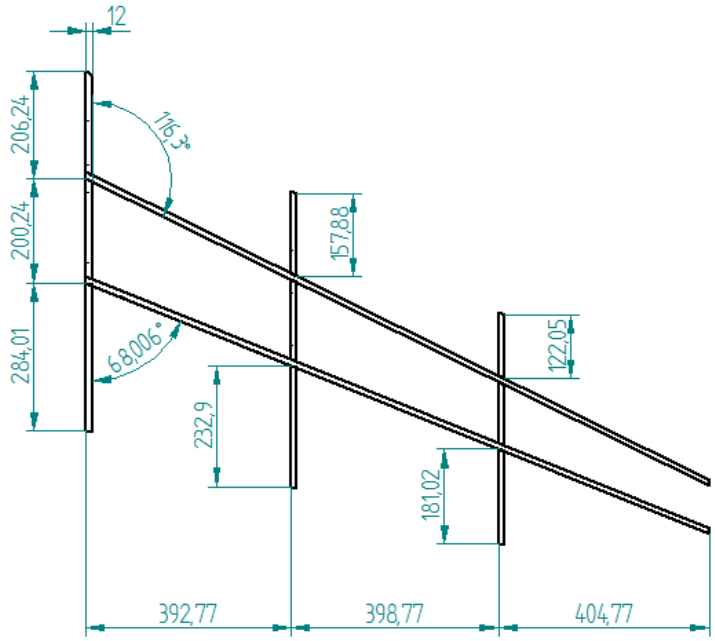

Figure H. 1: Internal Structure of the Onera M6 Wing

I Details of the Fluid Domain Mesh in the FSI Simulation of Onera M6 Wing

Defaults	
Physics Preference	CFD
Solver Preference	Fluent
Relevance	0
Sizing	
Use Advanced Size Fun...	On: Curvature
Relevance Center	Medium
Initial Size Seed	Active Assembly
Smoothing	Medium
Transition	Slow
Span Angle Center	Medium
Curvature Normal A...	Default (45.0 °)
Min Size	Default (7.8028e-003 m)
Max Face Size	Default (0.780280 m)
Max Size	Default (1.56060 m)
Growth Rate	1.30
Minimum Edge Length	1.2681e-004 m
Inflation	
Use Automatic Inflation	All Faces in Chosen Named Selection
Named Selection	wall_cfd_coupled
Inflation Option	Smooth Transition
Transition Ratio	0.272
Maximum Layers	5
Growth Rate	1.2
Inflation Algorithm	Pre
View Advanced Options	No

Figure I. 1: Details of the Fluid Domain Mesh in the FSI Simulation of Onera M6 Wing

J Mesh Details of the Onera M6 Wing Structure

Defaults	
Physics Preference	Mechanical
Solver Preference	Mechanical APDL
Relevance	0
Sizing	
Use Advanced Size Fun...	Off
Relevance Center	Medium
Element Size	1.e-002 m
Initial Size Seed	Active Assembly
Smoothing	Medium
Transition	Fast
Span Angle Center	Coarse
Minimum Edge Length	1.2681e-004 m

a)

Defaults	
Physics Preference	Mechanical
Solver Preference	Mechanical APDL
Relevance	0
Sizing	
Use Advanced Size Fun...	Off
Relevance Center	Medium
Element Size	2.e-002 m
Initial Size Seed	Active Assembly
Smoothing	Medium
Transition	Fast
Span Angle Center	Coarse
Minimum Edge Length	1.2681e-004 m

b)

Figure F. 1: a) Mesh specifications of simulation 2 b) Mesh specifications of Simulation 1 and 3

K Specifications of Remote Desktop Computer-Vibration Laboratory

2 x 12-Core Xeon E5-2670V3 2.3GHz, 30MB Cache, 9.6GT/Sec, 24 Threads, LGA 2011, Thermal solution is not included and may be ordered separately
2 x G.SKILL DDR4-2133 32GB Quad Channel Memory
1 x ASUS Z10PE-D16 Server MB, C612 Chipset, Dual 2011-3 Socket, 16 x DDR4 DIMM Slots, 5 x PCI-E, SATAII RAID, Int. VGA, 2 x GbE LAN, SSI EEB
1 x Western Digital WD4003FZEX Black 4 TB SATA 6 Gb/3.5""/64 MB/7200 RPM
2 x Corsair Hydro Series H75 Performance Liquid CPU Cooler - Slim 25mm radiator and dual PWM fans for compact, performance liquid CPU cooling
1 x Corsair 900D Super Tower PC Case with Side Window - Serious expansion flexibility and incredible cooling performance for advanced builders
1 x Corsair 1000W RM-1000 ATX Power Supply, 80 PLUS Gold Certified, Full Modular

Table K. 1: Memory used by the FSI simulations of the Onera M6 wing

Simulation	# of elements in Mesh wing structure	Hard Disk Space
Simulation 1	12,337	131 GB
Simulation 2	48,766	457 GB
Simulation 3	12,337	131 GB

Bibliography

Abobaker, M. H., et al. (2014). "ANSYS-FLUENT VALIDATION FOR TRANSONIC FLOW OVER ONERA-M6 WING AT DIFFERENT ANGLES OF ATTACK AND MACH NUMBERS." SRMA 2014 (THE FOURTH INTERNATIONAL SYMPOSIUM FOR STUDENTS): 14.

ANSYS (2006). "Modeling Turbulent Flows." 2015, from http://www.engr.uconn.edu/~barbertj/CFD%20Training/Fluent/5%20Modeling%20of%20Turbulent%20Flows.pdf.

ANSYS (2010). "Lecture 6. Turbulence Modeling." from http://imechanica.org/files/fluent_13.0_lecture06-turbulence.pdf.

ANSYS (2012). "Workshop 2, 2-way FSI for a Hyperelastic Flap Including Dynamic Remeshing.". Retrieved 10/06/2015, from https://crc.nd.edu/images/news-events/events/ansys_workshop/fsi/fluent-fsi_14.0_ws3_hyperelastic_flap_part1.pdf.

ANSYS (2013). "Lecture 3.Co-simulation Setup." Retrieved 06/07/2015, from http://es.slideshare.net/arstanle/fluent-fsi-145lect03cosimulationsetup-1.

ANSYS (2014). "Ansys Fluent User's Guide 14.5." Retrieved 20/06/2015, from http://www.afs.enea.it/project/neptunius/docs/fluent/html/ug/node1133.htm#Dynamic_Mesh.

Babel, L. V. (2008). "ONERA-M6 WING." Retrieved 5/03/2015, from http://lucvanbavel.com/capfte.html.

Castelló, W., et al. (2014). "Simulación numérica no lineal de una sección alar típica con oscilaciones autoexcitadas." Revista iberoamericana de ingeniería mecánica **18**(2): 137-151.

Chandrupatla, T. R., et al. (1997). Introduction to finite elements in engineering, Prentice Hall Upper Saddle River.

Chen, X., et al. (2010). "Delayed Detached Eddy Simulation of 3-D Wing Flutter with Fully Coupled Fluid-Structural Interaction." AIAA Paper **53**: 4-7.

Cook, R. D. (2007). Concepts and applications of finite element analysis, John Wiley & Sons.

De Hart, J., et al. (2003). "A three-dimensional computational analysis of fluid–structure interaction in the aortic valve." Journal of Biomechanics **36**(1): 103-112.

Dowell, E., et al. (2003). "Nonlinear Aeroelasticity." Journal of Aircraft **40**(5): 857-874.

Dowell, E. H. and D. Tang (2002). "Nonlinear aeroelasticity and unsteady aerodynamics." AIAA journal **40**(9): 1697-1707.

Eggenspieler, G. (2012). "Turbulence Modeling." Retrieved 3-09-2015, 2015, from http://www.ansys.com/staticassets/ANSYS/Conference/Confidence/San%20Jose/Downloads/turbulence-summary-4.pdf.

Elfeed, T. and I. Kostic (2014). "Influence of winglet added to Onera M6 wing on aerodynamic characteristics in transonic region." SRMA 2014 (THE FOURTH INTERNATIONAL SYMPOSIUM FOR STUDENTS): 9-13.

Frei, W. (2013). "Which Turbulence Model Should I Choose for My CFD Application?". Retrieved 3-09-2015, from http://www.comsol.com/blogs/which-turbulence-model-should-choose-cfd-application/.

Guru, G. and B. Chansup (1993). Fluid-structural interactions using Navier-Stokes flow equations coupled with shell finite element structures. 23rd Fluid Dynamics, Plasmadynamics, and Lasers Conference, American Institute of Aeronautics and Astronautics.

Houghton, E. L., et al. (2012). Aerodynamics for engineering students, Elsevier.

Joaquim Peiro, S. S. (2005). "FINITE DIFFERENCE, FINITE ELEMENT AND FINITE VOLUME METHODS FOR PARTIAL DIFFERENTIAL EQUATIONS." Retrieved 03-03-2015, from http://wwwf.imperial.ac.uk/ssherw/spectralhp/papers/HandBook.pdf.

Kesti, J. and S. Olsson (2014). Fluid structure interaction analysis on the aerodynamic performance of underbody panels, Chalmers University of Technology.

Korbahti, B., et al. (2011). "Subcritical, nontypical and period-doubling bifurcations of a delta wing in a low speed wind tunnel." Journal of Fluids and Structures **27**(3): 408-426.

Lee, B., et al. (1999). "Nonlinear aeroelastic analysis of airfoils: bifurcation and chaos." Progress in aerospace sciences **35**(3): 205-334.

Miller, E. (2012). "Starting ANSYS Products From the Command Line." Phoenix Analysis & Design Technologies Retrieved 3/10/2015, from http://www.padtinc.com/blog/the-focus/starting-ansys-products-from-the-command-line.

MSC.Software (2009). "MSC.Nastran Version 68, Aeroelastic Analysis User's Guide." from https://simcompanion.mscsoftware.com/infocenter/index?page=content&id=DOC9182.

NASA (2014). "Navier-Stokes Equations." from https://www.grc.nasa.gov/www/k-12/airplane/nseqs.html.

NASA (2015). "Dynamic Pressure." from https://www.grc.nasa.gov/www/k-12/airplane/dynpress.html.

Ponweiser, T., et al. (2013). "Fluid-Structure Simulations with OpenFOAM for Aircraft Designs." Partnership for Advanced Computing in Europe. Available at: http://www. prace-ri. eu/IMG/pdf/wp172. pdf (Accessed 27 February 2015).

Raja, R. S. (2012). Coupled fluid structure interaction analysis on a cylinder exposed to ocean wave loading.

Reimann, T., et al. (2014). "Numerical Simulation of a Turbulent FSI Benchmark Case." PAMM **14**(1): 631-632.

Roszak, R., et al. (2009). "Fluid-structure interaction for large scale complex geometry and non-linear properties of structure." Archives of Mechanics **61**(1): 3-27.

Ruck, S. and J. H. Oertel (2010). "Fluid-structure interaction simulation of an avian flight model." The Journal of experimental biology **213**(Pt 24): 4180-4192.

Schmitt, V. and F. Charpin (1979). "Pressure Distributions on the ONERA-M6-Wing at Transonic Mach Numbers." Experimental Data Base for Computer Program Assessment, Report of the Fluid Dynamics Panel Working Group 04, AGARD AR 138: B1-1.

Sigrist, J.-F. and S. Garreau (2007). "Dynamic analysis of fluid–structure interaction problems with modal methods using pressure-based fluid finite elements." Finite Elements in Analysis & Design **43**(4): 287-300.

Slater, J. W. (2008, Monday, 05-Jan-2015). "ONERA M6 Wing ". Retrieved 02/03/2015, 2015, from http://www.grc.nasa.gov/WWW/wind/valid/m6wing/m6wing.html.

Szabo, G. and G. Kristof (2010). Three-dimensional numerical flutter simulation. The 5th International Symposium on Computational Wind Engineering (CWE2010), Chapel Hill, North Carolina, USA.

Tech, V. (1998). "6. Aerodynamics of 3D Lifting Surfaces through Vortex Lattice Methods." from http://www.dept.aoe.vt.edu/~mason/Mason_f/CAtxtChap6.pdf.

Tooley, M. (2012). Fluid–Structure Interaction Using System Coupling. ansys-blog, ANSYS, Inc. **2015**.

USYD (2015). from http://aerodynamics.aeromech.usyd.edu.au/subsonic.pdf.

Yates, E. C., Jr "AGARD Standard Aeroelastic Configuration for Dynamic Response, Candidate Configuration I.-Wing 445.6." NASA TM 100492.

Zienkiewicz, O. C. and R. L. Taylor (2000). The finite element method: Solid mechanics, Butterworth-heinemann.